LBL-19551 c.2

Lawrence Berkeley Laboratory

UNIVERSITY OF CALIFORNIA

RECEIVED
BERKELEY LABORATORY
JUL 16 1985
LIBRARY AND
DOCUMENTS SECTION

APPLIED SCIENCE DIVISION

UNSTEADY HEAT TRANSFER DURING THE INTERACTION
OF A LAMINAR FLAME WITH A COLD WALL

S.R. Vosen
(Ph.D. Thesis)

TWO-WEEK LOAN COPY
This is a Library Circulating Copy
which may be borrowed for two weeks.

November 1983

APPLIED SCIENCE
DIVISION

Prepared for the U.S. Department of Energy under Contract DE-AC03-76SF00098

LBL-19551 c.2

DISCLAIMER

This document was prepared as an account of work sponsored by the United States Government. While this document is believed to contain correct information, neither the United States Government nor any agency thereof, nor the Regents of the University of California, nor any of their employees, makes any warranty, express or implied, or assumes any legal responsibility for the accuracy, completeness, or usefulness of any information, apparatus, product, or process disclosed, or represents that its use would not infringe privately owned rights. Reference herein to any specific commercial product, process, or service by its trade name, trademark, manufacturer, or otherwise, does not necessarily constitute or imply its endorsement, recommendation, or favoring by the United States Government or any agency thereof, or the Regents of the University of California. The views and opinions of authors expressed herein do not necessarily state or reflect those of the United States Government or any agency thereof or the Regents of the University of California.

LBL-19551

Unsteady Heat Transfer during the Interaction of a Laminar Flame with a Cold Wall

Steven Ray Vosen
Ph.D. Thesis

Lawrence Berkeley Laboratory
University of California
Berkeley, California 94720

November 1983

This work was supported by the Assistant Secretary for Conservation and Renewable Energy, Office of Transportation Programs, Division of Transportation Energy of the U.S. Department of Energy under Contract Number DE-AC03-76SF00098.

UNSTEADY HEAT TRANSFER DURING THE INTERACTION OF A LAMINAR FLAME WITH A COLD WALL

Ph.D. Steven Ray Vosen Mechanical Engineering

Sponsor: U.S. Department of Energy

Signature Committee Chairman

ABSTRACT

Measurements were made of the unsteady heat transfer to a wall during the quenching of premixed, methane-air flames. One dimensional laminar flames were produced in a constant volume chamber and the heat transfer was measured into the quenching surface by means of a platinum thin film resistance thermometer. The experiments were performed over a range of pressures varying from 1 to 4 atmospheres and over a range of equivalence ratios from 0.7 to 1.2. Possible catalytic effects of the gauge were appraised by comparing the heat flux as obtained from different types of gauges.

The experimental results were compared to the predictions of three numerical models. Two of the models were finite difference formulation of the conservation equations: one with detailed kinetics and the other with one step kinetics. The third model was an integral method with ignition temperature kinetics.

The main experimental results are: 1) the data were successfully correlated on the basis of the heat release rate of the flame prior to quenching. The effects of both equivalence ratio and pressure were included. 2) The maximum heat flux is related to the quenching distance and thus it may be possible to use measurements of the quenching distance to predict the maximum heat flux during quenching. 3) Catalytic effects of the platinum gauge on the heat transfer

measurement were determined to be undetectable for wall temperatures varying from 300 to 350 K.

A comparison of the experimental results and the numerical calculations revealed that: 1) compression heating in the constant volume chamber affected the heat transfer. This was accounted for by considering the variation of thermal properties of the gas near the wall. 2) A one step reaction model predicts the heat transfer as well as a detailed kinetics model, to within 15% of the experimental results. 3) The integral model predicted the heat transfer as well as the finite difference models with only a modest computational effort. 4) Thermal diffusion and the chemical reaction rate of combustion are the dominant processes which determine the heat flux during quenching.

ACKNOWLEDGEMENTS

The completion of this work reflects the talents, experience and generosity of many individuals. At this time, I wish to express my appreciation to them and to their contribution to my thesis.

I thank my parents, brother, grandparents, aunts, uncles and cousins for their moral support, and for encouraging me to pursue my career. I am also grateful to Mary Ann for her love and support.

My advisor, Professor Ralph Greif contributed much to my learning, through his guidance in the course of my research, and his patience during the writing of this dissertation. This work also benefited from the thoughtful comments and suggestions of the other members of my thesis committee, Professors Robert Sawyer and Sumner Davis.

Throughout the years, both Professors Chang-Lin Tien and Antoni Oppenheim have given their support and knowledge. To them I am deeply indebted.

The enthusiasm which Dr. Charles Westbrook of Lawrence Livermore National Laboratory has shown in my project has been greatly appreciated. He has spent numerous hours discussing by research and performing the calculations for the finite difference modeling.

Ken Hom, Dick Jensen, Horton Stewart, Gary Hubbard, Al Shaw, and the staff of the Hesse Hall and Etcheverry Hall machine shops are to be thanked for their parts in the design, maintenance and operation of the experiments.

Finally, I would to express my appreciation to the students and staff of Hesse Courtyard for their comradery, and for making life as a graduate student more bearable.

TABLE OF CONTENTS

page

ACKNOWLEDGEMENTS i

TABLE OF CONTENTS ii

LIST OF FIGURES iv

LIST OF TABLES ix

NOMENCLATURE x

CHAPTER

1 Introduction 1
- 1.1 Heat Transfer Studies 2
  - 1.1.1 Steady State Combustion with Heat Transfer 2
  - 1.1.2 Unsteady Combustion with Heat Transfer 2
- 1.2 Quenching Distance Studies 4
- 1.3 Flame Quenching Models 5
- 1.4 The Present Work 6

2 Experimental System and Procedure 7
- 2.1 Apparatus 7
  - 2.1.1 Chamber 7
  - 2.1.2 Gas Metering and Ignition 7
  - 2.1.3 Instrumentation 10
    - 2.1.3.1 Pressure 10
    - 2.1.3.2 Heat Flux 10
    - 2.1.3.3 Optics 15
- 2.2 Calibrations 15
  - 2.2.1 Thin Film Resistance Thermometer 15
  - 2.2.2 Pressure Gauge 16
  - 2.2.3 Flow System 16
- 2.3 Procedure 17
  - 2.3.1 Quenching in a Constant Volume Combustion Chamber 17
  - 2.3.2 Control of the Pressure at Quench 21
  - 2.3.3 Rational for Data Acquisition 22
  - 2.3.4 Experimental Procedure 25
  - 2.3.5 Data Reduction 26

3 Experimental Results 28
- 3.1 Interpretation of Results 31
- 3.2 Nondimensional Results 34
- 3.3 The Assumption of Constant Pressure 45
- 3.4 Run to Run Variations 45
- 3.5 The Effects of Protective Coatings 45

4 Numerical Results 52
4.1 Detailed vs. One-Step Kinetics Models 54
4.2 One-Step Kinetics Model 54
4.3 Integral Method 58
4.4 Thermal Boundary Layer Effects 64

5 Comparison of Experimental and Numerical Results 69
5.1 Experimental Results and Modeling 69
5.2 Comparison with Other Experiments 73
5.2.1 Heat Transfer Experiments 73
5.2.2 Relationship of the Heat Flux to the Quenching Distance 78

6 Conclusions and Recommendations 83
6.1 Conclusions 83
6.1.1 Experimental Results 83
6.1.2 Experimental and Numerical Results 84
6.2 Recommendations for Further Research 85

APPENDIX

A Determination of the Wall Heat Flux from Wall Temperaure Variation 87

B The Governing Equations 90

C Numerical Models 93

D Experimental and Numerical Data 108

E Fluid and Flame Properties 145

F Isshiki & Nishiwaki 150

REFERENCES 153

LIST OF FIGURES

Figure	Caption	
Figure 2.1	Photograph of fully instrumented constant volume combustion chamber.	8
Figure 2.2	Machine drawing of constant volume combustion chamber.	9
Figure 2.3	Detail of combustion chamber showing thin film gauge and spark gap.	11
Figure 2.4	Schematic of the experiment.	12
Figure 2.5	Thin film gauge.	13
Figure 2.6	Detail of thin film gauge holder. The Assembly is inserted into the combustion chamber with the thin film gauge directed towards the center of the chamber.	14
Figure 2.7a	Sequence of events in an experimental run. The mixture is quiescent and is about to be ignited in the center of the chamber.	18
Figure 2.7b	Sequence of events in an experimental run. The flame has propagated symetrically outwards. The temperature profile is shown.	19
Figure 2.7c	Sequence of events in an experimental run. The flame has just consummed the last of the reactants (solid line). Temperature profiles from previous times are shown (dotted lines).	20
Figure 2.8a,f	Photographic sequence of flame propagation. The mixture is methane-air at an equivalence ratio of one. Initial pressure is one atmosphere.	23
Figure 2.9	Wall temperature and pressure in chamber. The lower figure is detail of the upper figure.	24
Figure 3.1	Heat release, heat flux, flame position as predicted from numerical calculations.	32
Figure 3.2	Typical wall heat flux variation as measured in the experiment.	33
Figure 3.3	Experimental results - wall heat flux vs. time - all conditions.	35
Figure 3.4	Experimental results - maximum heat flux vs. pressure - all conditions.	36

Figure 3.5a	Experimental results - wall heat flux vs. time - p = 1.1 Atmospheres.	38
Figure 3.5b	Experimental results - wall heat flux vs. time - p = 2.7 Atmospheres.	39
Figure 3.6	Experimental results - time for quenching to occur vs. pressure - all conditions.	40
Figure 3.7	Pressure scaled experimental results (Eqn 3.3) - wall heat flux vs. time - all conditions.	41
Figure 3.8	Pressure scaled experimental results (Eqn 3.3) - time for quenching vs. pressure - all conditions.	43
Figure 3.9	Pressure scaled experimental results (Eqn 3.3) - maximum heat flux vs. pressure - all conditions.	44
Figure 3.10a	Heat flux as measured by a platinum gauge for four consecutive runs.	46
Figure 3.10b	Heat flux as measured by a nickel gauge for four consecutive runs.	47
Figure 3.11	Resistance across the thin film as measured through a coating of quartz.	49
Figure 3.12	Comparison of a platinum gauge and a platinum gauge coated with quartz.	51
Figure 4.1	One step kinetics model - wall heat flux vs. time - all conditions.	55
Figure 4.2	One step kinetics model - maximum heat flux vs. pressure - all conditions.	56
Figure 4.3	One step kinetics model - time for quenching vs. pressure - all conditions.	57
Figure 4.4	Integral model - maximum wall heat flux vs. ignition temperature.	60
Figure 4.5	Integral model - maximum wall heat flux vs. time for quenching.	61
Figure 4.6	Integral model - wall heat flux vs. time for four ignition temperatures.	62
Figure 4.7	Comparison of integral and one step kinetics models - wall heat flux vs. time.	63

Figure 4.8	Comparison of integral and one step kinetics models - reaction zone size.	65
Figure 5.1	Comparison of experimental results, pressure scaled experimental results (Eqn 3.3), and one step kinetics model - maximum wall heat flux vs. pressure.	71
Figure 5.2	Comparison of experimental results, pressure scaled experimental results (Eqn 3.3), and one step kinetics model - time for quenching vs. pressure.	72
Figure 5.3	Comparison of pressure scaled experimental results (Eqn 3.3) and one step kinetics model - wall heat flux vs. time.	74
Figure 5.4	Comparison of pressure scaled experimental results (Eqn 3.3) and integral models - wall heat flux vs. time.	75
Figure 5.5	Results of Isshiki & Nishiwaki.	79
Figure C.1	Definitions for the variables in the integral model.	102
Figure D.1	Experimental results - wall heat flux vs. time - P = 1.10 atm., phi = 0.70.	109
Figure D.2	Experimental results - wall heat flux vs. time - P = 1.12 atm., phi = 0.80.	110
Figure D.3	Experimental results - wall heat flux vs. time - P = 1.17 atm., phi = 0.90.	111
Figure D.4	Experimental results - wall heat flux vs. time - P = 1.19 atm., phi = 1.00.	112
Figure D.5	Experimental results - wall heat flux vs. time - P = 1.18 atm., phi = 1.10.	113
Figure D.6	Experimental results - wall heat flux vs. time - P = 1.17 atm., phi = 1.20.	114
Figure D.7	Experimental results - wall heat flux vs. time - P = 1.58 atm., phi = 1.00.	115
Figure D.8	Experimental results - wall heat flux vs. time - P = 2.64 atm., phi = 0.80.	116
Figure D.9	Experimental results - wall heat flux vs. time - P = 2.67 atm., phi = 0.90.	117

Figure D.10 Experimental results - wall heat flux vs. time - P = 2.84 atm., phi = 1.00. 118

Figure D.11 Experimental results - wall heat flux vs. time - P = 2.81 atm., phi = 1.10. 119

Figure D.12 Experimental results - wall heat flux vs. time - P = 2.74 atm., phi = 1.20. 120

Figure D.13 Experimental results - wall heat flux vs. time - P = 3.38 atm., phi = 0.80. 121

Figure D.14 Experimental results - wall heat flux vs. time - P = 3.65 atm., phi = 1.00. 122

Figure D.15 Pressure scaled experimental results (Eqn 3.3) - wall heat flux vs. time - P = 1.10 atm., phi = 0.70. 123

Figure D.16 Pressure scaled experimental results (Eqn 3.3) - wall heat flux vs. time - P = 1.12 atm., phi = 0.80. 124

Figure D.17 Pressure scaled experimental results (Eqn 3.3) - wall heat flux vs. time - P = 1.17 atm., phi = 0.90. 125

Figure D.18 Pressure scaled experimental results (Eqn 3.3) - wall heat flux vs. time - P = 1.19 atm., phi = 1.00. 126

Figure D.19 Pressure scaled experimental results (Eqn 3.3) - wall heat flux vs. time - P = 1.18 atm., phi = 1.10. 127

Figure D.20 Pressure scaled experimental results (Eqn 3.3) - wall heat flux vs. time - P = 1.17 atm., phi = 1.20. 128

Figure D.21 Pressure scaled experimental results (Eqn 3.3) - wall heat flux vs. time - P = 1.58 atm., phi = 1.00. 129

Figure D.22 Pressure scaled experimental results (Eqn 3.3) - wall heat flux vs. time - P = 2.64 atm., phi = 0.80. 130

Figure D.23 Pressure scaled experimental results (Eqn 3.3) - wall heat flux vs. time - P = 2.67 atm., phi = 0.90. 131

Figure D.24 Pressure scaled experimental results (Eqn 3.3) - wall heat flux vs. time - P = 2.84 atm., phi = 1.00. 132

Figure D.25 Pressure scaled experimental results (Eqn 3.3) - wall heat flux vs. time - P = 2.81 atm., phi = 1.10. 133

Figure D.26 Pressure scaled experimental results (Eqn 3.3) - wall heat flux vs. time - P = 2.74 atm., phi = 1.20. 134

Figure D.27 Pressure scaled experimental results (Eqn 3.3) - wall heat flux vs. time - P = 3.38 atm., phi = 0.80. 135

Figure D.28 Pressure scaled experimental results (Eqn 3.3) - wall heat flux vs. time - P = 3.65 atm., phi = 1.00. 136

Figure D.29 One step kinetics model - wall heat flux vs. time - P = 1.13 atm., phi = 0.80. 137

Figure D.30 One step kinetics model - wall heat flux vs. time - P = 1.21 atm., phi = 1.00. 138

Figure D.31 One step kinetics model - wall heat flux vs. time - P = 1.19 atm., phi = 1.20. 139

Figure D.32 One step kinetics model - wall heat flux vs. time - P = 2.59 atm., phi = 0.80. 140

Figure D.33 One step kinetics model - wall heat flux vs. time - P = 2.88 atm., phi = 1.00. 141

Figure D.34 One step kinetics model - wall heat flux vs. time - P = 2.78 atm., phi = 1.20. 142

Figure D.35 One step kinetics model - wall heat flux vs. time - P = 3.42 atm., phi = 0.80. 143

Figure D.36 One step kinetics model - wall heat flux vs. time - P = 3.70 atm., phi = 1.00. 144

LIST OF TABLES

Table	Caption	Page
Table 2.1	Calibration Constants (K/volt) for Several Thin Film Gauges	16
Table 3.1	Experimental Conditions - Pressure in Atmospheres During Quenching	28
Table 3.2	Experimental Results - Pressure Rise During Quenching	29
Table 3.3	Experimental Results - Heat Flux and Time for Quenching	30
Table 4.1	Numerical Results	58
Table C.1	Table of Reaction Rates for Detailed Kinetic Model of Methane-Air Combustion. Rates in cgs units, $k = A\,T^{m} \exp(-E_a/RT)$.	94
Table E.1	Coefficients for Fluid Property Variation.	146
Table E.2	Dependence of Flame Speed and Flame Temperature on Equivalence Ratio.	148

NOMENCLATURE

A ≡ frequency factor of a chemical reaction

a ≡ speed of sound

b ≡ temperature exponent of reaction rate

C ≡ mass concentration

C_p ≡ specific heat at constant pressure

D ≡ mass diffusivity

E ≡ activation energy

$F_S(\varphi)$ ≡ functional dependence of flame speed on φ

$F_T(\varphi)$ ≡ functional dependence of flame temperature on φ

f ≡ temperature dependence of chemical reaction rate

G ≡ functional dependence of flame speed on T and p

h ≡ specific enthalpy

$I_{()}$ ≡ Integral of ( ) over appropriate interval

j ≡ mass flux

k ≡ thermal conductivity

M ≡ Mach number

Pe ≡ Peclet number $\equiv \dfrac{\text{bulk heat transfer}}{\text{conductive heat transfer}} = \dfrac{\text{(length) (velocity)}}{\text{thermal diffusivity}}$

$Pr \equiv$ Prandtl number $\equiv \dfrac{\text{kinematic viscosity}}{\text{thermal diffusivity}} \equiv \dfrac{\mu}{\rho\alpha}$

$p \equiv$ pressure

$q \equiv$ heat flux

$R \equiv$ gas constant

$r \equiv$ nondimensional flame thickness

$S \equiv$ flame speed

$T \equiv$ temperature

$t \equiv$ time

$t_f \equiv$ time scale for quenching – determined by Isshiki and Nishiwaki, from wall temperature measurements

$t_q \equiv$ time scale for quenching – the time over which the wall heat flux increases from 50% to 100% of its maximum value

$u \equiv$ gas velocity

$x \equiv$ spatial distance from the wall

$Y \equiv$ specie mass fraction

$z \equiv$ nondimensional distance flame front

$\alpha \equiv$ thermal diffusivity

$\gamma \equiv$ ratio of specific heats $\equiv \dfrac{C_p}{C_v}$

$\Delta(\ )_f$ ≡ difference across the flame

$\Delta(\ )_q$ ≡ difference across quenching layer

δ ≡ quenching distance

δ_T ≡ quenching distance as defined in Equation 5.4

ϑ ≡ nondimensional temperature

κ ≡ bulk viscocity

λ ≡ variable of integration

μ ≡ dynamic viscocity

ρ ≡ density of the gas

τ ≡ sheer stress (Appendix B)

≡ nondimensional time (Appendix C)

φ ≡ equivalence ratio

ψ ≡ distance in mass coordinates

ω ≡ chemical reaction rate

subscripts

b ≡ referenced burnt gas conditions, just behind the flame

c ≡ characteristic of steady flame propagation

D ≡ in the diffusion dominated (preheat) region of the flame

f ≡ at the begining of the reaction zone of the flame

o ≡ referenced initial conditions

ig ≡ ignition conditions

max ≡ maximum value (as a function of time)

p ≡ characteristic of pressure rise in chamber

≡ at the front of the preheat region of the flame (in Appendix C only)

q ≡ during quenching

R ≡ in the reaction region of the flame

S ≡ at steady state

st ≡ at stoichiometric conditions

u ≡ referenced the unburnt gas conditions

w ≡ conditions at the wall

∞ ≡ at infinity (very far from the wall)

superscripts

o ≡ reference conditions

* ≡ pressure corrected for thermal boundary effects

– ≡ average for all conditions

~ ≡ nondimensional value

CHAPTER 1

INTRODUCTION

The unsteady heat transfer to the walls of a combustion chamber depends upon many factors, some of which are not well understood. In practical devices, such as internal combustion engines, several complicated and closely coupled processes occur simultaneously. For example, the flow is turbulent, boundary conditions are unsteady, the quality of the fuel can vary, and radiation can be significant. A detailed model of the combustion in a chamber based on a knowledge of the physical processes involved would require a fundamental understanding of some of the following complicated phenomena: the ignition process (since this affects the propagation of the flame); the dynamics of turbulent flames in unsteady, three dimensional flow fields; the formation of soot; and the dynamics of the flame-wall interaction. A complete discribtion of system in which these process occur would be a formidable task.

In an attempt to obtain a basic understanding of the above phenomena, many of them have been studied separately [Afgan & Beer, 1974 ; Mondt, 1982]. The purpose of this work was to obtain measurements and develop models to predict the unsteady heat transfer during flame-wall interactions (flame quenching). Specifically, the unsteady interaction of laminar, premixed, methane-air flames in stagnating flows were studied as they approached a cold wall.

Heat transfer measurements have been made in systems with steady combustion and are discussed in section 1.1.1; unsteady combustion experiments are presented in section 1.1.2. Connections between the heat transfer and the quenching distance are discussed in section 1.2, and models of flame quenching are reviewed in section 1.3.

1.1 HEAT TRANSFER STUDIES

1.1.1 STEADY STATE COMBUSTION WITH HEAT TRANSFER

Several experimental methods have been used to study the region between flames and quenching surfaces. Temperature distributions in the gas above a burner have been measured using thermocouples [Tewari & Weinberg, 1966], and in steady boundary layers using laser Raman spectroscopy [Bechtel & Blint, 1979 ; Clendening, Shackelford & Hilyard, 1981]. Laser diagnostics have also been used to determine species concentrations in two dimensional flows [Bechtel & Blint, 1979 ; Clendening, et al., 1981]. Experiments such as these provide detailed information concerning flame quenching, but are limited to regions away from the quenching surface. Wall heat transfer measurements are usually made by considering the temperature distribution in the solid, or if the quenching surface is being cooled from behind, from an energy balance of the wall.

Correlations for steady state and time averaged heat transfer data from premixed flames are available for torch flames impinging on cold walls [Schulte, 1972 ; Kilham & Purvis, 1978], and in combusting boundary layers [Rosner, 1975]. Heat transfer and quenching distance data for a steady flame stabilized on a porous plug burner were obtained by Yamazaki & Ikai (1971), who successfully modeled their results with a thermal theory of flame propagation. A comparison of the results of Yamazaki & Ikai with the results of this study (see Section 5.2.1) indicate that there are basic differences between steady and unsteady quenching.

1.1.2 UNSTEADY COMBUSTION WITH HEAT TRANSFER

Data and models for unsteady heat transfer are available for combustion from the side walls of detonation tubes [Paillard, et al., 1981], from the end

walls of shock tubes [Keiper & Spurk, 1981 ; Heperkan, 1980], in constant volume combustion chambers [Isshiki & Nishiwaki, 1974 ; Woodard, 1982], and in internal combustion engines [Eichelberg, 1939 ; Annand, 1963 ; Alkidas & Meyer, 1979]. The analysis of unsteady combustion processes is difficult. Combustion in apparently simple systems is often accompanied by complex flow patterns, and even in experiments which are nearly two dimensional, instabilities occur which may wrinkle the flame or generate turbulence [Markstein, 1964 ; Groff, 1981]. Thus, models of unsteady combustion are most successful in predicting heat transfer in one dimensional systems.

Paillard,et al., (1981) measured the heat transfer in a detonation tube as a detonation wave moved normal to the wall. Predictions of the heat transfer were good in the region near the detonation front, but there was disagreement in the region behind the front.

Measurements have been made of the heat transfer at the end wall of a shock tube containing a combustible mixture [Keiper & Spurk, 1981 ; Heperkan, 1980]. In these studies, a shock wave was passed through the mixture which was ignited after the reflection of the shock wave from the end wall. Quenching then occurred at the end wall. The fluid dynamics just before ignition is understood quite well [Liepmann & Roshko, 1957], and thus this experiment provides a clear method for directly examining the effects of kinetics and nonequilibrium on the heat transfer. Keiper & Spurk (1981) have examined the effects of nonequilibrium on combustion. The experimental results were compared with a model which divided the flow into a frozen and an equilibrium regime. Unexplained discrepancies existed between the experiment and the model for small times after ignition, but the agreement for equilibrium flow was good. Heperkan (1980) treated the kinetics in equilibrium flow in an approximate way and was able to predict the wall heat transfer.

Isshiki & Nishiwaki (1974) measured and correlated the unsteady heat transfer in a constant volume combustion chamber. In their study, heat transfer measurements were made for one dimensional hydrogen-oxygen-nitrogen flames for a variety of pressures (and the data were successfully correlated in an empirical manner). The measurements are essentially the same as those made in this study. There appears to be good agreement between the work of Isshiki & Nishiwaki and the present results and a comparison of the results is given in Chapter 5.

Measurements of the heat transfer have been made in two dimensional systems [Woodard, 1982], and were related to the flame position (from photographs) and the pressure in the system. However, due to the complex nature of two dimensional combusting flows, no modeling of this experimental configuration was made.

Measurements made in internal combustion engines [Eichelberg, 1939 ; Alkidas & Meyer, 1979 ; Mondt, 1982] provide an indication of the heat transfer rates, but difficulties in quantifying the conditions inside of the chamber make prediction of the heat transfer very difficult. Correlations of heat transfer in internal engines have existed for some years [Krieger & Borman, 1966 ; Woschni, 1967], but these correlations are on an overall system basis. Current modeling includes some fundamental processes which occur in engines [Borgnakke et al., 1980].

1.2 QUENCHING DISTANCE STUDIES

Perhaps the easiest quenching measurement to make in steady flows is the determination of the closest approach of the flame to the wall (the "quenching distance"). This may be done by a variety of techniques as discussed in Chapter 5. The relevance of conventional quenching measurements to quenching distances under unsteady conditions was noted by Daniel (1956). Recently, Ballal

& Lefebvre (1977) have shown that the ratio of the quenching distance to the flame thickness is approximately constant for both laminar and turbulent flows, and for a variety of gaseous mixtures, thus extending the usefulness of the concept of a quenching distance.

It is shown in Chapter 5 that the maximum heat flux during quenching is inversely proportional to the quenching distance. Based on this relationship, correlations of the quenching distance [Ishikawa, 1978] for methane-air flames were compared to measurements of the maximum wall heat transfer rate.

1.3 FLAME QUENCHING MODELS

The earliest quenching models were developed for steady flames propagating normal to a wall. In these theories, known as thermal theories, the heat loss to the wall is considered to be the important process governing the quenching, and the reaction rate is considered to be only a function of temperature. Using this approximate theory, von Karman and Millan (1952) were able to obtain the temperature profile for a flame propagating normal to one wall. Spalding (1957) considered a flame propagating down a narrow tube, and was able to account for the existence of flammability limits at finite flame speeds.

Assuming quenching to be one dimensional and the kinetics as unimolecular, Kurkov (1967) was able to predict the evolution of temperature and fuel profiles in the gas. The heat transfer and fuel mass fraction remaining at the wall were studied over a limited range of Lewis number and activation energy of the reaction.

The concept of an unburnt fuel layer at the wall is supported by models which utilize unimolecular or global kinetics, but not by kinetic schemes composed of many elementary reactions [Westbrook, et al., 1981]. Hocks, et al. (1981) has shown that complete combustion is predicted if a two step chemical

reaction is assumed.

Two dimensional steady models have been developed for steady and unsteady flows. Steady, finite difference models developed by Carrier, Fendell, & Feldman (1980) and by Aly & Hermance (1981), have been used to study reacting flows between parallel plates. Activation energy asymptotics [Buckmaster, 1979], limited to flow speeds much greater than the laminar flame speed, have also been used to solve two dimensional problems.

Recent efforts have been made to model unsteady two dimensional and axisymmetric flame propagation [Cloutman, et al., 1982]. These models are presently limited to simplified kinetic schemes due to computational restrictions.

1.4 THE PRESENT WORK

The present work is an experimental and numerical study of the heat transfer during one dimensional premixed laminar flame quenching. A description of the constant volume combustion chamber and the associated instrumentation is given in Chapter 2. The experimental results and a correlation of the data are presented in Chapter 3. The numerical models used to predict the heat transfer are presented in Chapter 4, along with the numerical results. In Chapter 5, the experimental and numerical results are compared. Conclusions and recommendations for further study are presented in Chapter 6.

CHAPTER 2

EXPERIMENTAL SYSTEM AND PROCEDURE

2.1 APPARATUS

2.1.1 CHAMBER

The experiments were performed in a constant volume combustion chamber. The chamber was designed specifically for these experiments, but with the flexibility for use as a general purpose, low pressure container with good accessibility to its interior. The final design (Figure 2.1) proved to be quite flexible, providing excellent optical access, as well as space for instrumentation.

The combustion chamber was constructed from 5/8" thick, type 303 stainless steel seamless tubing (Figure 2.2). The interior of the container has the shape of two 3.50 inch diameter cylinders 7 inches long, intersecting at right angles. Along the third axis, instrumentation ports were provided on the top and bottom of the container. Two additional ports on the off optical axis provide for the introduction of fresh reactants, and the exhausting of burnt gases.

2.1.2 GAS METERING AND IGNITION

The oxidizer (air) and fuel (99.98% pure methane) are obtained from high pressure bottles, and individually flow through rotameters before being mixed at approximately 8 psi.

Ignition of the unburnt gases was accomplished by means of an 8 kilovolt, 200 millijoule discharge across a .035 inch gap between 0.020 inch tungsten electrodes. The electrodes are mounted in the chamber through one of the 4 inch ports that are off of the optical axis. A plexiglass insert with compression

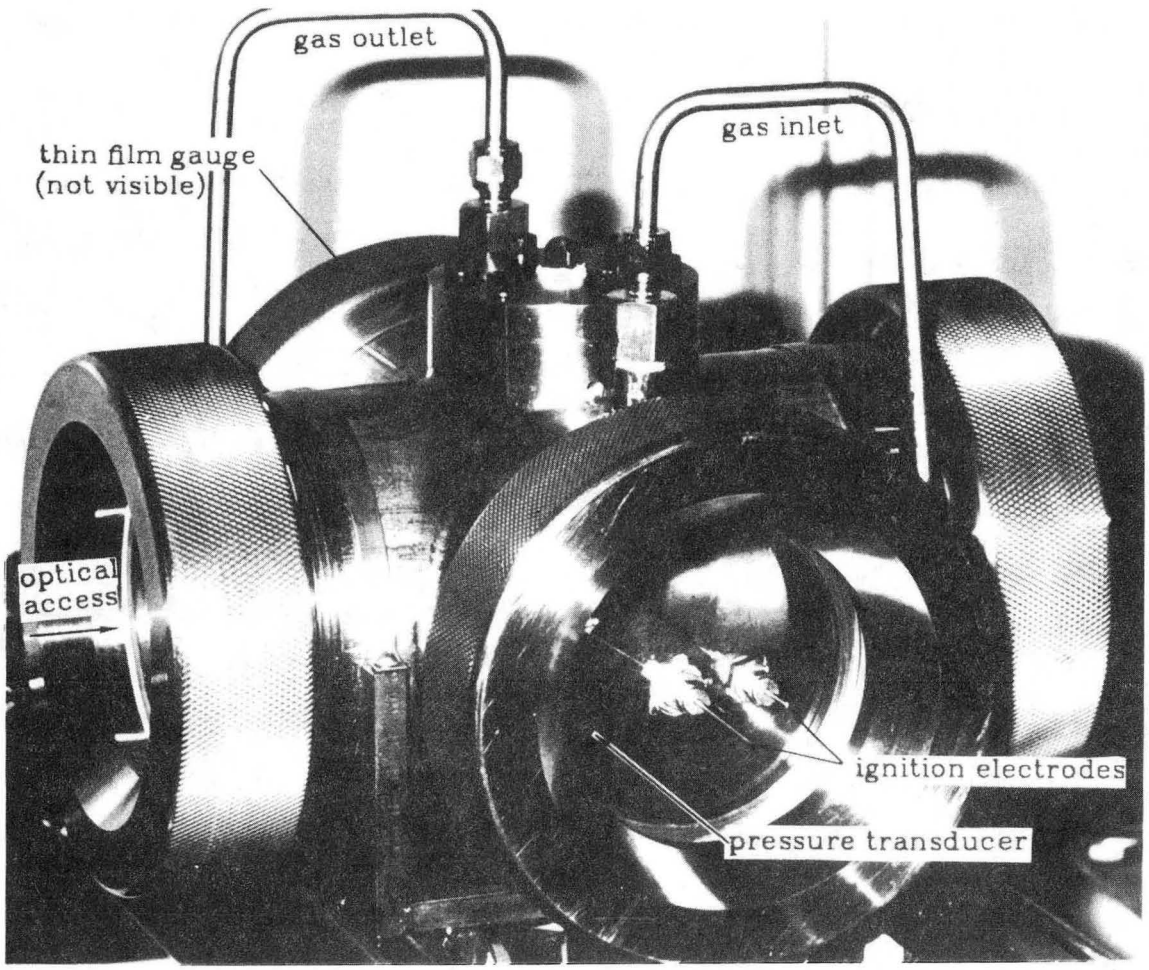

XBB 854-2871

Figure 2.1 Photograph of fully instrumented constant volume combustion chamber.

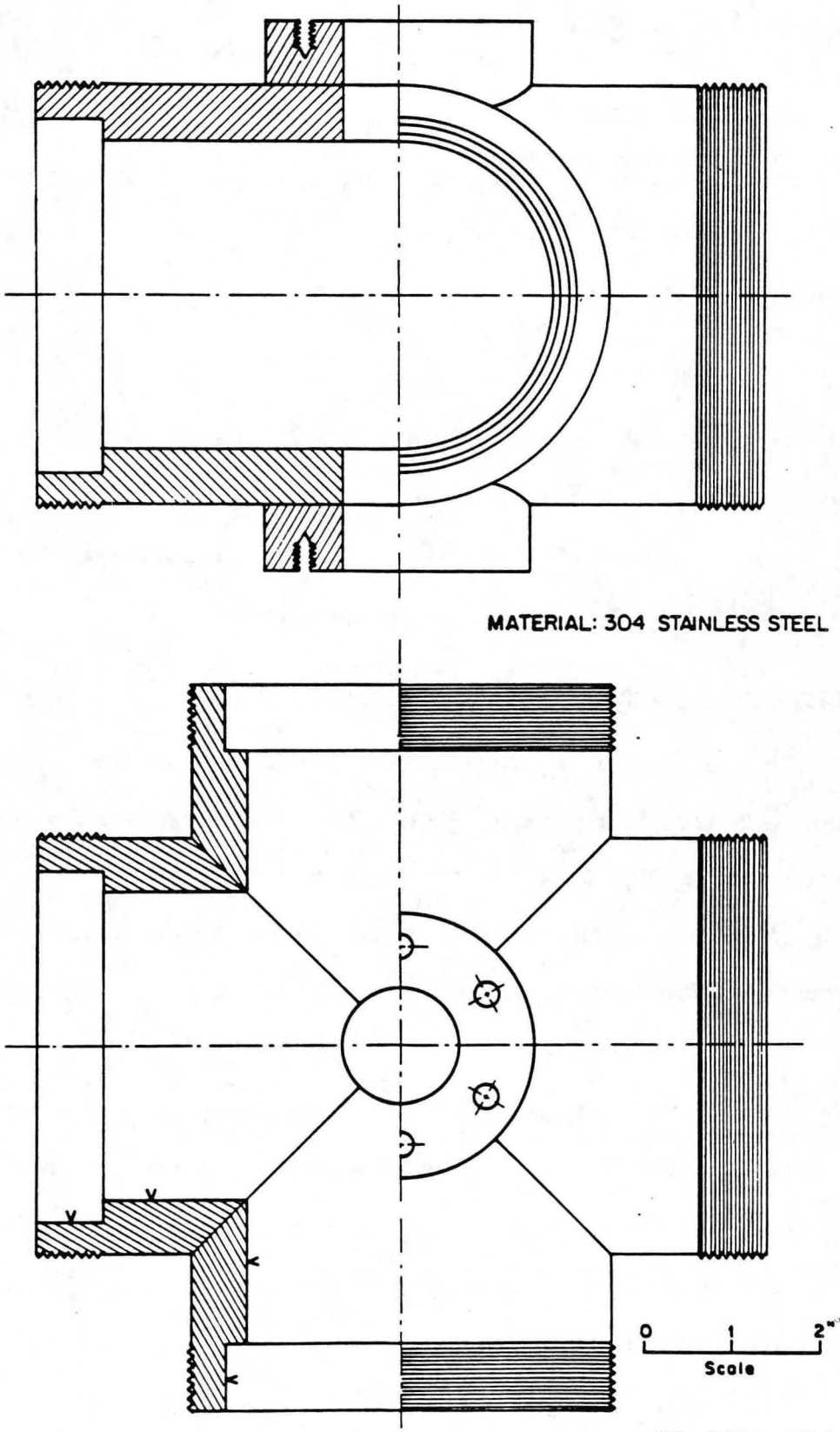

-- XBL 8411-4672 --

Figure 2.2 Machine drawing of constant volume combustion chamber.

fittings provides a convenient way of adjusting the electrode gap and position in the chamber (see Figure 2.3).

2.1.3 INSTRUMENTATION

Three measurements are made during an experimental run: the chamber pressure, the wall heat flux at one point, and schlieren or shadowgraph photography. A schematic of the experimental setup is shown is Figure 2.4.

2.1.3.1 PRESSURE

The pressure in the chamber was measured at the bottom instrumentation port. The output of the pressure transducer, which was of the piezioelectric type (AVL model 12QP300cvk), was passed through a charge amplifier (Kistler model 566) and was recorded on an oscilloscope.

2.1.3.2 HEAT FLUX

The wall heat flux was determined from measurements made with a thin film resistance thermometer (Figure 2.5). The gauge was mounted flush in a metal fixture (Figure 2.6), which was in turn mounted in the chamber (Figure 2.3). A detailed discussion of the determination of the heat flux from the wall temperature measurements is given in Appendix A.

Three types of sensors were used : Pt, Pt- SiO_2, and Ni. All three types consisted of a 2000 - 3000 Angstrom thick layer of the metal on a ceramic substratum (Macor, Corning Glass Works). The nickel coatings were vacuum deposited, and the platinum coatings were achieved by baking of a platinum laden paint (Hanovia Liquid Platinum, Englehard Corporation). For more detail on the gauge coatings, see section 3.5.

Leads from the thin film pass through the ceramic base to a bridge amplifier [Heperkan, 1980], and the output was recorded on an oscilloscope.

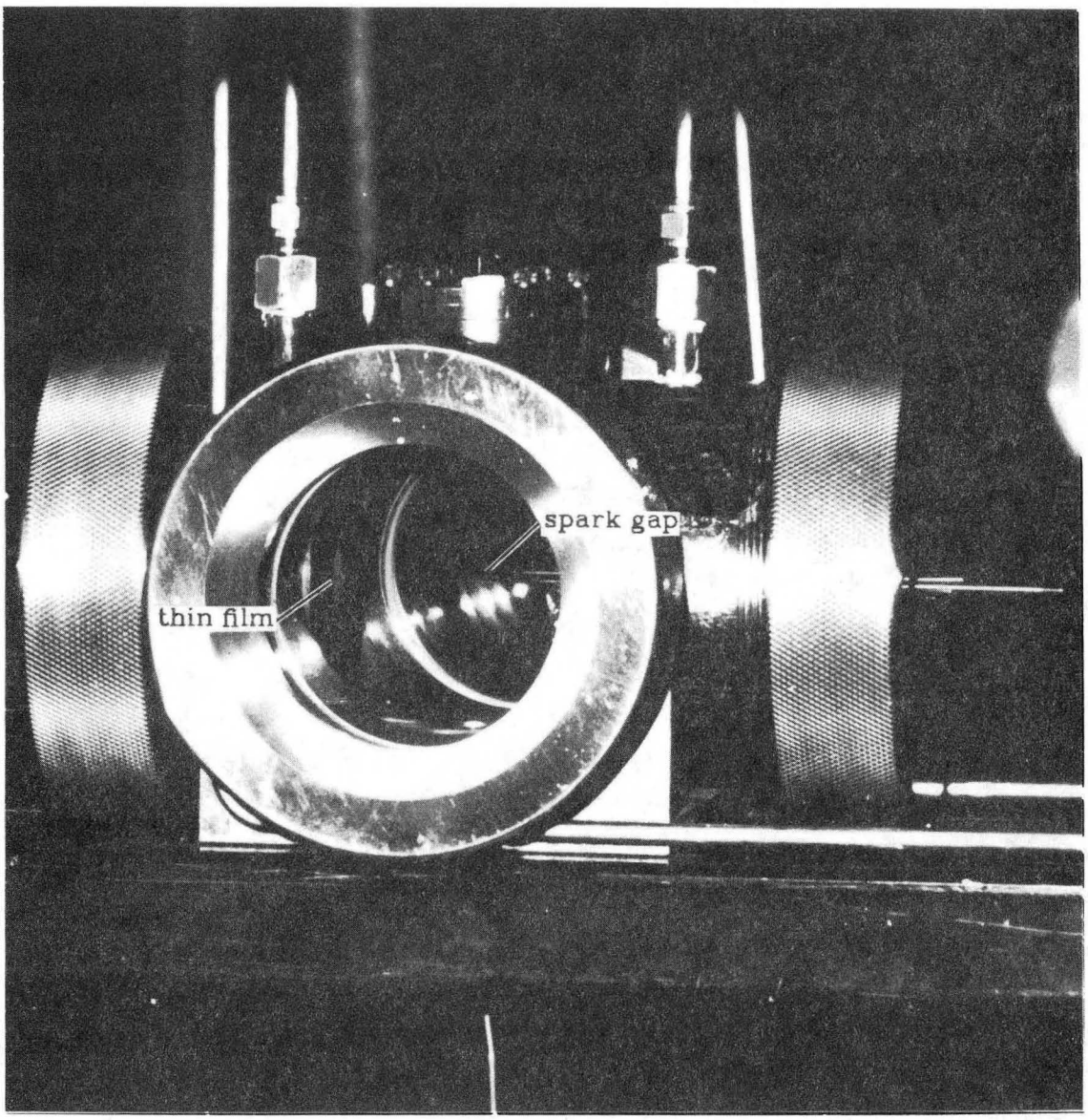

XBB 854-2870

Figure 2.3 Detail of combustion chamber showing thin film gauge and spark gap.

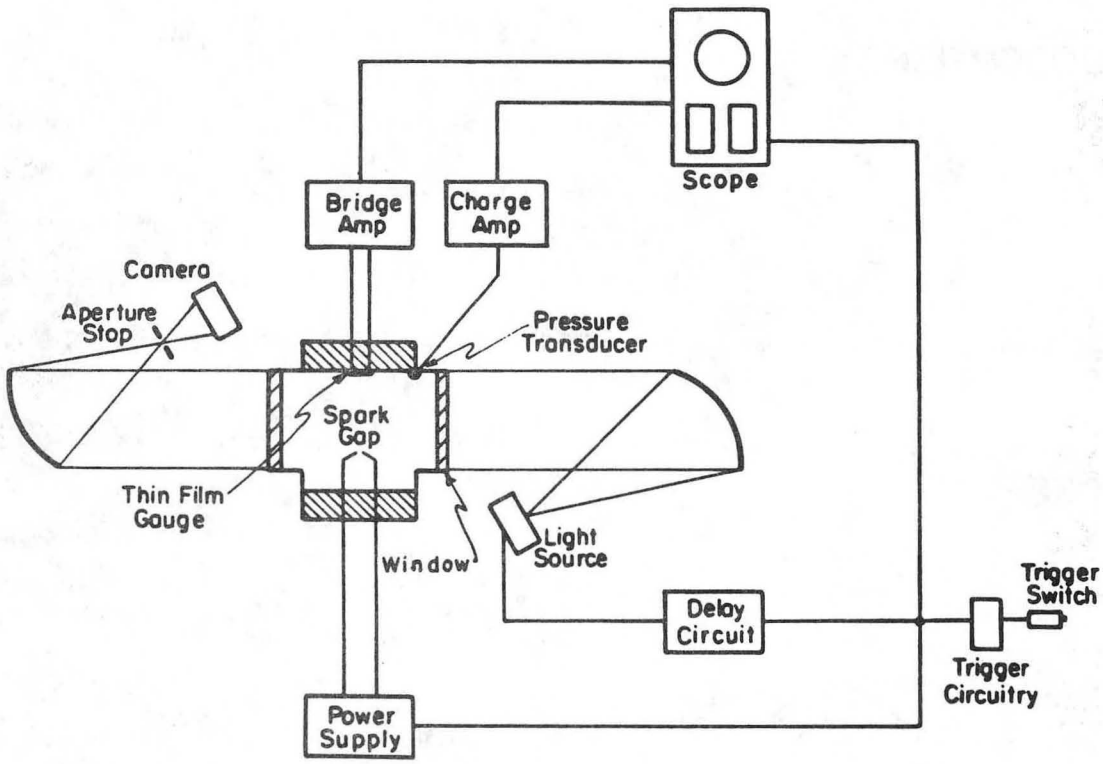

-- XBL 833-5420 --

Figure 2.4 Schematic of the experiment.

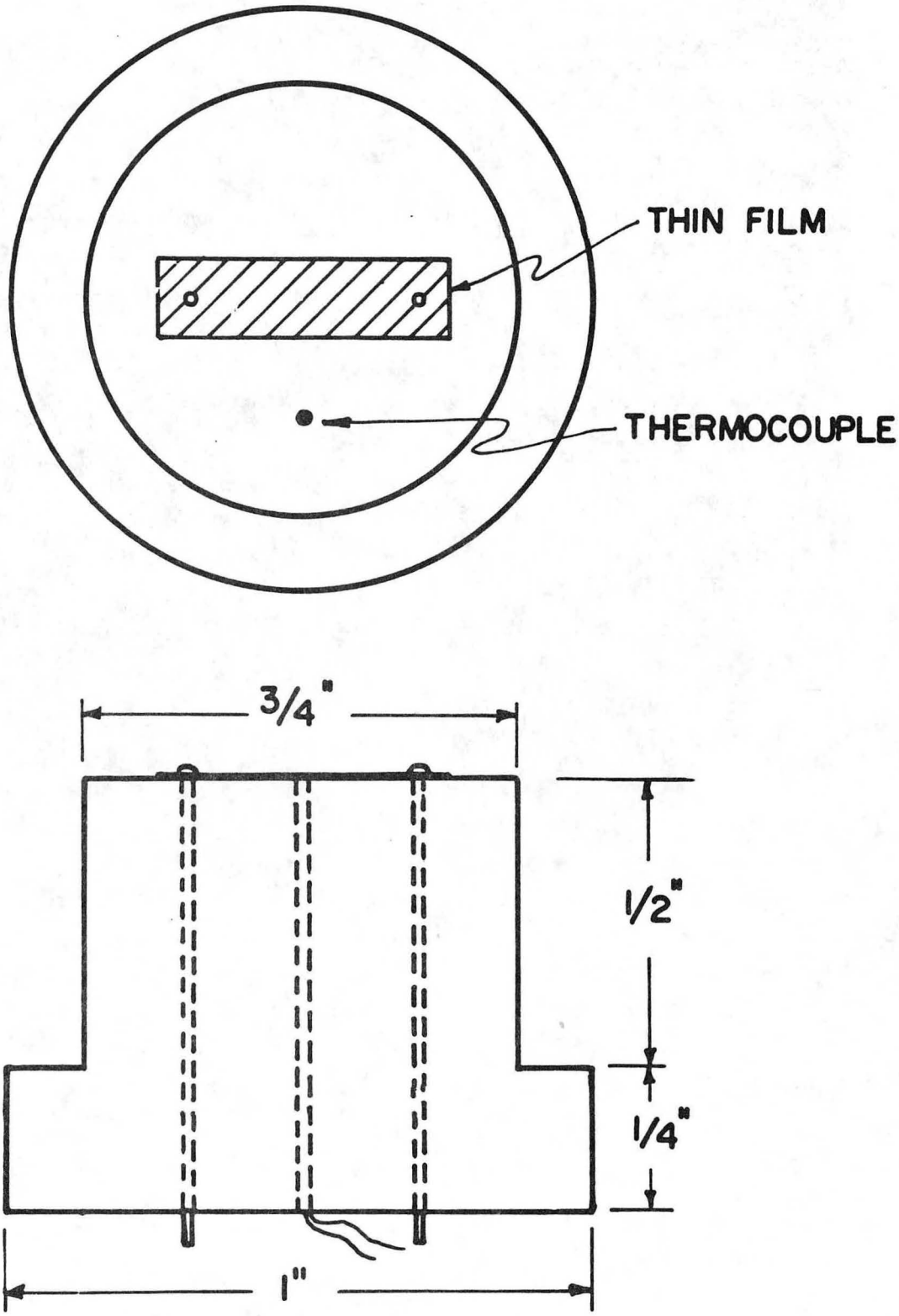

Figure 2.5 Thin film gauge.

-- XBL 8411-4671 --

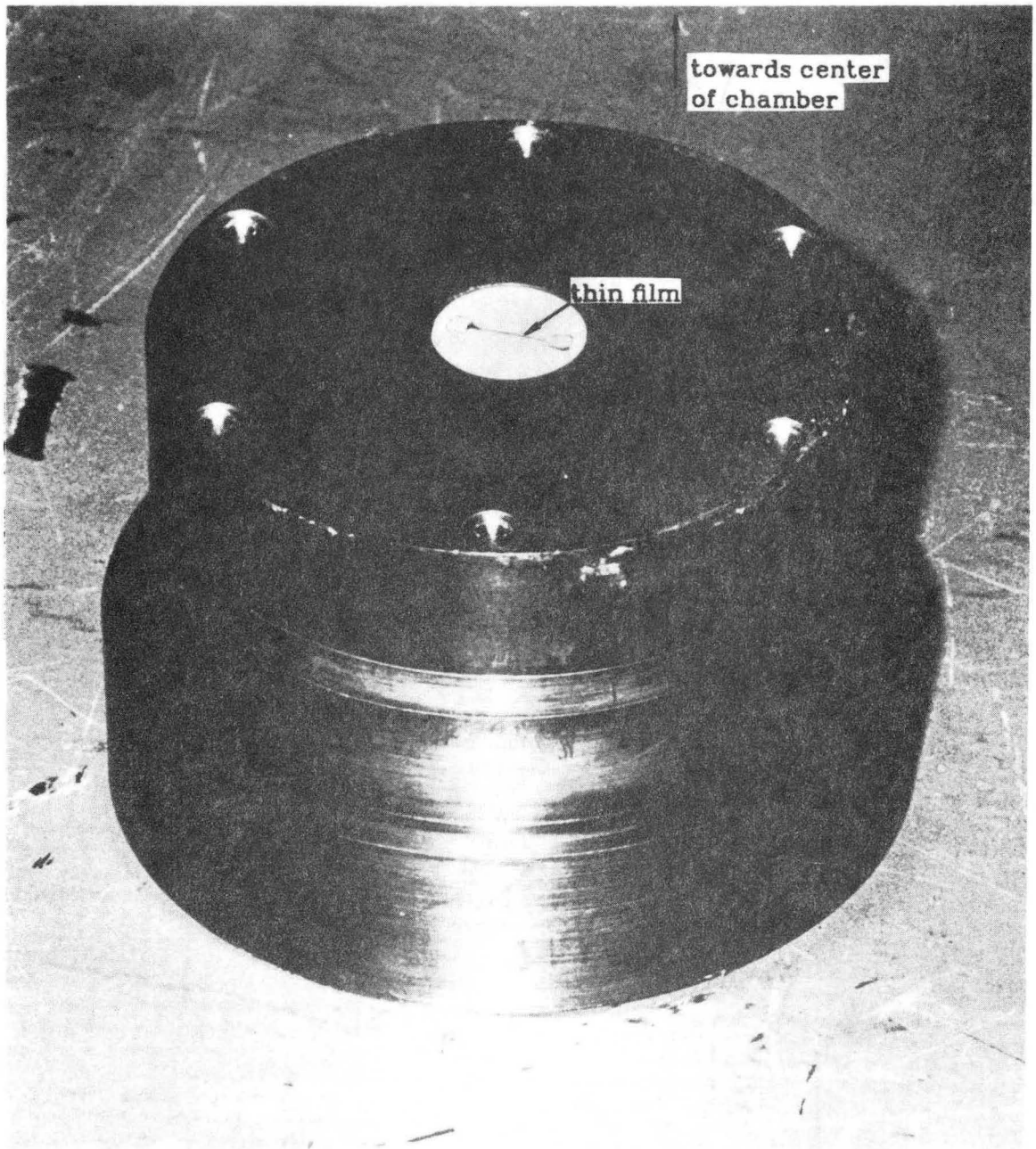

XBB 854-2872

Figure 2.6 Detail of thin film gauge holder. The Assembly is inserted into the combustion chamber with the thin film gauge directed towards the center of the chamber.

2.1.3.3 OPTICS

Optical measurements were obtained from either schlieren or shadowgraph photography, made by use of the standard Z configuration schlieren (Figure 2.4). The light source was a delayed microsecond spark light for stills, and a continuous source for use with a 5000 frame per second movie camera (Hycam model 41-0004). An aperture and razor edge were both tried for the schlieren pictures. Due to the three dimensional structure of the flame, the aperture worked best for an overall view of the flame.

2.2 CALIBRATIONS

2.2.1 THIN FILM RESISTANCE THERMOMETER

To determine the wall heat flux, the wall temperature as a function of time was measured with a thin film temperature sensor (Appendix A). The thermal properties of the substratum are known from the manufacturer (Corning Glass Works). Thus the primary step in the calibration procedure was the determination of the output of the thin film and associated electronics as a function of the temperature of the thin film.

The temperature sensor - amplifier combination was calibrated quasi-steadily in an oven. A thermocouple embedded in the ceramic (Figure 2.5) gave an absolute measure of the temperature, which was then compared to the bridge amplifier output. The calibration determined in this manner was linear to within three percent over the temperature range of 25 to 75 °C. A calibration constant, in degrees Kelvin per volt output, was thus obtained for each gauge. Some typical calibration constants are listed in Table 2.1, showing the differences between gauge materials, as well as differences among the platinum gauges. The calibration constant changes slightly with usage, and so the gauges were periodically calibrated between tests.

In general, the gauges were dependable, and gauges which gave repeatable calibration were used twenty to fifty times. When gauges did fail after being used in many tests, the connection between the film and the connecting wires appeared to be the point at which failure occurred.

Table 2.1
Calibration Constants (K/volt)
of Several Thin Film Gauges

Gauge type	Gauge number	Initial Calibration	Recalibrations (every 30 – 50 runs)	
Pt	1	147	152	-
	2	149	147	148
	3	126	126	-
	4	145	150	-
	5	143	147	151
Ni	6	63	-	-
	7	62	-	-
	8	64	-	-

2.2.2 PRESSURE GAUGE

The pressure transducer and charge amplifier were calibrated periodically both statically, on a dead weight tester, and dynamically, in a shock tube. The accuracy for both methods was about the same, approximately 2%.

2.2.3 FLOW SYSTEM

The gas flow rates while the chamber was being charged was monitored by rotameters (Matheson), and were adjusted by needle valves. The rotameters were calibrated by the soap bubble method. This method of calibration gave an uncertainty in the equivalence ratio of approximately 2%.

2.3 PROCEDURE

Measurements were made in the experimental apparatus described in section 2.1 to determine the unsteady heat transfer from a flame, propagating in stagnation flow, to a cold wall. Wall heat flux data were obtained for pressures varying from one to four atmospheres (section 2.3.2), and for equivalence ratios varying from 0.70 to 1.20†. Before discussing the sequence of events in an actual experiment, it is instructive to examine what would happen in an idealized spherical combustion chamber with isothermal walls.

2.3.1 QUENCHING IN A CONSTANT VOLUME COMBUSTION CHAMBER

Figures 2.7a-c depict an idealized experiment in which a combustible gaseous mixture is contained in a rigid, spherical chamber with isothermal walls. Prior to ignition, the gas temperature is the same as the wall temperature, T_u, and there is no gas motion (Figure 2.7a). The gas is ignited at the center of the hypothetical sphere, and the flame propagates spherically outward.

At a later time, the gas is in the state shown in Figure 2.7b. The increase in the pressure in the container results in the compression heating of the gas. The container walls maintain an essentially constant temperature, causing a thermal boundary layer to develop at the walls. The conditions in the gas between the flame and the thermal boundary layer are uniform, and thus the gas in this region is adiabatically compressed, with its temperature given by $T_u = T_o \left[\frac{P_q}{P_o}\right]^{\frac{\gamma-1}{\gamma}}$, where T_o and P_o are the initial gas temperature and pressure, respecitvely. The temperature of the gas decreases to the value of the isothermal wall ($T_w = T_o$) across a thermal boundary layer. The flame produces an increase in the enthalpy, which results in a temperature difference (ΔT_f) across

† The equivalence ratio is defined as the fuel to air ratio divided by the stoichiometric fuel to air ratio

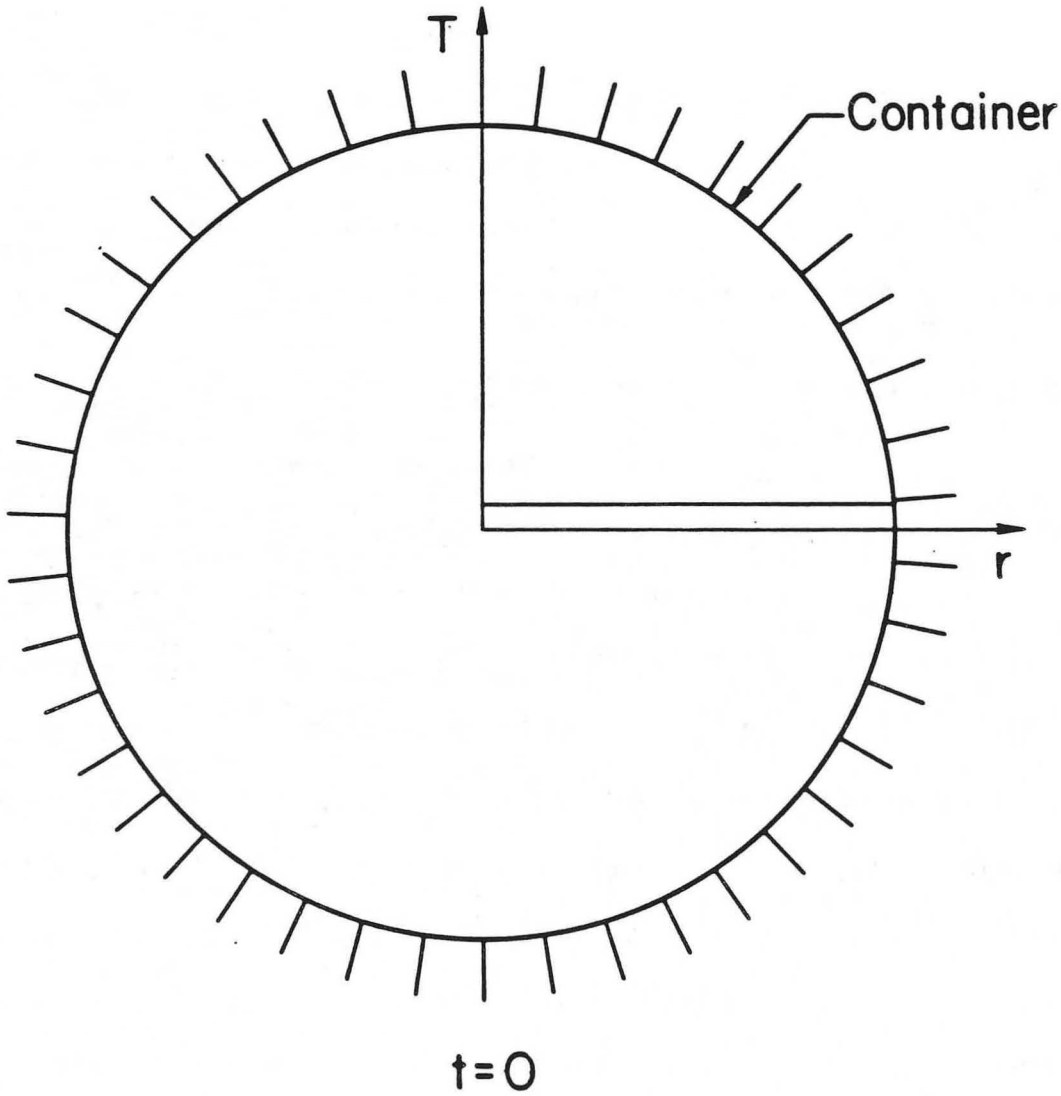

-- XBL 833-1362 --

Figure 2.7a

Sequence of events in an experimental run. The mixture is quiescent and is about to be ignited in the center of the chamber.

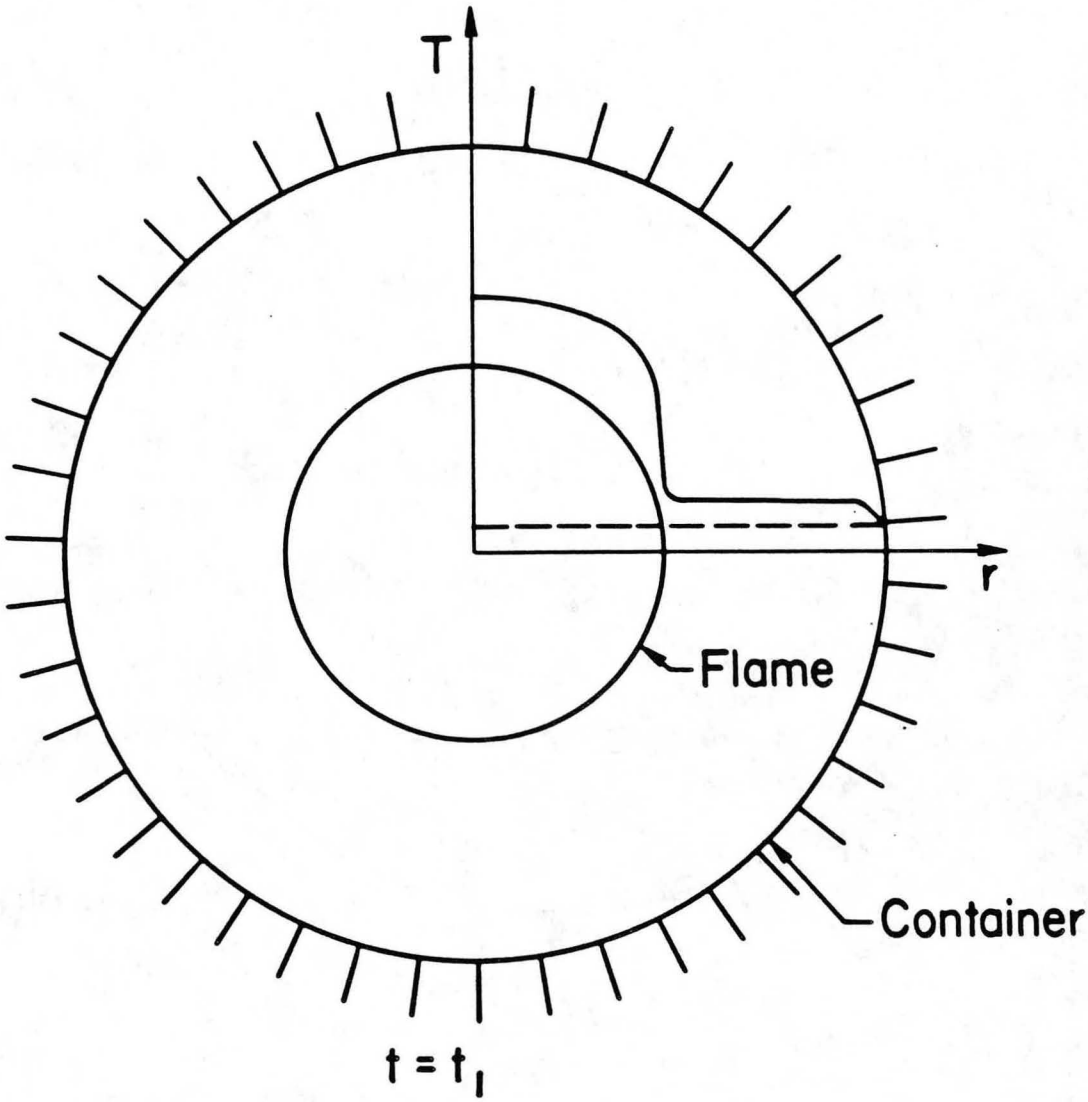

-- XBL 833-1361 --

Figure 2.7b

Sequence of events in an experimental run. The flame has propagated symetrically outwards. The temperature profile is shown.

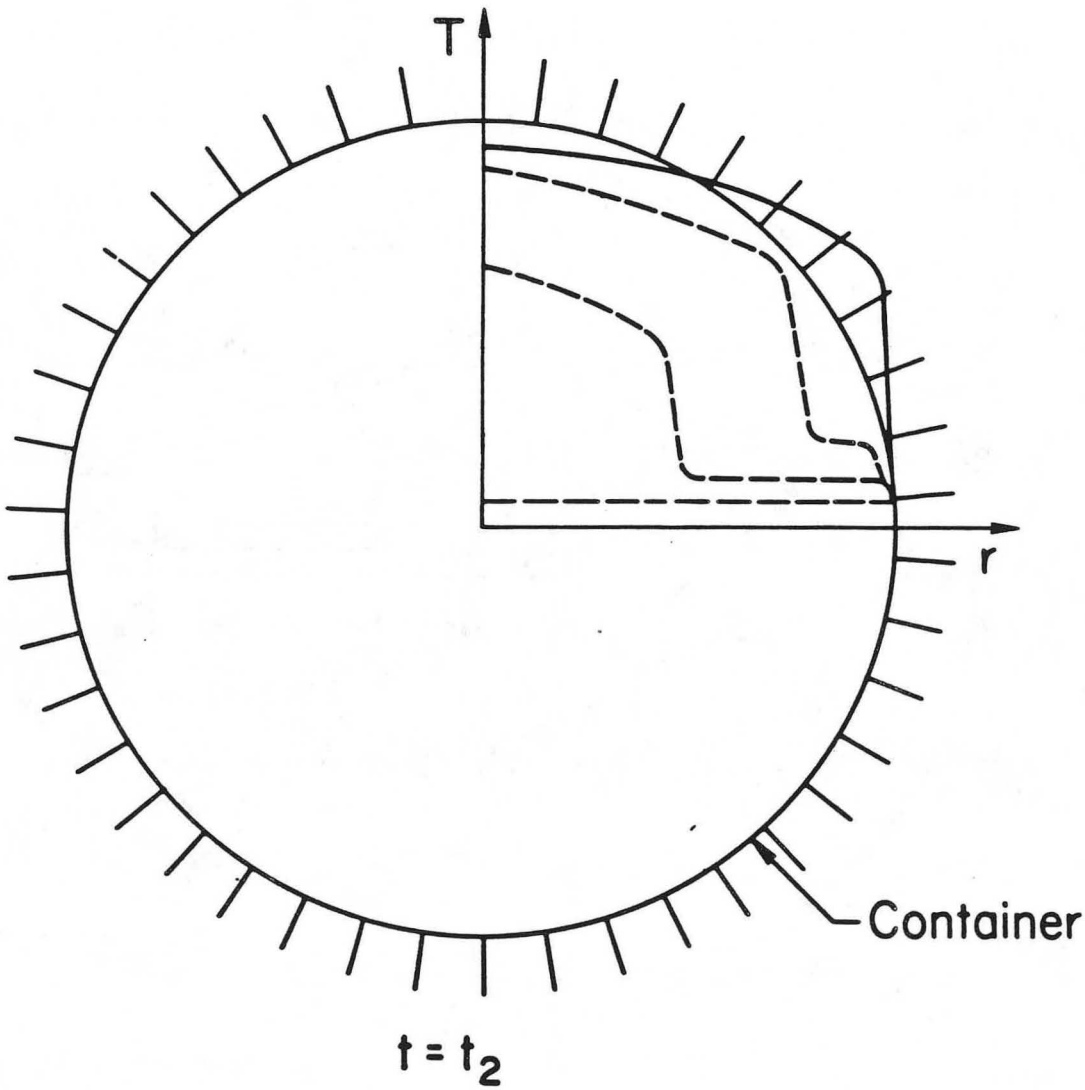

-- XBL 833-1363 --

Figure 2.7c

Sequence of events in an experimental run. The flame has just consummed the last of the reactants. Temperature profiles from previous times are shown.

the flame, independent of the conditions in the unburnt gases. Gases which are compressed after combustion, such as those at the center of the sphere, are at a higher temperature than those that have just undergone combustion. As a result, a temperature gradient is generated with the highest temperature at the center of the sphere.

The flame continues to burn until the walls of the sphere are reached (Figure 2.7c). At this moment, the wall heat transfer reaches a maximum. The time during which the flame interacts with the wall is of primary interest.

2.3.2 CONTROL OF THE PRESSURE AT QUENCH

In the idealized experiment described above, the flame quenches everywhere at once, at a pressure which is determined mainly by the initial thermodynamic conditions. Thus, to cause the flame to quench at different pressures, the initial pressure and/or temperature must be varied. However, if one is willing to sacrifice the symmetry of the idealized experiment, an easier method may be used to obtain pressures between the initial and maximum values. For a given combustible mixture, the pressure as a function of time in the chamber is not very dependent on the location of the ignition source. Thus the pressure in the chamber during quenching (in the vicinity of the heat transfer gauge) is related to the time needed for the flame to reach the gauge. When the spark gap was close to the gauge, quenching occurred at a pressure only slightly above the initial pressure; larger relative distances resulted in larger pressures at quenching. Thus it was possible to predetermine the pressure at quench by adjusting the position of the spark gap.

The initial pressure and temperature for all experimental runs were one atmosphere and room temperature. The pressure during quenching, and the time required to obtain that value depend upon the fuel used, the mixture, and the location of the ignition source. A sequence of photographs from an

experiment conducted with stoichiometric methane - air is shown in Figures 2.8a-f. These schlieren pictures were taken using the experimental setup shown in Figure 2.3. Initially, the flame was spherical (Figures 2.8a-b). As the flame approached the walls, it flattened out (Figures 2.8c-d), and was nearly planar when quenching occurred near the thin film gauge (Figure 2.8e). In fact, as long as the ignition point was located more than one quarter of the chamber width away from the thin film gauge, the quenching was nearly planar. This condition was met in all of the experiments.

Data for a similar experiment is shown in Figure 2.9. Due to differences in the experimental set up, the time at which quenching occurs differs from that in previous example by 10 milliseconds, but the essential features of the pressure and wall temperature data are the same. A maximum pressure of 6.4 atmospheres was reached 58 milliseconds after ignition. The flame was in close contact with the heat transfer gauge at 34.7 milliseconds, which corresponded to a pressure of 3.80 atmospheres. The time during which the wall temperature was increasing at its greatest rate corresponded to the time when the flame is closest to the wall (Figure 2.8e).

If the flame propagated too far before reaching the thin film gauge, the flame became become unstable, breaking into cellular structures [Groff, 1981]. The present study is of laminar flame quenching, and so this condition was avoided. The initial pressure in the system was one atmosphere, which limited the maximum pressure to about four atmospheres.

2.3.3 RATIONALE FOR DATA ACQUISITION

The purpose of this work was to study the interaction of laminar flames with cold walls. From this point of view, the heat transfer in a constant volume combustion chamber may be divided into the following time intervals:

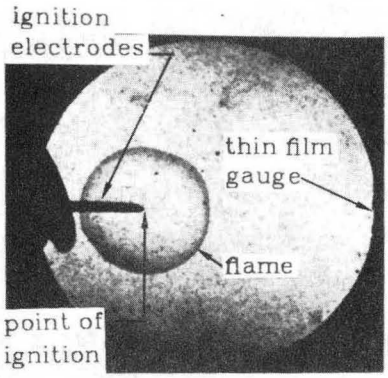

10 milliseconds
Figure 2.8a

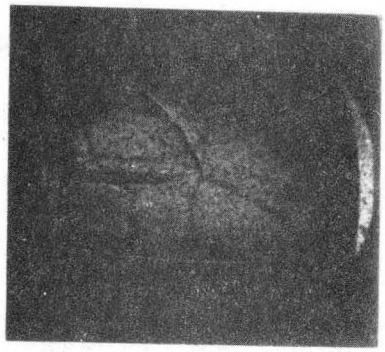

Figure 2.8d

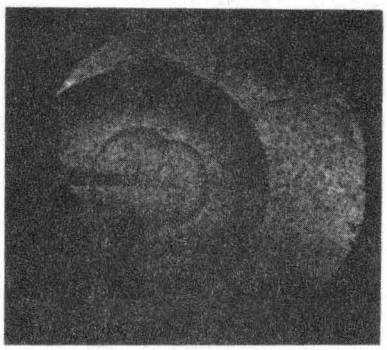

20 milliseconds
Figure 2.8b

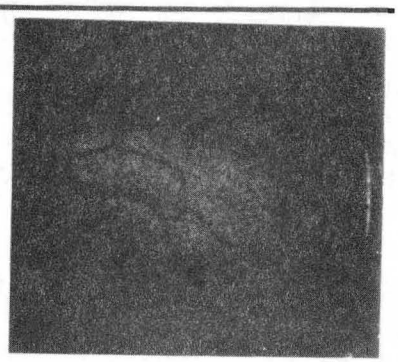

Figure 2.8e

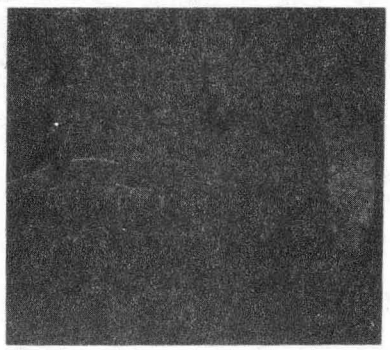

30 milliseconds
Figure 2.8c

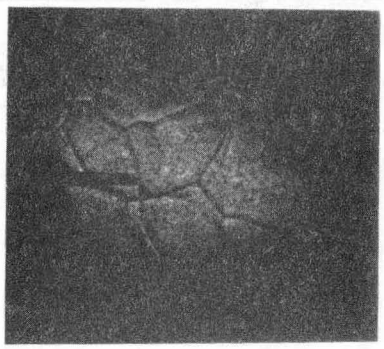

Figure 2.8f

XBB 854-2873

Figure 2.8a,f

Photographic sequence of flame propagation. The mixture is methane-air at an equivalence ratio of one. Initial pressure is one atmosphere.

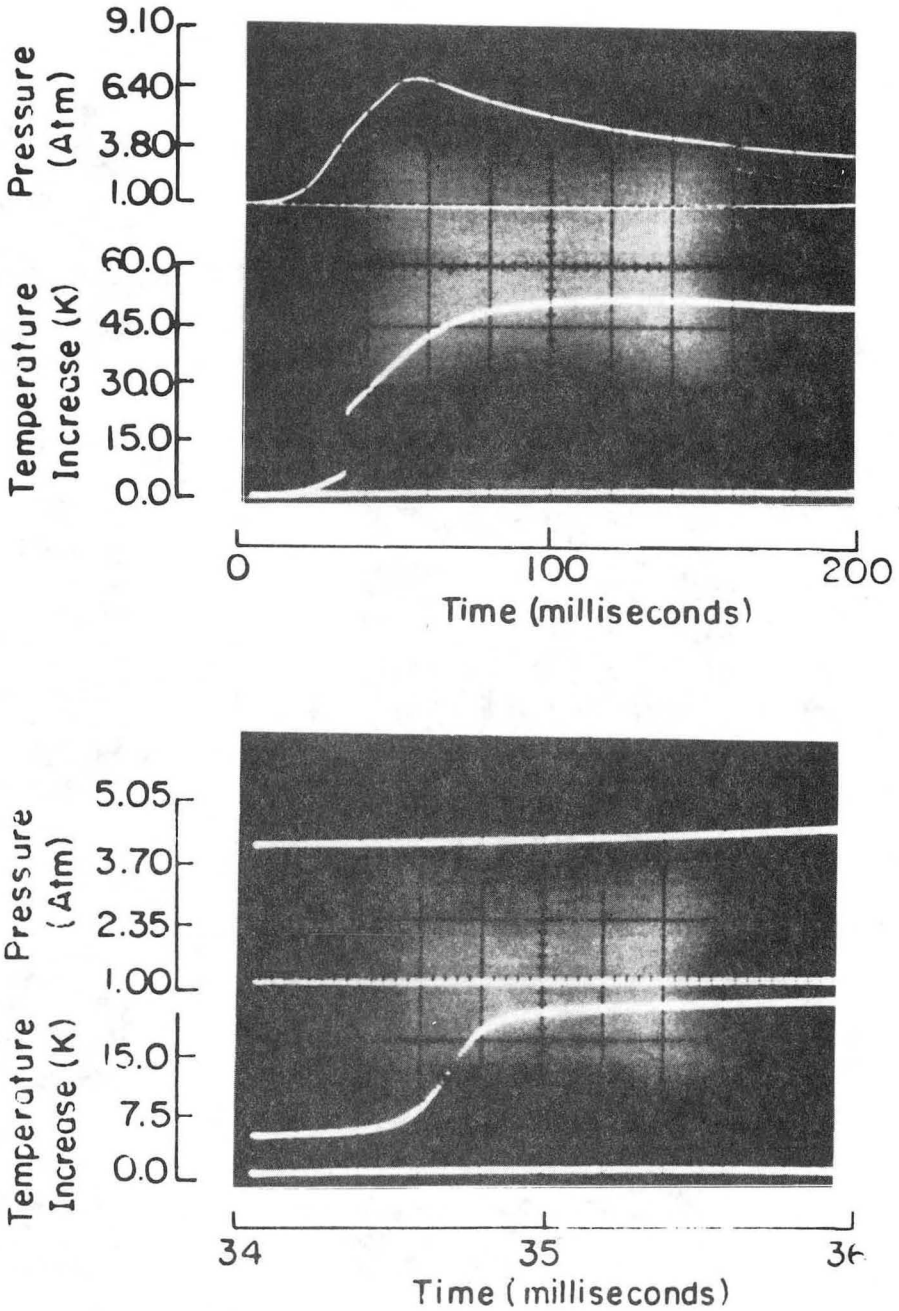

XBB 854-392A

Figure 2.9

Wall temperature and pressure in chamber. The lower figure is detail of the upper figure.

1) Ignition to flame arrival (10 to 40 milliseconds), and

2) Flame - wall interaction (0.5 - 2.5 milliseconds).

The mechanism of the heat transfer to the wall is reasonably well understood during the first interval [Grief et.al., 1979 ; Keck, 1980]. The flame motion during an experiment was very slow ($M<<1$), and so the pressure in the chamber was spatially uniform [Sivashinsky, 1979]. The heat transfer was the same as that for a gas which was being compressed by a piston [Nikanjam & Grief, 1978 ; Keck, 1980], and thus can be computed from the knowledge of the variation of the pressure with time.

The interval of time that the flame was near the wall is short compared to the total time of the experiment (one to two percent), and an understanding of the heat and mass transfer during this time interval is exceedingly difficult due to chemical reactions occurring near the wall. Measurements of the heat flux provide a unique way to study the flame structure, dominant heat transfer modes, and fluid dynamics during quenching.

By concentrating on the shorter interval, however, an error was made by not taking data prior to this time. This error is approximately equal to the value of the heat flux due to the compression of the gas just before quenching. This was found to be 5 per cent of the value of the maximum heat flux.

2.3.4 EXPERIMENTAL PROCEDURE

The procedure consisted of the following steps:

1) The chamber was purged with a fresh mixture. The flow rates were controlled by rotameters to give the desired fuel to air ratio. Tests showed†

† The larger the purge volume, the closer the mixture in the chamber will be to the fresh, inflowing mixture. The results obtained from using progressively larger purging volumes was compared to the results from very large purge volumes (over 100 times the chamber volume). It was determined that there was no change in the experimental measurements when the purge volume was over 15 times the chamber volume. This value was used in all of the experiments.

that it was required to purge the chamber with 15 times the chamber volume.

2) The flow was shut off, the chamber sealed, and one minute was allowed for gas motion to stop.

3) The ignition voltage was set, and the instrumentation was readied.

4) The appropriate delay time was set for the oscilloscope. If still photographs were to be taken, then the delay for the light source was set.

5) If movies were to be taken, then the camera was started by hand one second before step 6 to insure that the camera was working at full speed.

6) The experiment was started by depressing a trigger switch. This discharges the spark used for ignition. The trigger also activates all delay circuits.

7) At the conclusion of the experiment, the data was recorded from the oscilloscope, and the film was retrieved from the camera.

8) The voltage setting on all high voltage components was lowered.

9) The purge cycle was repeated.

2.3.5 DATA REDUCTION

As discussed in Chapter 2.1.3, the output of the thin film gauge and the pressure transducer were recorded on an oscilloscope. The oscilloscope traces were then digitized using a model 4662 Tektronics plotter driven by a PDP 11/34 computer.

After being digitized, the appropriate calibration constants were applied, and linear interpolation was used between data points which were evenly spaced in time. From the wall temperature as a function of time, it is possible to derive the wall heat flux as a function of time, as described in Appendix A.

The data from 3 - 10 runs were averaged to give the results presented in

Chapter 3. In all cases the run to run variation in the data produced an error in the heat flux was only 5% of the value of the maximum heat flux. As noted in section 2.3.3, there is also an error of 5% of the maximum heat flux associated with the limited amount of time over which data is taken. Thus the the error associated with the measurement of the heat flux is approximately 8%.

CHAPTER 3

EXPERIMENTAL RESULTS

The experimental results from this study are the unsteady wall heat fluxes during the quenching of a planar, laminar methane-air flame. Using the apparatus described in Chapter 2, data were obtained over the range of conditions shown in Table 3.1. The runs are identified by the equivalence ratio and by a nominal pressure, which was the approximate pressure during quench.

Unlike experiments involving more complex geometries [Woodard, 1982], all of the results in the constant volume cell show similar trends. The wall heat flux increases slowly until the flame reaches the vicinity of the wall where the heat flux gauge was located. The wall heat flux then increases rapidly to a maximum value, after which the flux falls as the inverse root of the time. In order to characterize the shape of the curves, the interval of time required for the heat flux to increase from 50% of the maximum heat flux to the maximum heat flux (t_q) will be used. These time intervals and the values of the maximum heat flux for all of the conditions listed in Table 3.1 are presented in Table 3.2. The wall heat fluxes as a function of time may be found in Appendix D, Figures D.1 to D.14.

TABLE 3.1
Experimental Conditions
Pressure in Atmospheres During Quench

Nominal Pressure	Equivalence Ratio .7	.8	.9	1.0	1.1	1.2
1.1	1.10	1.12	1.17	1.19	1.18	1.17
1.6				1.58		
2.7		2.64	2.67	2.84	2.81	2.74
3.5		3.38		3.65		

Table 3.2
Experimental Results
Heat Flux and Time for Quenching

p_{nom} (Atmos)	p_q (Atmos)	φ	t_q (msec)	$q_{w_{max}}$ $\left(\frac{MW}{m^2}\right)$	t_c (msec)	q_c $\left(\frac{MW}{m^2}\right)$	$\frac{t_q}{t_c}$	$\frac{q_{w_{max}}}{q_c}$	$\frac{t_q^*}{t_c}$ From Eqn 3.3	$\frac{q_{w_{max}}^*}{q_c}$ From Eqn 3.3
1.1	1.10	0.7	.85	.20	.416	.499	2.03	.40	1.96	.41
	1.12	0.8	.56	.28	.238	.771	2.41	.36	2.31	.37
	1.17	0.9	.24	.45	.153	1.07	1.60	.42	1.51	.44
	1.19	1.0	.20	.51	.100	1.38	2.00	.37	1.87	.39
	1.18	1.1	.19	.61	.095	1.43	2.06	.43	1.94	.45
	1.17	1.2	.22	.53	.119	1.21	1.90	.44	1.79	.46
1.6	1.58	1.0	.25	.69	.080	1.79	3.11	.39	2.62	.43
2.7	2.64	0.8	.35	.53	.118	1.68	3.15	.32	2.19	.40
	2.67	0.9	.17	.81	.0778	2.26	2.35	.36	1.62	.45
	2.84	1.0	.14	1.00	.0498	3.03	2.85	.33	1.92	.42
	2.81	1.1	.11	1.20	.0464	3.13	2.38	.38	1.61	.48
	2.74	1.2	.16	1.05	.0592	2.61	2.83	.40	1.94	.51
3.5	3.38	0.8	.29	.58	.0961	2.10	3.28	.28	2.07	.37
	3.65	1.0	.13	1.16	.0405	3.81	3.22	.30	1.98	.41

Additional results are the pressure variations up to the time of quenching, and photographs of the flame development. The pressure at the time of quenching and the rate of pressure increase are shown in Table 3.3.

Table 3.3
Experimental Results
Pressure Rise During Quenching

p_{nom} (Atmos)	p_q (Atmos)	φ	t_p (msec)	t_q (msec)	$\frac{t_q}{t_p}$
1.1	1.10	0.7	92	.85	.0092
	1.12	0.8	50	.56	.0112
	1.17	0.9	31	.24	.0077
	1.19	1.0	25	.20	.0080
	1.18	1.1	24	.19	.0079
	1.17	1.2	39	.22	.0056
1.6	1.58	1.0	17	.25	.015
2.7	2.64	0.8	25	.35	.014
	2.67	0.9	17	.17	.010
	2.84	1.0	12	.14	.0115
	2.81	1.1	11	.11	.0098
	2.74	1.2	15	.16	.0105
3.5	3.38	0.8	37	.29	.0078
	3.65	1.0	24	.13	.0053

$$t_p = \frac{p_q}{\left.\frac{dp}{dt}\right|_q}$$

The results from one experiment will be presented first, and an interpretation of the results will be given. The complete set of results will then be nondimensionalized, accounting for the effects of changes in the pressure at quenching and equivalence ratio. The assumption of constant pressure during quenching will also be examined. Causes of run to run variations will be considered and, lastly, the effects of the thin film material on the heat flux measurement

will be shown to be negligible.

3.1 INTERPRETATION OF RESULTS

It is helpful to utilize some results from numerical calculations (Chapter 4) to aid in the interpretation of the experimental results. In Figure 3.1, some pertinent information is presented. The top curve shows the distance from the flame to the wall as a function of time. The two curves on the bottom half of the Figure show the variation of the total chemical heat release and the wall heat flux on the same time scale.

Initially, the flame speed and heat release in the flame are not affected by the wall, even though the wall heat flux (which is small) rises at an increasing rate. As the wall heat flux increases, the effect of the wall on the flame propagation also increases.

Eventually, the flame begins to decelerate, and the heat release in the flame starts to drop. During this time, the wall heat flux is increasing almost linearly with time.

The flame eventually reaches a position where the heat losses are so great that it can no longer progress. The flame then remains stationary while fuel near the wall is heated by the flame and expands into the flame. The wall heat flux reaches a maximum value and then decreases as the last of the fuel is consumed.

This interpretation is supported by the experimental results of Figure 3.2†, in conjunction with the corresponding photographic sequence (Figures 2.8a-f). As stated above, from the time of ignition to t = 40 milliseconds, the flame is far from the wall, and the heat flux is small. The heat transfer rate reaches a maximum at time t = 45 milliseconds (which corresponds to t = 0 in Figure 3.2),

† In Figure 3.2, as with all of the heat flux data, the time t = 0 corresponds to the time at which the maximum heat flux occurs.

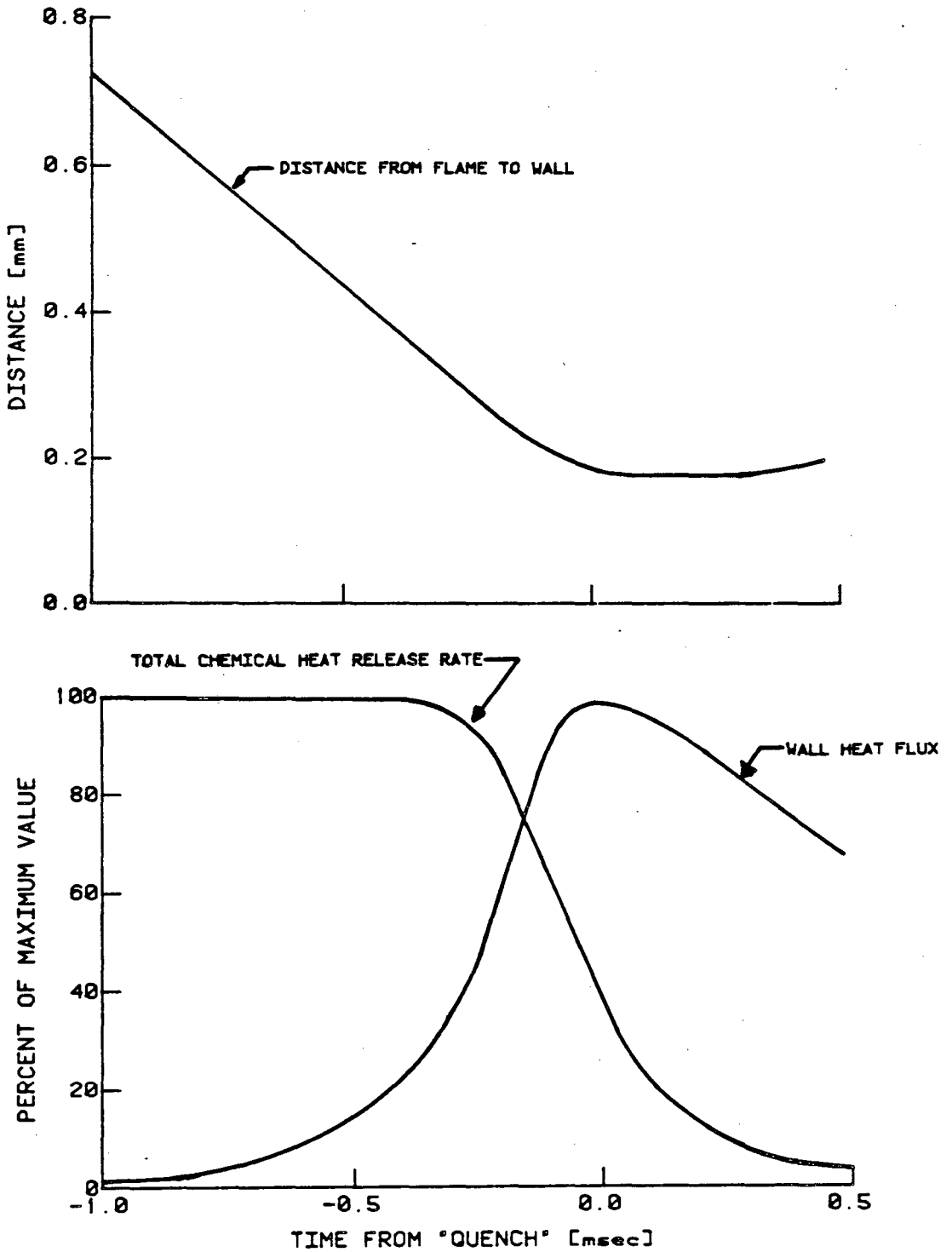

-- XBL 8411-4673 --

Figure 3.1 Heat release, heat flux, flame position as predicted from numerical calculations.

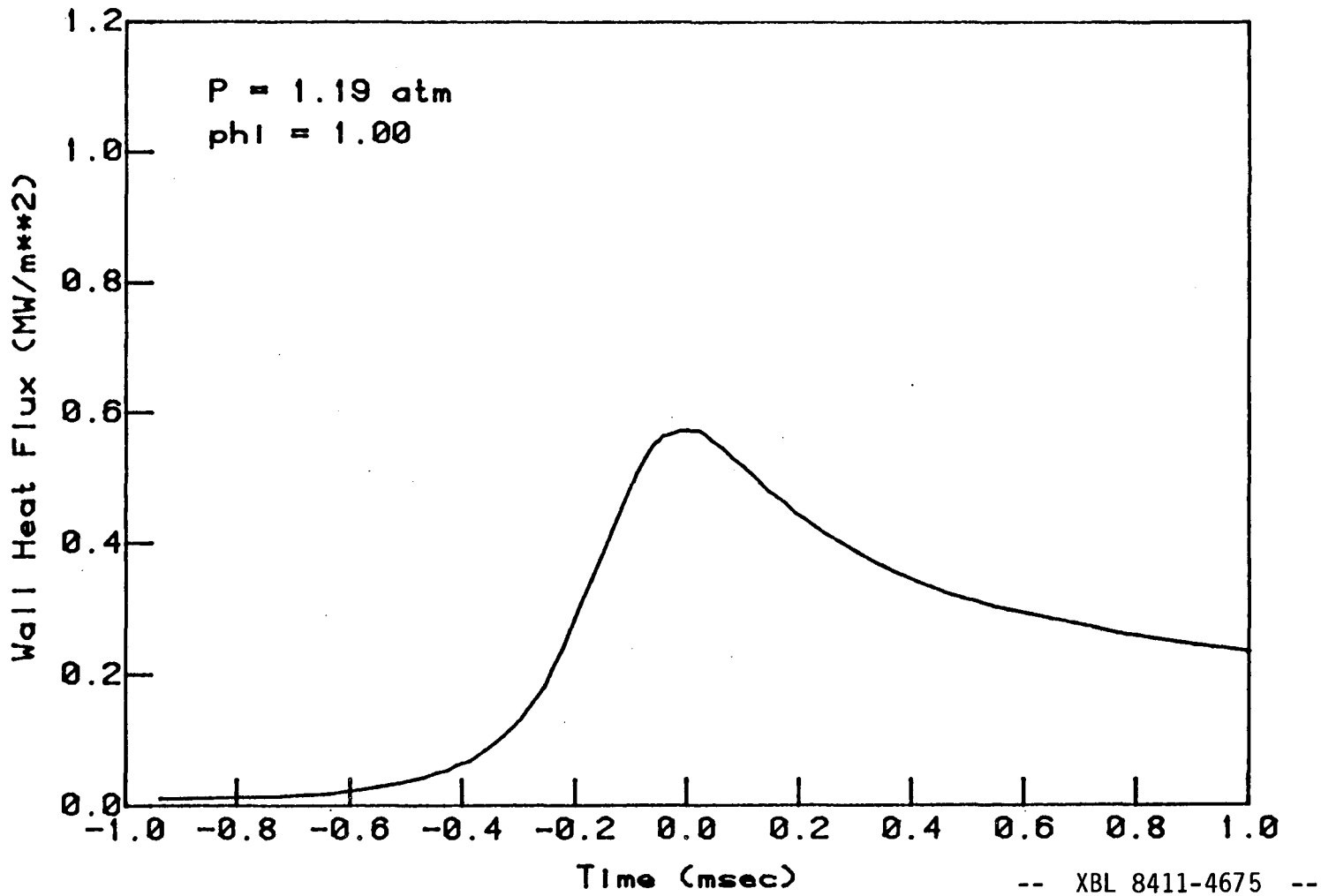

Figure 3.2 Typical wall heat flux variation as measured in the experiment.

when the flame is near the heat transfer gauge (Figure 2.8e). The flux then decreases with time.

3.2 NONDIMENSIONAL RESULTS

The experimental data were nondimensionalized based on the properties for a flame propagating into a gas at a pressure of p_q and a temperature of T_u, that is, for the conditions outside of the thermal boundary layer, at the moment that quenching occurs. For methane-air flames, the Lewis number is near one, and the time, length, and heat flux can be scaled by the thermal properties of a freely propagating flame. The characteristic time is given by the flame speed and thermal diffusivity according to:

$$t_c = \left(\frac{\alpha}{S_u^{\,2}}\right)_{p_q,T_u} \quad . \tag{E.18}$$

The characteristic heat flux is given by the heat release rate in an undisturbed flame:

$$q_c = (\rho S_u c_p \Delta T_f)_{p_q,T_u} \quad . \tag{E.19}$$

The values of t_c and q_c for methane-air may be found in Appendix E. The results for all of the experimental conditions (Table 3.1) are shown on Figure 3.3. By nondimensionalizing the heat flux with the steady state heat release rate in a flame, and the time with the characteristic time for flame propagation, most of the effects which influence the unsteady heat been taken into account.

The nondimensional maximum heat flux, $\frac{q_{w\,max}}{q_c}$, was found to be dependent on the pressure, and independent of the equivalence ratio. The maximum heat flux is listed in Table 3.2, and is shown as a function of the pressure in Figure 3.4. A least squares fit to the data gave

$$\frac{q_{w\,max}}{q_c} = 0.42\left(\frac{p_q}{p_o}\right)^{-0.209} \quad . \tag{3.1}$$

This relation correlated all of the data to within 25%.

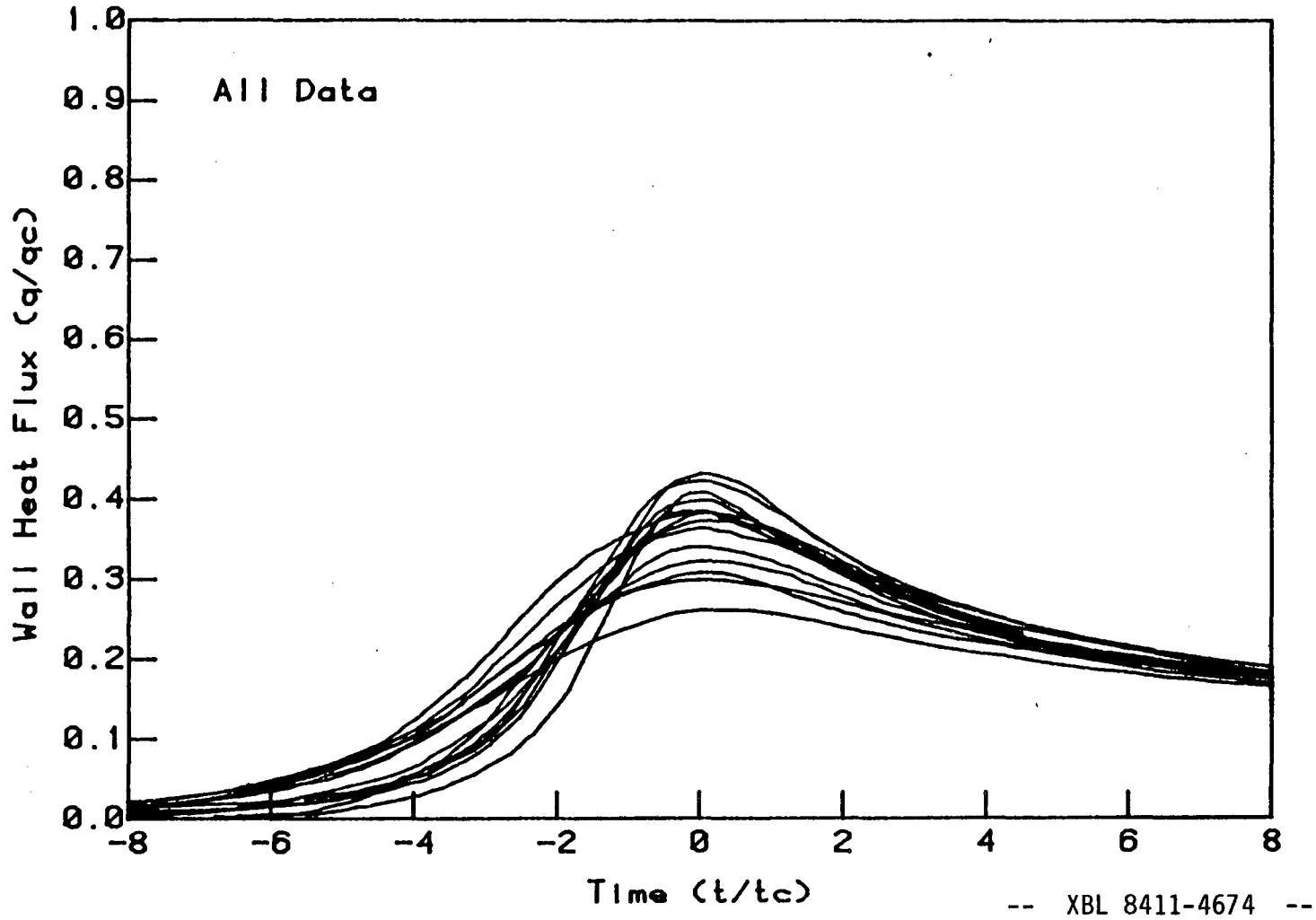

Figure 3.3 Experimental results - wall heat flux vs. time - all conditions.

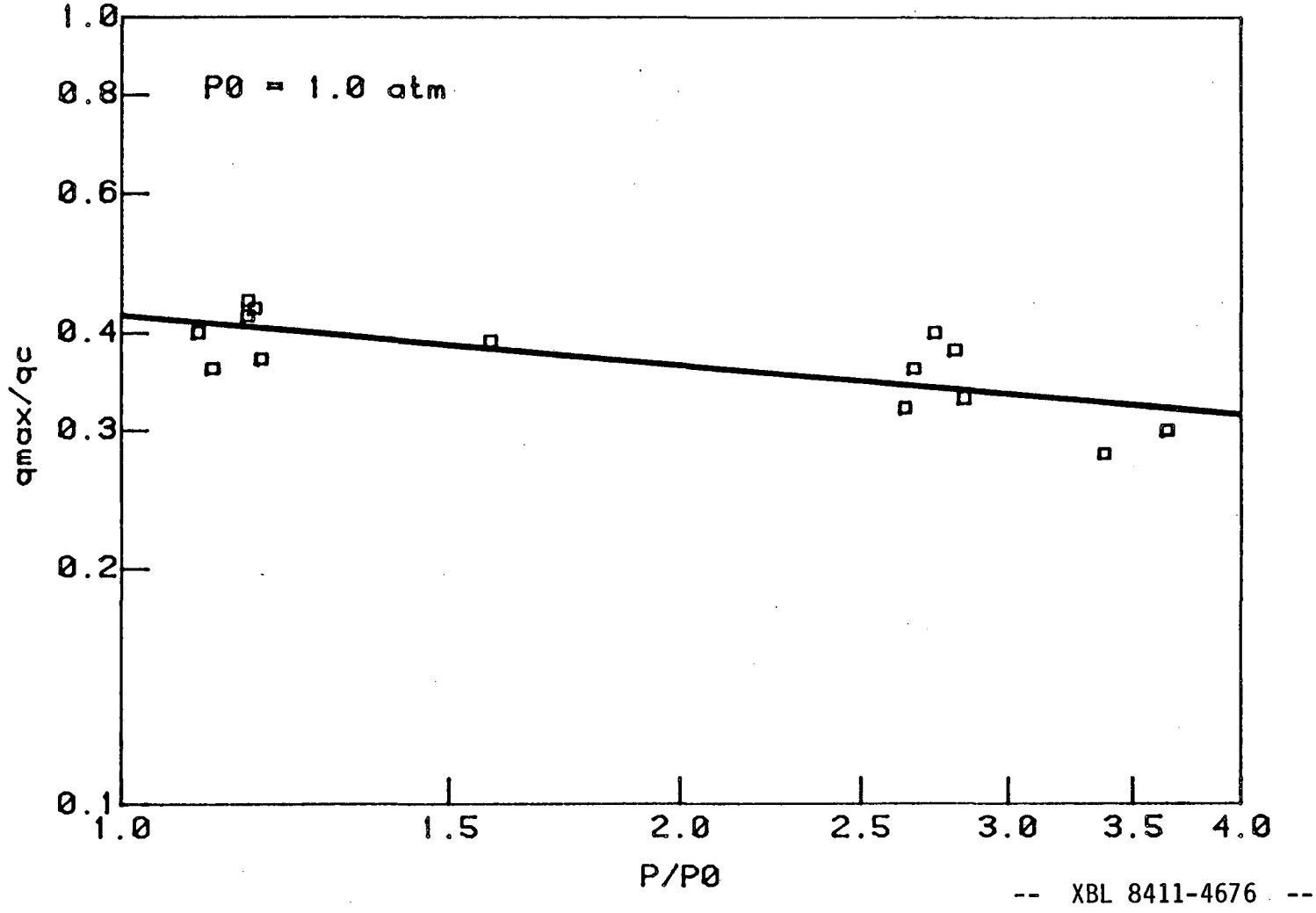

Figure 3.4 Experimental results - maximum heat flux vs. pressure - all conditions.

There is also a dependency of the nondimensional time for quenching $\frac{t_q}{t_c}$ (as defined in the introduction to Chapter 3) on pressure. This is evident when comparing the nondimensional results for two different pressures, as in Figures 3.5a and 3.5b. At 1.10 atmospheres (Figure 3.5a), $t_q = 2.0t_c$, and at 2.70 atmospheres (Figure 3.5b) $t_q = 2.7t_c$. This trend, of longer times for quenching at higher pressures, was found to hold for all of the data. Values for $\frac{t_q}{t_c}$ are listed in Table 3.2, and the variation of $\frac{t_q}{t_c}$ with pressure is shown in Figure 3.6. A least squares fit to the data gave:

$$\frac{t_q}{t_c} = 1.88\left(\frac{p_q}{p_o}\right)^{0.376} \tag{3.2}$$

to within 25%.

Based on the correlations given in Equations 3.1 and 3.2, new time and heat flux variables may be defined which scale with pressure, and which eliminate the trends in the nondimensional experimental results. Specifically, by defining

$$t^* = t\left(\frac{p_q}{p_o}\right)^{-0.376} ,$$

and

$$q^* = q\left(\frac{p_q}{p_o}\right)^{0.209} , \tag{3.3}$$

the heat flux as a function of time may be scaled according to

$$\frac{q^*}{q_c} = fn\left(\frac{t^*}{t_c}\right) . \tag{3.4}$$

Using Equation 3.3 and 3.4, the experimental results shown in Figure 3.3 (and individually in Figures D.1 to D.14) were scaled with the pressure to give the curve in Figure 3.7. The individual curves may be found in Figures D.15 to D.28.

The nondimensional values $\frac{t_q^*}{t_c}$ and $\frac{q_{w\,max}^*}{q_c}$ are related to $\frac{t_q}{t_c}$ and $\frac{q_{w\,max}}{q_c}$

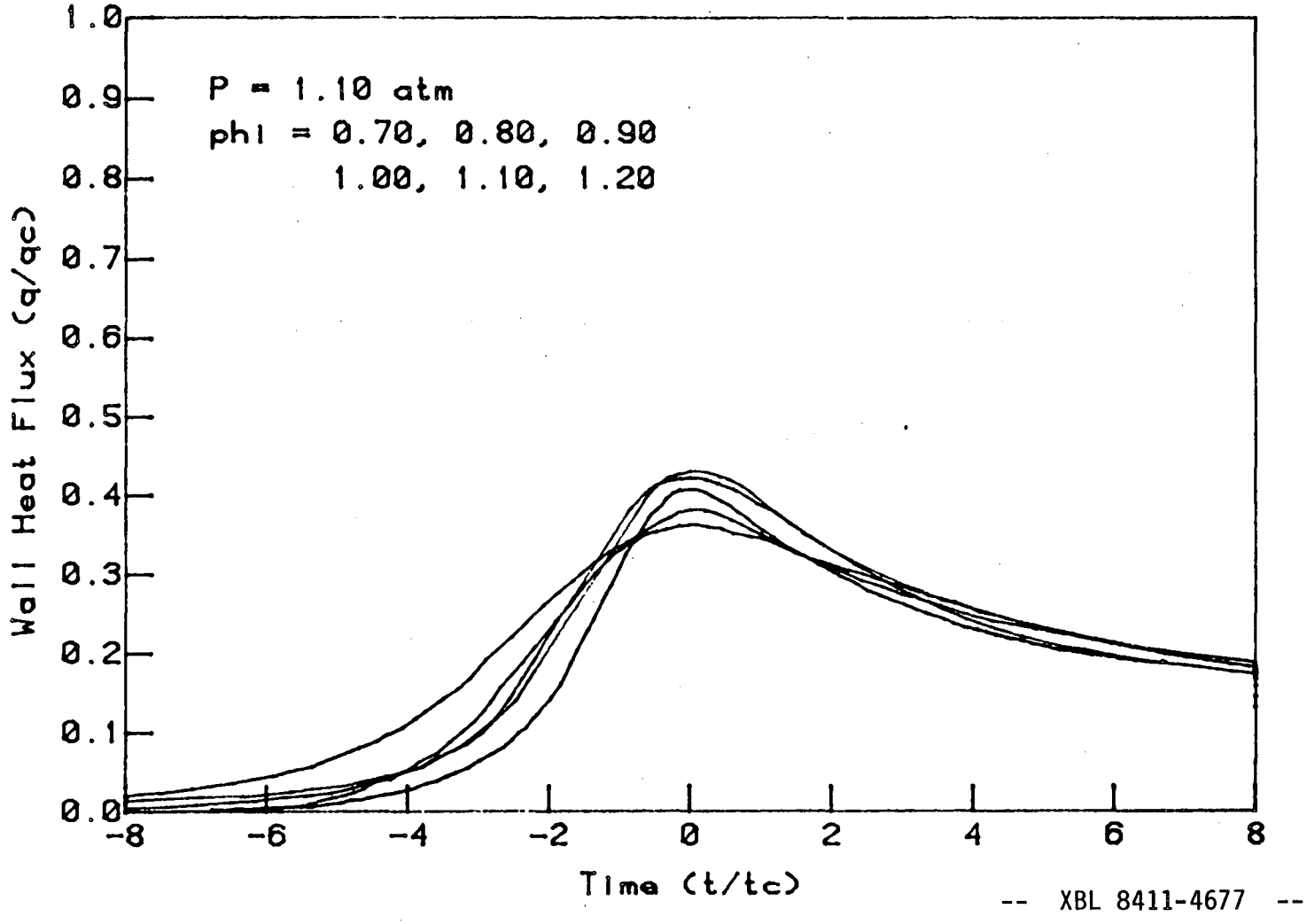

Figure 3.5a Experimental results - wall heat flux vs. time - p = 1.1 Atmospheres.

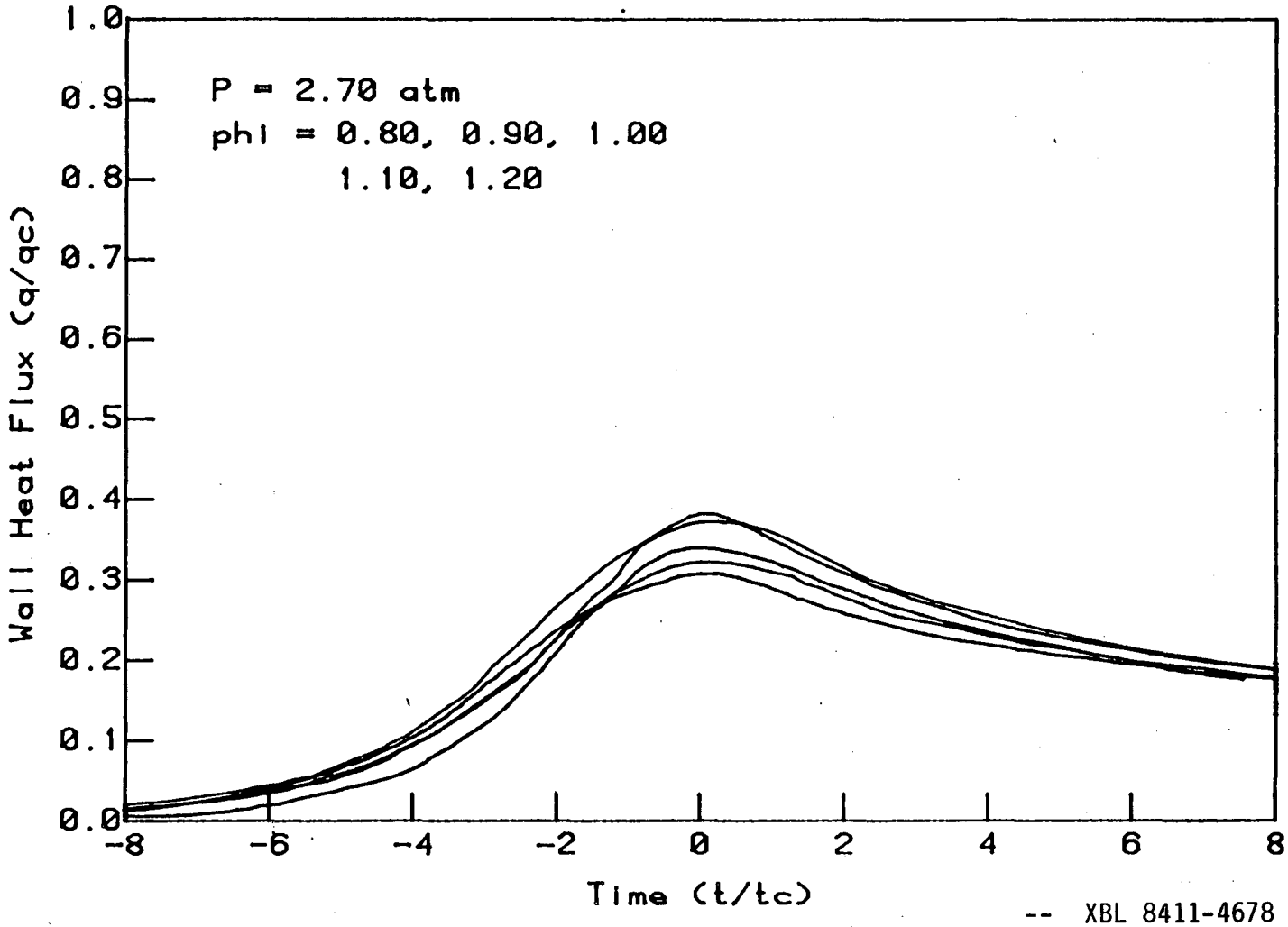

-- XBL 8411-4678 --

Figure 3.5b Experimental results - wall heat flux vs. time - p = 2.7 Atmospheres.

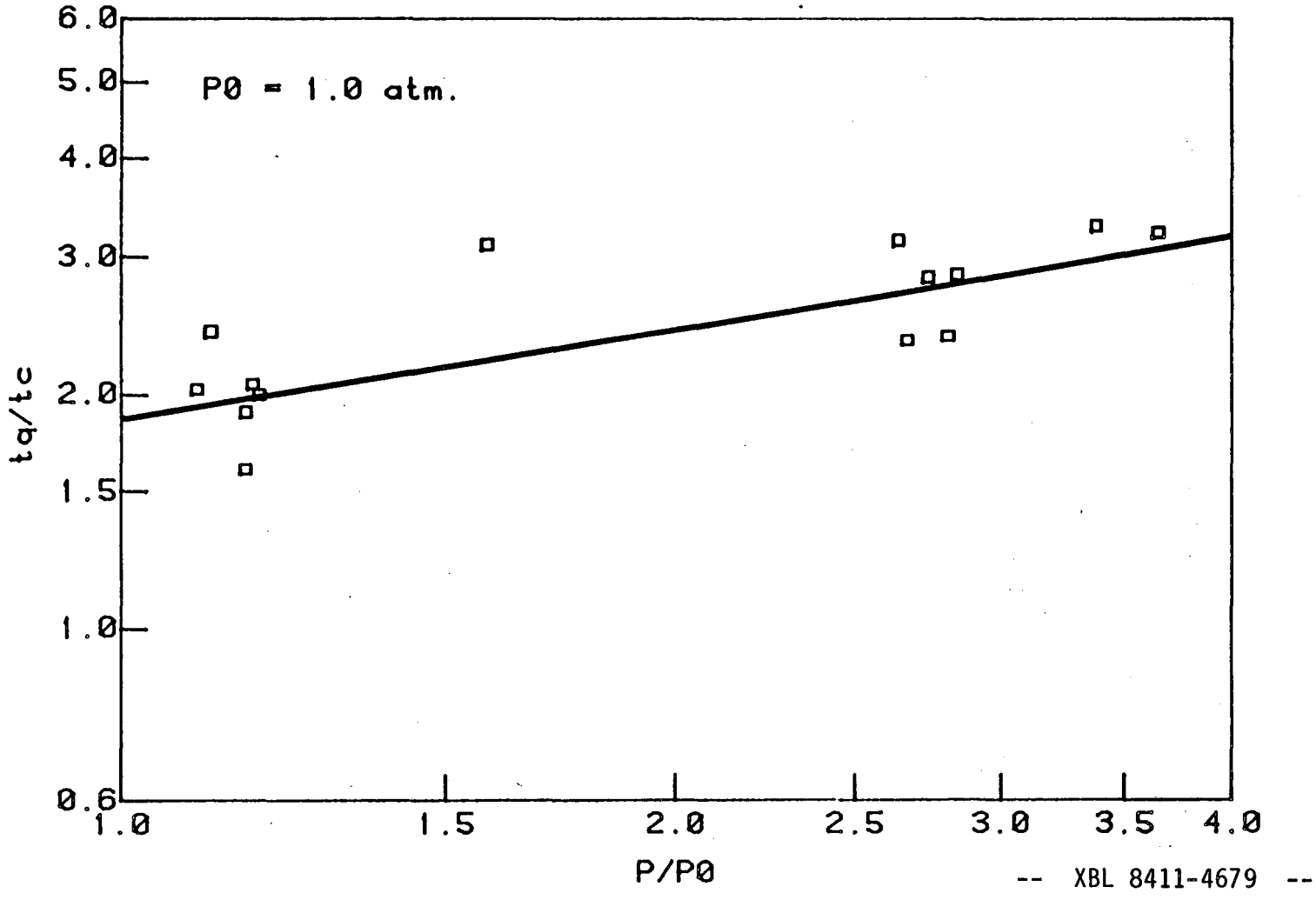

Figure 3.6 Experimental results - time for quenching to occur vs. pressure - all conditions.

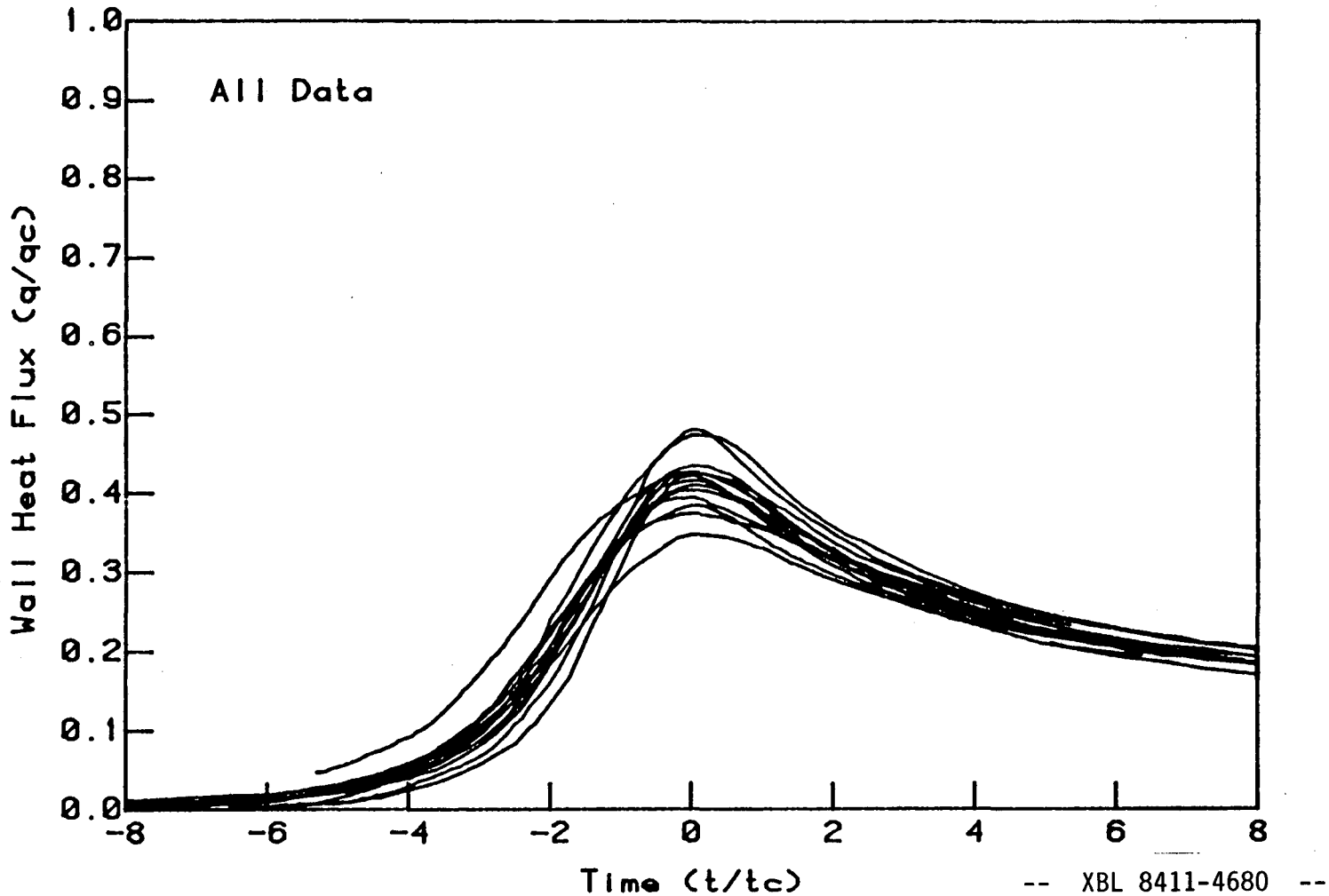

Figure 3.7 Pressure scaled experimental results (Eqn 3.3) - wall heat flux vs. time - all conditions.

through:

$$\frac{t^*_q}{t_c} = \frac{t_q}{t_c}\left(\frac{p_q}{p_o}\right)^{-0.376} \tag{3.5}$$

and

$$\frac{q^*_{w_{max}}}{q_c} = \frac{q_{w\,max}}{q_c}\left(\frac{p_q}{p_o}\right)^{0.209}.$$

These values are shown in Figures 3.8 and 3.9, and are tabulated in Table 3.2. The average values of $\frac{t_q^*}{t_c}$ and $\frac{q_{w\,max}^*}{q_c}$ are:

$$\overline{\frac{t_q^*}{t_c}} = 1.88 \tag{3.6}$$

$$\overline{\frac{q_{w\,max}^*}{q_c}} = 0.42$$

In summary, it is noted that the following were accomplished in this section:

1) The heat flux as a function of time during flame quenching was rendered nondimensional by the heat release rate and time of propagation for the steady flame which existed just before quenching (Equations E.18 and E.19).

2) It was noted that the nondimensional results exhibited trends with the pressure at which quenching occured (Equations 3.1 and 3.2).

3) The results were scaled for the pressure trends by introducing a new time and heat flux variable (Equation 3.3).

4) In terms of the pressure scaled variables, the heat flux as a function of time during flame quenching was reduced to one curve (Figure 3.7).

A possible explanation for the pressure dependence of the nondimensional results is presented in Section 4.4.

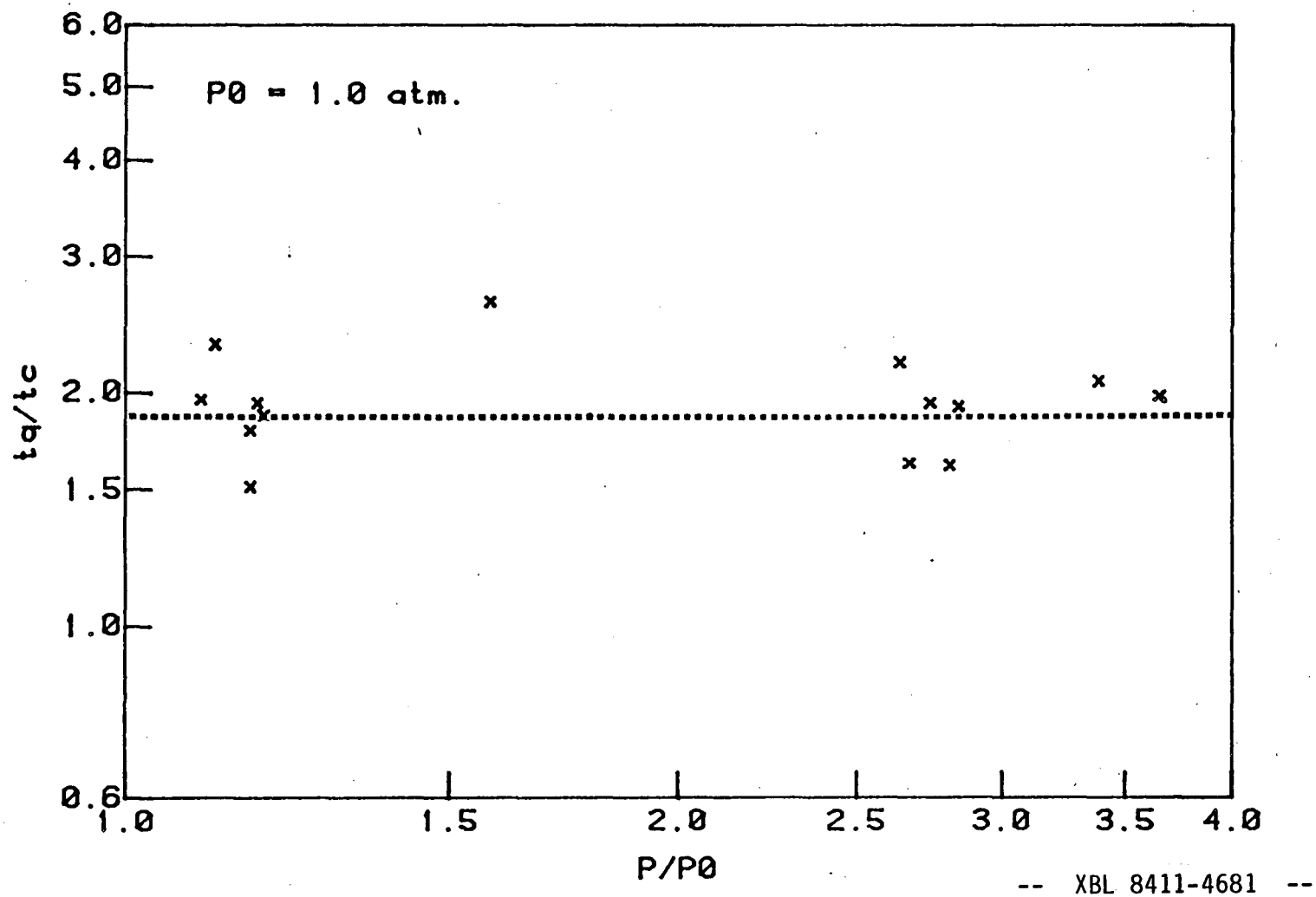

Figure 3.8 Pressure scaled experimental results (Eqn 3.3) - time for quenching vs. pressure - all conditions.

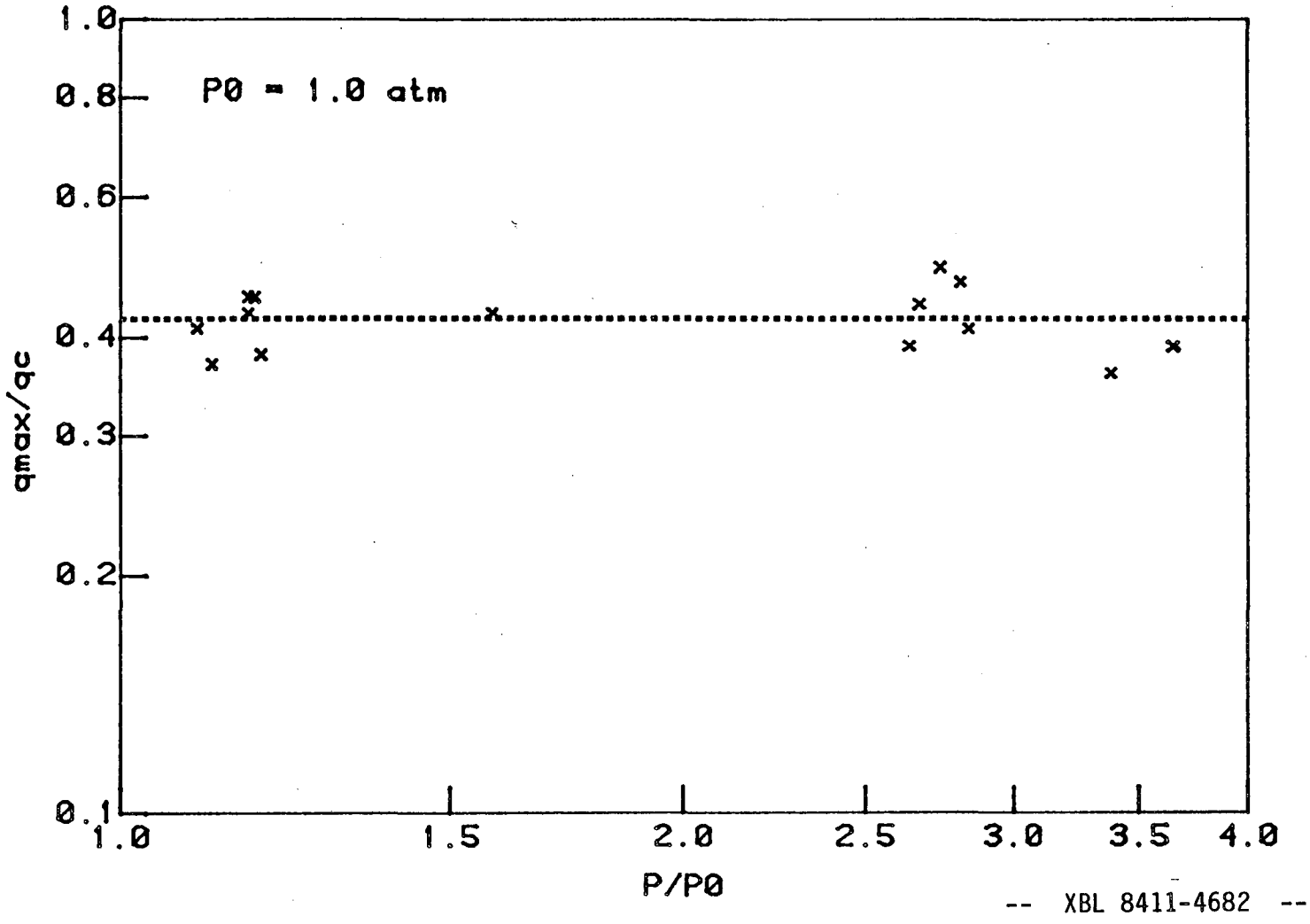

Figure 3.9 Pressure scaled experimental results (Eqn 3.3) - maximum heat flux vs. pressure - all conditions.

3.3 THE ASSUMPTION OF CONSTANT PRESSURE

It is assumed in the calculations of Chapter 4 that the pressure is constant during quenching. The validity of this assumption may be assessed by comparing the time required for quenching to occur, t_q, to the relative rate of the pressure increase,

$$t_p = \frac{p_q}{\left.\frac{dp}{dt}\right|_q} \tag{3.7}$$

In Table 3.2, the value of t_q / t_p is presented for each experimental condition. Since t_q / t_p is small for all conditions, we may conclude that the pressure is essentially constant during quenching. In addition, the Mach number of the flow in the combustion chamber,

$$M = \frac{u}{a} \approx \frac{S_b}{\sqrt{\gamma R T_b}}$$

is also small. Thus the pressure is approximately uniform as well as constant.

3.4 RUN TO RUN VARIATION

For the data to be considered reliable, it was required that the heat flux did not vary by more than the experimental error in the measurement, which was approximately 8% (see section 2.3.5). Optical measurements of the flame front (section 2.1.3.3) showed that the reliability criteria were met over a wide range of experimental conditions as long as the flame surface was free of wrinkles. In Figure 3.10a, the data for a flame which is free of wrinkles are presented. The curves follow the same trends, and appear to be identical to an accuracy greater than that of the measurement. In contrast, the heat flux for a wrinkled flame was found to vary by 20 % or more from run to run.

3.5 THE EFFECTS OF PROTECTIVE COATINGS

A comparison of three types of gauges was conducted in order to evaluate

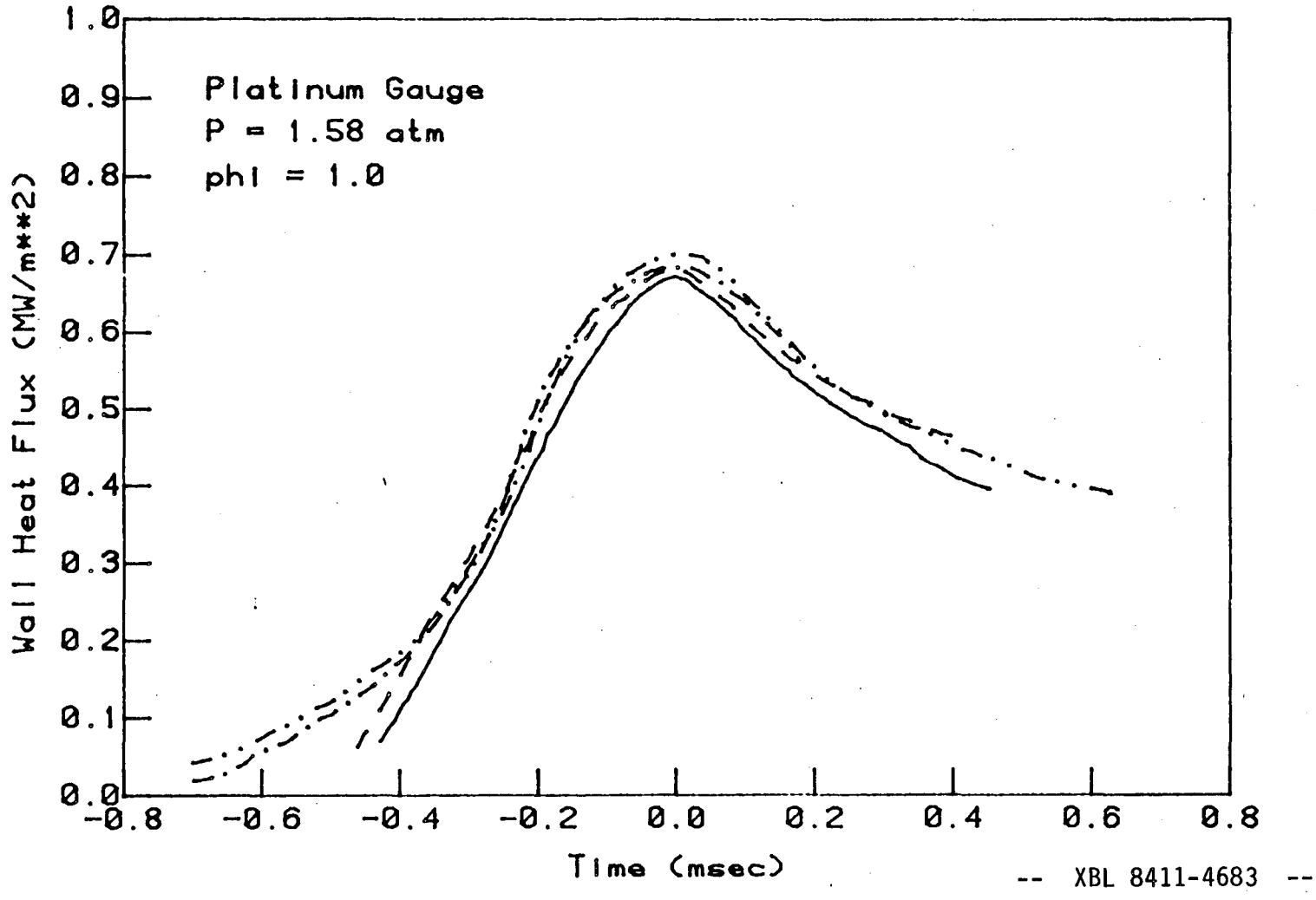

Figure 3.10a Heat flux as measured by a platinum gauge for four consecutive runs.

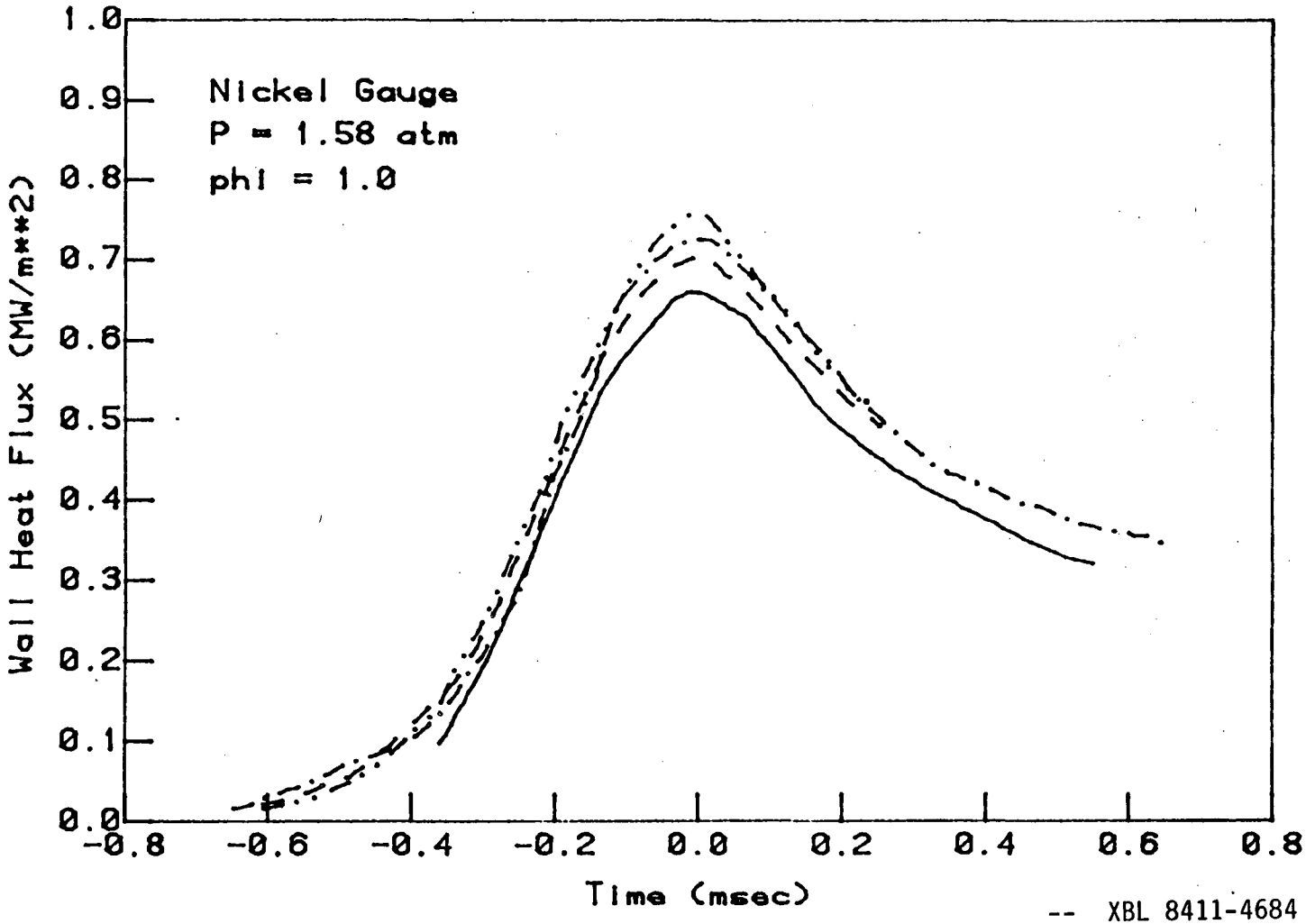

-- XBL 8411-4684 --

Figure 3.10b Heat flux as measured by a nickel gauge for four consecutive runs.

the effect of the thin film material on the heat transfer measurements. The catalytic effects of the platinum were considered to be a potential problem since the catalytic reactions might occur on the platinum surface during quenching. Although catalytic reactions might not be expected to occur at temperatures as low as those which the platinum was exposed to in this experiment (less than 350 K), it was felt that it would be worth while to experimentally determine if such reactions occur, and if they would interfere with the heat transfer measurements.

The chosen thin films were an uncoated platinum gauge, a platinum gauge coated with quartz, and an uncoated nickel gauge. The platinum was deposited from platinum paint, as described in Section 2.1.3.2. The nickel film and the quartz coating on the platinum film were achieved by vacuum deposition.

The purpose of the quartz overcoating was to render the platinum chemically inert to the surrounding gases. As an indirect measure of the insulating effects of the quartz, it was assumed that a chemically inert film would also be electrically insulating; thus the following test was performed to estimate the thickness of he overcoating required:

1) A platinum film was coated with a layer of quartz.

2) From the area coated and the weight of quartz used, the thickness of the coating was determined.

3) The electrical resistance across length of the film, as measured *through* the overcoating, was determined.

   By repeating this process, the curve in Figure 3.11 was produced, giving the measured resistance versus coating thickness. It was determined that an overcoating of 2000 Angstroms provided adequate protection from possible catalytic reactions.

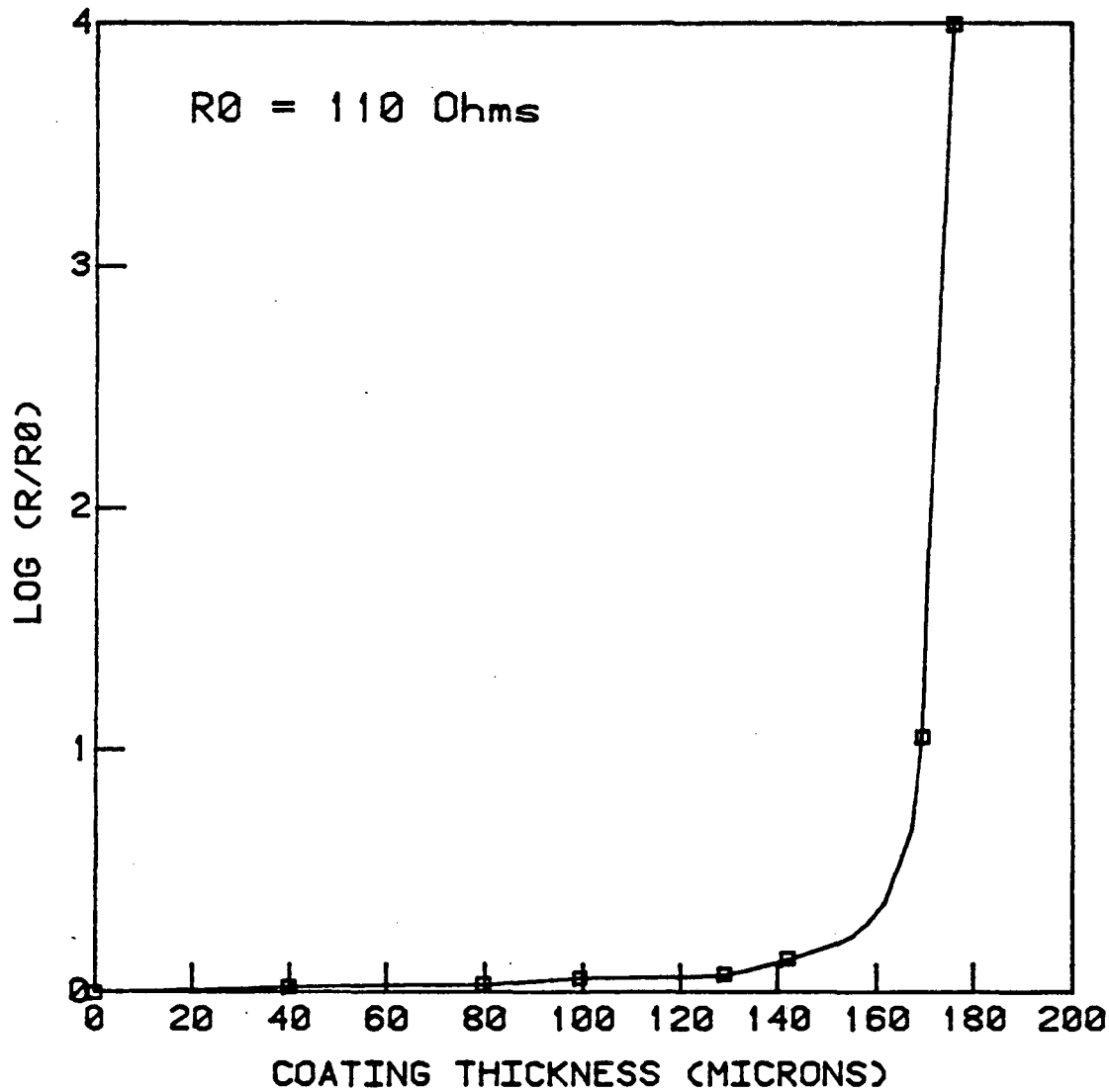

-- XBL 8411-4685 --

Figure 3.11 Resistance across the thin film as measured through a coating of quartz.

The results of the Platinum-Nickel comparison are presented in Figures 3.10a and 3.10b. Each of the curves in these figures was obtained from individual experiments. Thus it can be seen that the heat flux, as measured by either gauge, differed by no more than the run to run variation.

The results of the Platinum-Platinum SiO_2 comparison is shown in Figure 3.12. Each of these curves is the average of four individual experiments. The differences between the two gauges is of the same order as the differences between the Platinum and Nickel gauges.

It therefore appears that the differences in the heat flux measured by the three types of gauges is small. This conclusion is supported by the work of other researchers who have studied catalytic reactions on platinum surfaces. Hydrocarbon combustion on heated platinum surfaces were studied by Schefer & Robben (1980), who found that the reaction rates where very low at the wall temperatures near room temperature. Mori, Ohtake, & Ishizuka (1972) measured the heat transfer to both bare and coated platinum wires for a range of wire temperatures, and found that for room temperature surfaces the heat transfer was not affected by catalytic reactions.

Although the reaction rates of catalytic reactions would be low at low temperatures [Schefer & Robben, 1980], this does not mean that catalytic reactions never take place on the uncoated platinum film surface. Since all of the gauges were used many times, it is possible that the supposedly uncoated surface contained impurities which, in turn, blocked catalytic reactions. It is also possible that the differences were not greater than the experimental uncertainty of the measurements (8%).

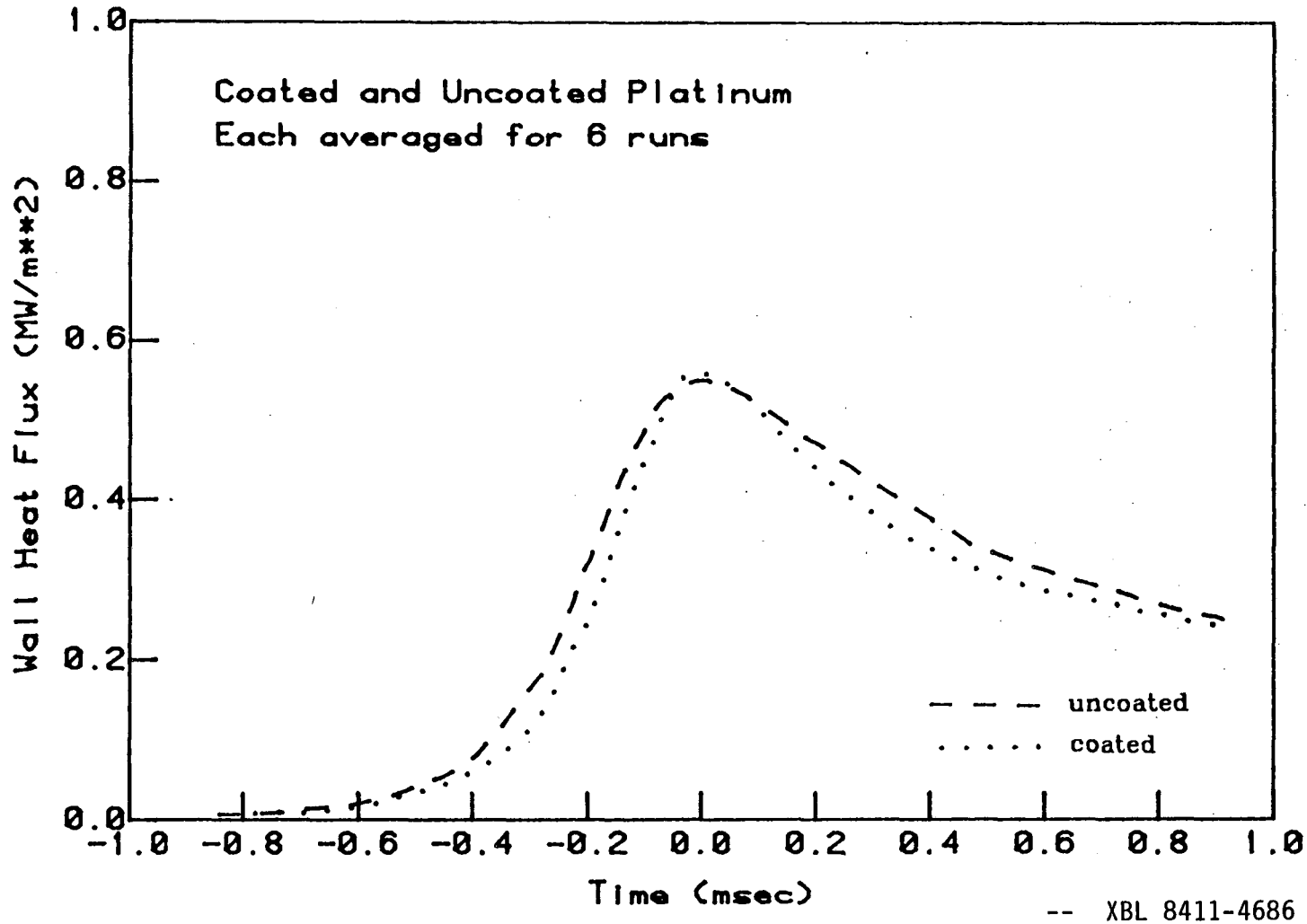

-- XBL 8411-4686 --

Figure 3.12 Comparison of a platinum gauge and a platinum gauge coated with quartz.

CHAPTER 4

NUMERICAL RESULTS

Three models of the quenching process were used to predict the unsteady heat transfer. The models ranged in complexity from an integral model using an ignition temperature and unimolecular kinetics, to a finite difference model using an extensive set of elementary reactions (Appendix C). In each of the models, the conservation equations governing reactive-diffusive gas mixtures were used (see Appendix B). It was assumed that species diffusion was dominated by concentration gradients, and that radiative heat transfer is not important.

In two of the models, a finite difference formulation of the governing equations was used [Lund, 1978]. In these models, the kinetics were of Ahrrenius form, with the difference between them being the complexity of the reaction scheme. One of the models utilized the known set of elementary reactions for methane-air combustion, with experimental values for the kinetics constants. This will be referred to as the "detailed kinetics model" (Appendix C.1). The other finite difference model used a one step, global reaction, where the kinetic constants where chosen to give reasonable agreement with experimental values of flame speed and temperature [Westbrook & Dryer, 1978]. This will be referred to as the "one step kinetics model" (Appendix C.2).

For the third model, the conservation equations were integrated for use with an integral method. The reaction was assumed to be unimolecular, and the reaction rate was simplified by assuming an ignition temperature (Appendix C.3).

The conditions in the experiment were modeled by considering the interaction of a steady laminar flame with an impervious wall of very large heat

capacity. Since the rate of pressure increase in the experiment was small (see section 3.3), the pressure in the calculations was assumed to constant. This was accomplished by considering the gas to be of semi-infinite extent, bounded only by the wall at which quenching occurs. Thus the compression heating of the gas, as discussed in section 2.3.1, has been neglected. Consistent with this assumption, the temperature of the reactants and of the wall were assumed to be equal, thus eliminating the thermal boundary layer at the wall. Specifically, from the time of ignition to the time of quenching, the pressure increases from p_o to p_q, the gas which is far from the wall is adiabatically compressed, causing an increase in the unburnt gas temperature from T_o to $T_o\left(\frac{p_q}{p_o}\right)^{\frac{\gamma-1}{\gamma}}$. Due to differences between the thermal properties of the gas and the wall, there is only a small increase in the wall temperature†. In the models, the constant value of the pressure is chosen to be the value at the time of quenching, p_q. The unburnt gas far in front of the flame is taken to be uniform, at the temperature $T_u = T_o\left(\frac{p_q}{p_o}\right)^{\frac{\gamma-1}{\gamma}}$. Furthermore, is is assumed that the wall temperature is also at T_u so that there is no thermal boundary layer at the wall, and no wall heat flux prior to quenching. This approximation is discussed in detail in section 4.4. Briefly, it is noted that this approximation yields meaningful results for the temperature profile in the gas because the temperature difference across the thermal boundary layer is much less than the temperature difference across the flame. The assumption of constant pressure in the constant volume combustion chamber is examined in section 3.C, and it is found to be a valid approximation.

† For example, in the experiments, the wall temperature increased by less than 15 ° K during quenching, and the temperature rise across the flame was calculated to be 2100 ° K. Thus the change in the wall temperature is seen to be small in comparison with the temperature differences in the gas.

Details of the models and the calculations are presented in Appendix C.

4.1 DETAILED KINETICS VS. ONE STEP KINETICS MODELS

Calculations were preformed using the detailed and the one step kinetics models at the same conditions. Predictions for the heat flux differed by less than 10% of the maximum heat flux. The agreement between the two models was not unexpected, since the kinetic constants in the one step model were chosen to produce the proper flame speed and temperature [Westbrook & Dryer, 1978].

Because of the agreement of the results of these two models, and because the one step model requires much less computer time than the detailed model, one step kinetics were chosen for all of the subsequent finite difference calculations.

4.2 ONE STEP KINETICS MODEL

Using the one step kinetics model, the effects of pressure (at the time of quenching) and equivalence ratio on the heat transfer were studied. The results are included in Appendix D, and a summary of the results is presented in Table 4.1. The results, rendered dimensionless by the parameters of Chapter 3.2, are shown in Figure 4.1. It is seen that the results for all of the cases, i.e. for the different pressures and equivalence ratios, are collapsed onto one curve. The variation with pressure of the maximum heat flux and the time for quenching are shown in Figures 4.2 and 4.3. These results are very similar to the results of Kurkov (1967), who also used a one step reaction.

The maximum heat flux was found to be

$$q_{w\,max}(T_u) = 0.40 q_c \quad , \tag{4.1}$$

where

$$q_c \equiv \left[\rho S_u c_p \Delta T_f\right]_{p_q, T_u} \quad , \tag{E.19}$$

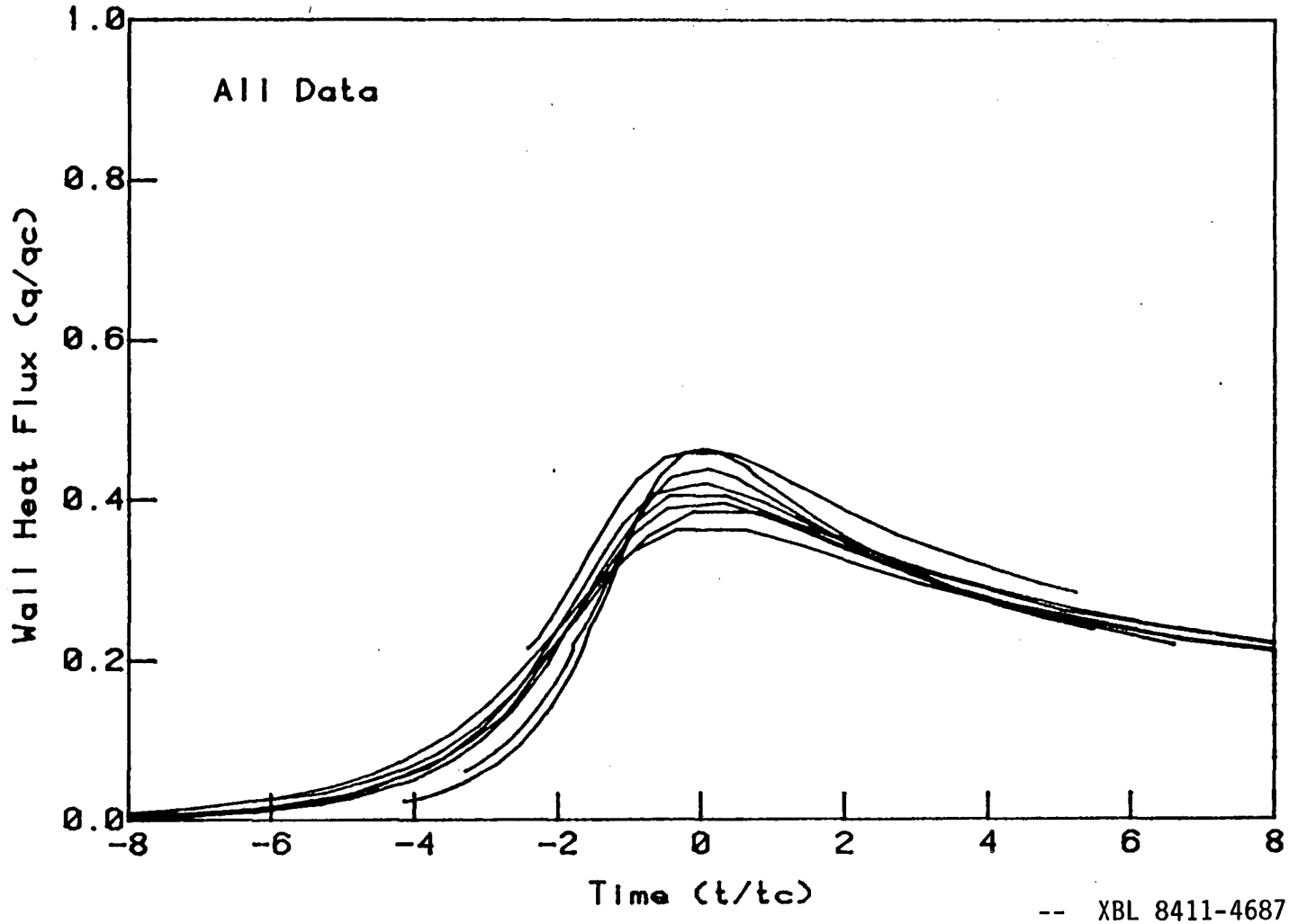

-- XBL 8411-4687 --

Figure 4.1 One step kinetics model - wall heat flux vs. time - all conditions.

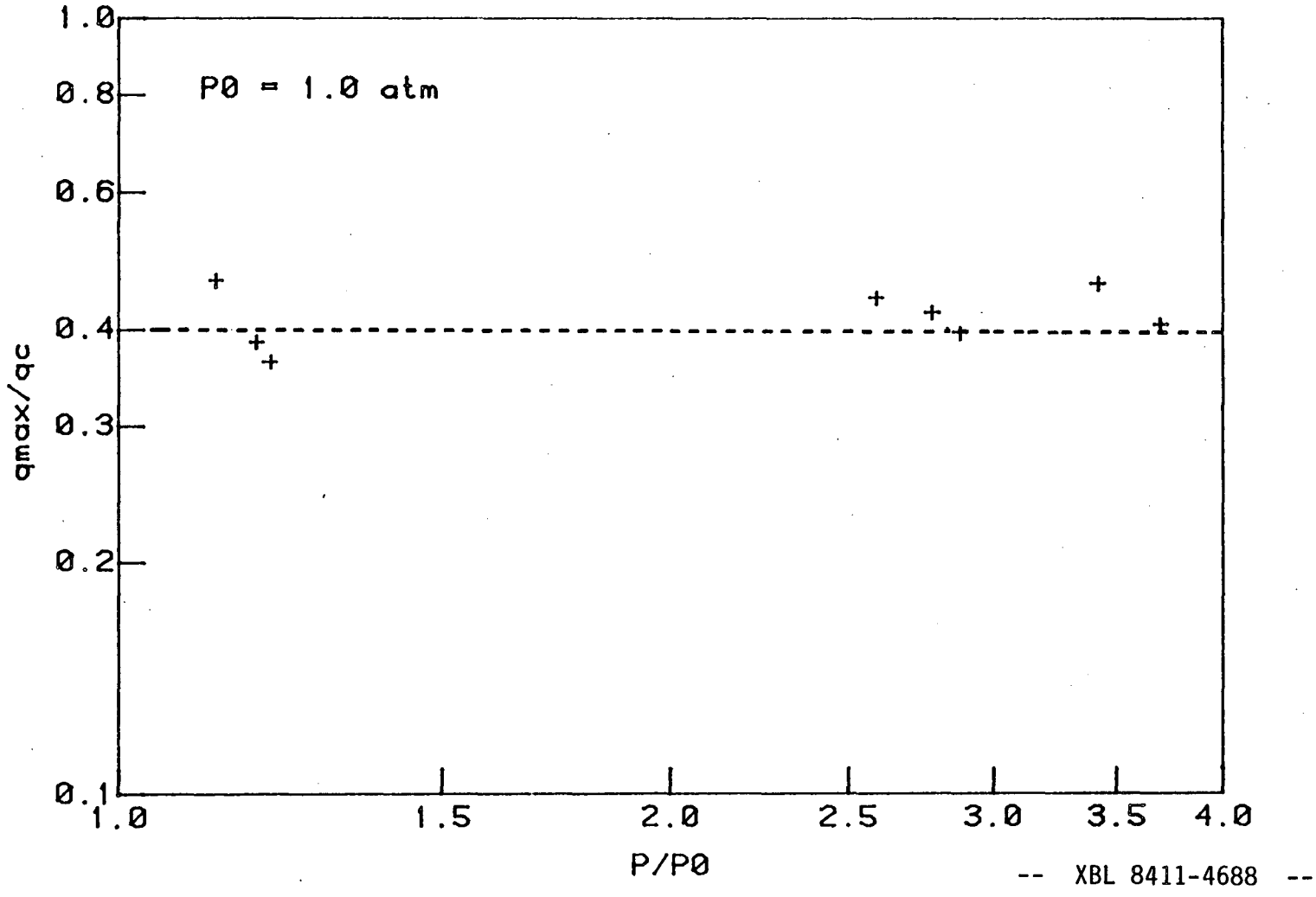

Figure 4.2 One step kinetics model - maximum heat flux vs. pressure - all conditions.

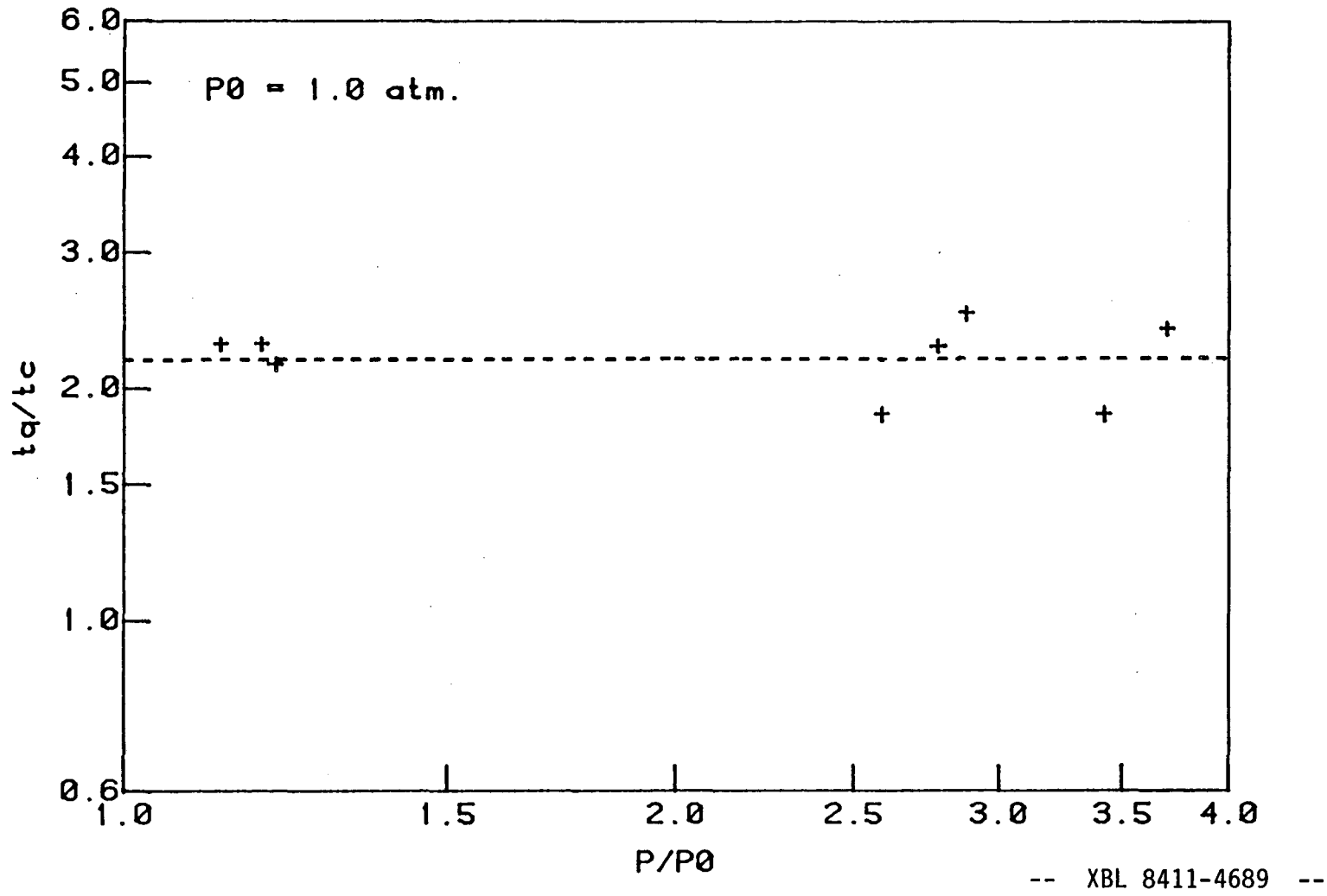

Figure 4.3 One step kinetics model - time for quenching vs. pressure - all conditions.

and the time required for the heat flux to increase from one half of the maximum heat flux to the maximum heat flux was

$$t_q(T_u) = 2.2t_c \quad , \tag{4.2}$$

where

$$t_c \equiv \left[\frac{\alpha}{S_u{}^2}\right]_{p_q,T_u} \quad . \tag{E.18}$$

Table 4.1
Numerical Results

P_{nom} (*Atmos*)	P_q (*Atmos*)	φ	$\frac{t_q}{t_c}$	$\frac{q_{w_{max}}}{q_c}$
1.1	1.13	0.8	2.28	.463
	1.21	1.0	2.15	.363
	1.19	1.2	2.28	.385
2.7	2.59	0.8	1.85	.439
	2.88	1.0	2.50	.396
	2.78	1.2	2.27	.421
3.5	3.42	0.8	1.85	.458
	3.70	1.0	2.27	.421

A comparison of the numerical predictions with the experimental results is presented in section 5.1.

4.3 INTEGRAL METHOD

The integral method was used in conjunction with the concept of an ignition temperature and one step kinetics (Section C.3). When the appropriate equations (Appendix C) where nondimensionalized, it was found that the solution to the problem was a family of solutions, with a nondimensional ignition temperature as the parameter:

$$\vartheta_{ig} = \frac{T_b - T_{ig}}{T_b - T_u} \quad . \tag{C.21}$$

As discussed in Appendix C, this can be interpreted as being either a measure of

an ignition temperature, or alternatively, as a measure of the flame thickness.

During the quenching of a real flame the reaction rates of the elementary reactions are all approaching zero. The importance of the individual reactions is thus changing with time, as is the temperature of the combustion products. Thus the concept of a constant ignition temperature, which may be meaningful in some circumstances, can only be considered to be a rough approximation during quenching.

The dimensionless ignition temperature was varied from ϑ_{ig} = 0 to 1. The case ϑ_{ig} = 0.0 corresponds to a flame sheet, where all combustion takes place at the flame temperature. The flame sheet propagates close to the wall which results in a very large heat flux and a small characteristic time. For values of ϑ_{ig} approaching unity, the flame becomes thicker and does not approach as close to the wall as the flame sheet does. As a result, the maximum heat flux is smaller and the characteristic time is larger. In Figure 4.4 the maximum heat flux is shown to be a decreasing function of the ignition parameter. Since the total heat transfer is the same for all ignition parameters, the characteristic time follows the opposite trend; for larger values of ϑ_{ig}, the flame requires a longer period of time to quench. This is evident from Figure 4.5, which shows both the time for quenching and the maximum heat flux as a function of ϑ_{ig}.

In Figure 4.6, nondimensional results are shown for a range of ignition temperature parameters. The results show essentially the same trends as do the more complete models (see Figure 4.1). In this formulation, the preheat region of the flame is of finite extent. Thus the conditions in front of the flame are uniform, $T_w = T_u$, and there is no heat flux to the wall before the front of the flame reaches the wall. In Figure 4.7, the results from the one step kinetics model are shown with the integral model results for values of ϑ_{ig} which come closest to the predictions of the one step kinetics model. For the value ϑ_{ig} =

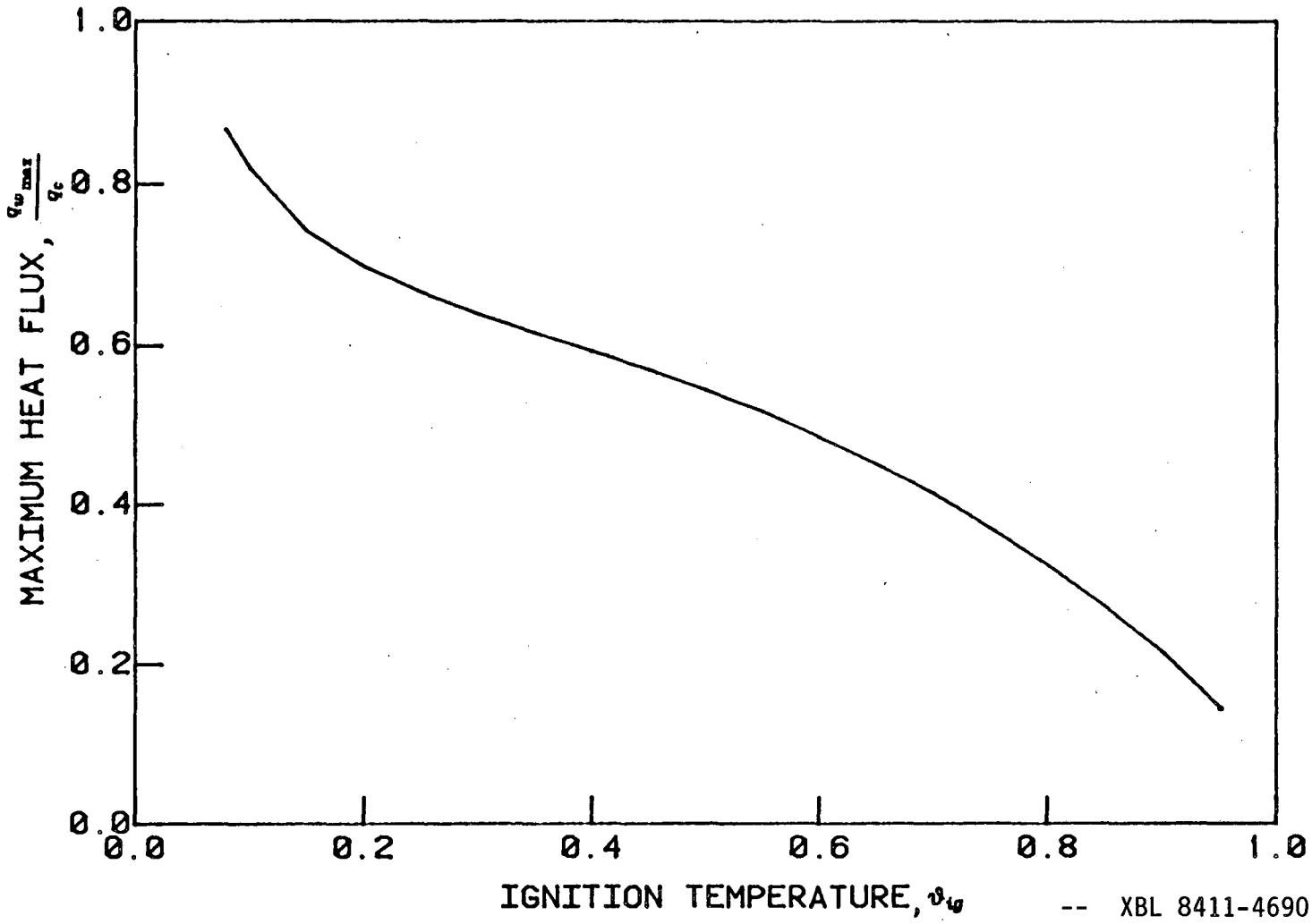

-- XBL 8411-4690 --

Figure 4.4 Integral model - maximum wall heat flux vs. ignition temperature

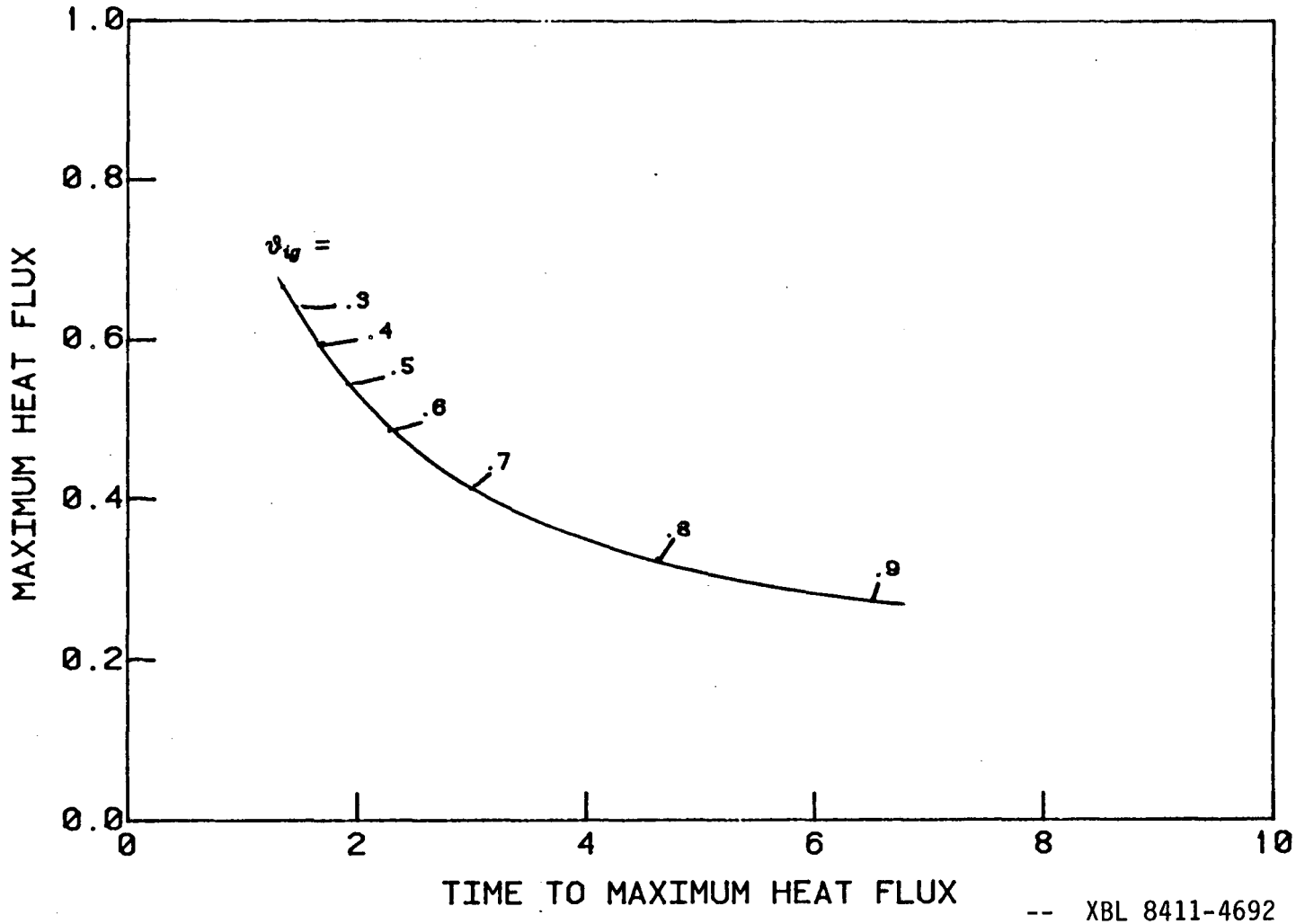

-- XBL 8411-4692 --

Figure 4.5 Integral model - maximum wall heat flux vs. time for quenching

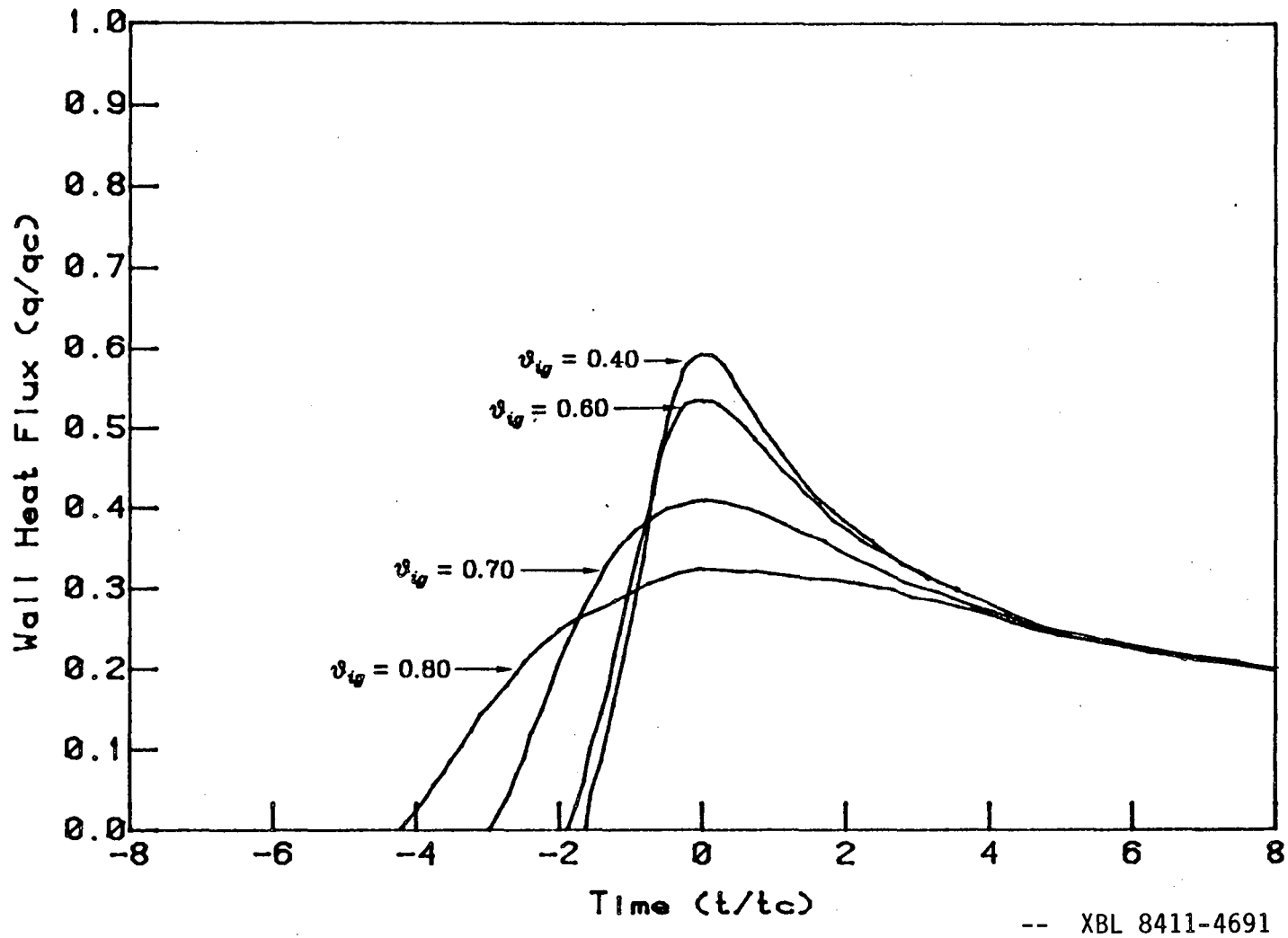

-- XBL 8411-4691 --

Figure 4.6 Integral model - wall heat flux vs. time for four ignition temperatures.

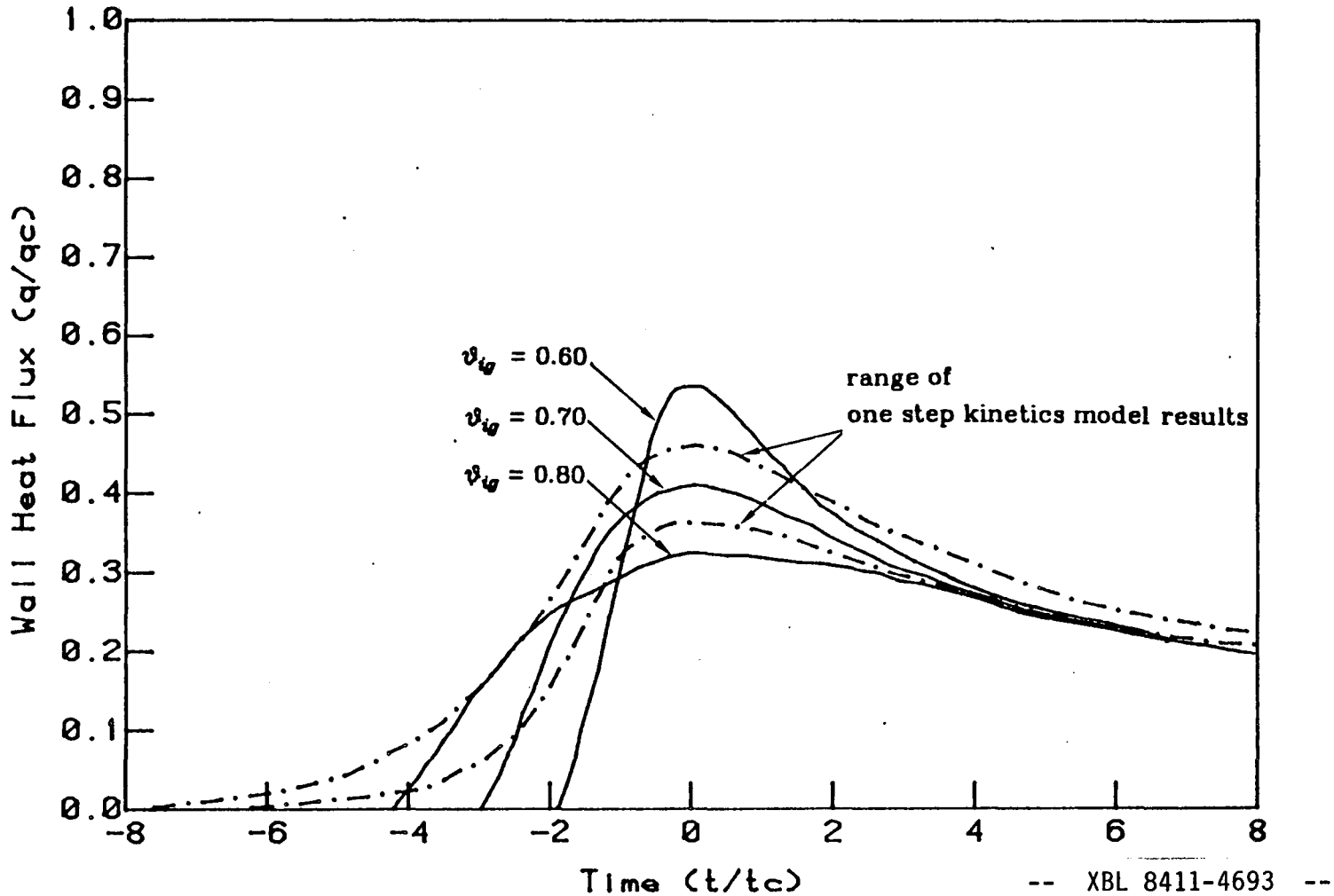

Figure 4.7 Comparison of integral and one step kinetics models - wall heat flux vs. time.

0.70, the heat flux as predicted by the integral model comes very close to the predictions of the one step kinetics model. For a stoichiometric methane air flame at one atmosphere, and a reactant temperature of 300 K, this corresponds to an effective ignition temperature of 875 K. In addition to the agreement of the predicted heat flux, the step kinetics model and the integral model both give reaction zones which are approximately of the same size (Figure 4.8).

The results of the models used in this study indicate that the thickness of the reaction zone during quenching is approximately the same as the distance from the wall to the reaction region. Thus it is necessary to consider the flame thickness, and hence the reaction rates, in order to study the interaction of the flame with a wall.

In section 5.1.2, the results of the integral method are compared to the experimental results.

4.4 THERMAL BOUNDARY LAYER EFFECTS

The calculations presented up to this point were made with the pressure assumed to be constant, $p = p_q$, and with the wall temperature at that associated with the unburnt gas temperature,

$$T_u = T_o \left(\frac{p_q}{p_o} \right)^{\frac{\gamma-1}{\gamma}}$$

In the experiment the wall temperature increases only slightly above its initial temperature T_o; thus the approach taken in the calculations neglects the thermal boundary layer at the wall.

In order to include a thermal boundary layer with the same temperature difference as that in the experiment, the wall temperature was lowered from T_u to T_o at a time prior to quenching†. It was found that the effect of a thermal

† As long as the wall temperature was changed at least $5t_c$ before the maximum heat flux

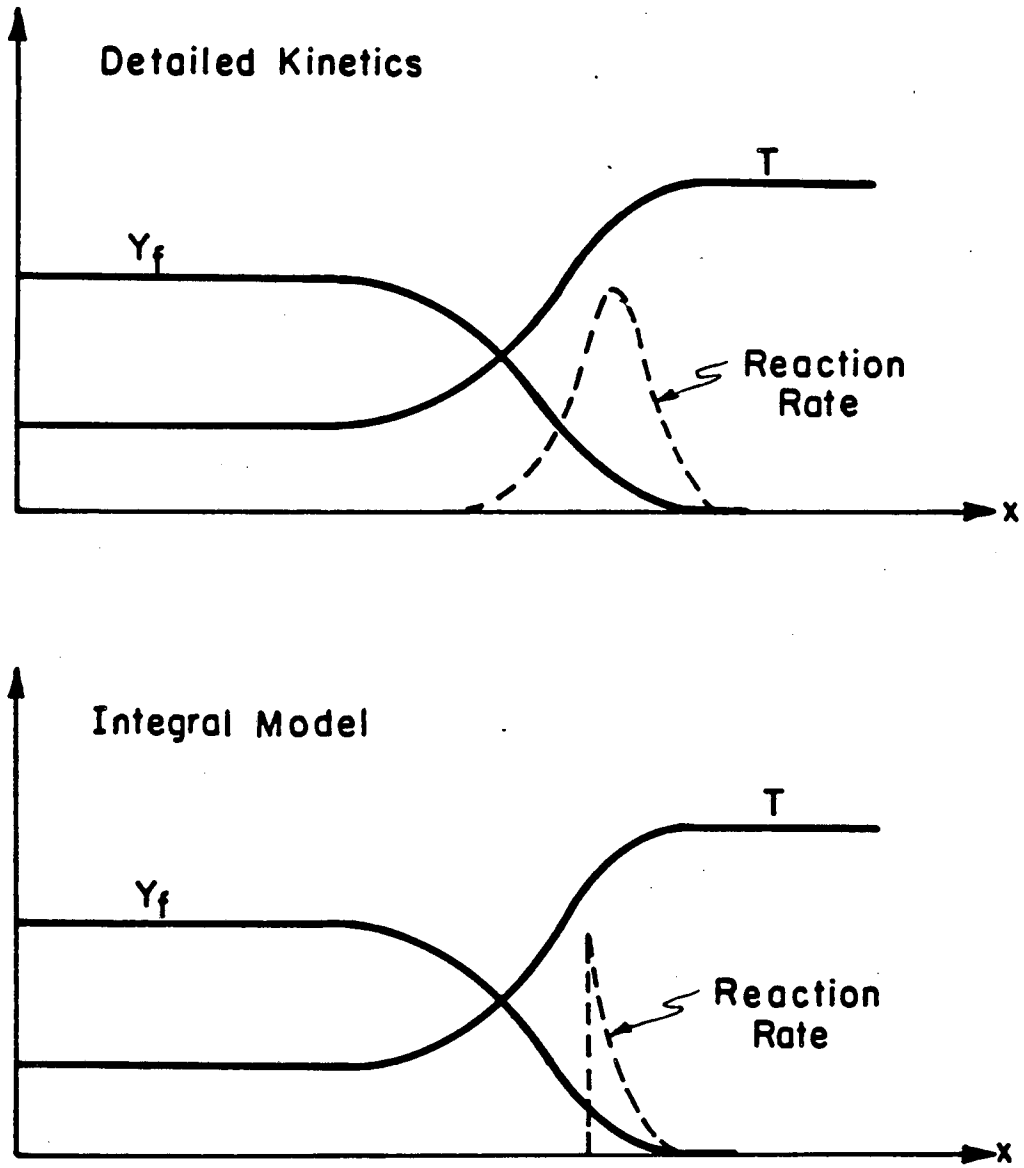

-- XBL 8411-4694 --

Figure 4.8

Comparison of integral and one step kinetics models - reaction zone size.

boundary layer, with the wall temperature lower than that of the surrounding gases, was to decrease the maximum wall heat flux, and to increase the time required for the flame to quench. The effect was quite drastic: when the temperature difference across the thermal boundary layer ($T_u - T_w$) was 5% of the temperature difference across the flame ($T_b - T_u$), the maximum heat flux decreased by 20% (from the case where $T_u - T_w = 0$), with a corresponding increase in the time required for quenching to occur.

To understand the cause of the decrease in the heat flux, consider the maximum flux to be a function of the wall temperature:

$$q_{w\,max}(T_w) = -k_w \left.\frac{\partial T}{\partial x}\right|_{w_{max}} \quad . \tag{4.3}$$

It was found that the temperature profile in the gas is not appreciably affected by a small change in the wall temperature, that is for

$$T_u - T_w \ll T_b - T_u \quad . \tag{4.4}$$

Thus the temperature gradient at the wall is insensitive to the wall temperature, providing that Equation 4.4 is satisfied. However, the thermal conductivity of the gas is strongly dependent upon temperature. For air near standard conditions, the thermal conductivity depends on the gas temperature as

$$k \sim T^{0.832} \quad . \tag{E.1}$$

Thus the maximum heat flux is dependent upon the wall temperature mainly through the variation of the thermal conductivity. For a change in the wall temperature from T_u to T_o Equation 4.3 therefore gives

$$\frac{q_{w\,max}(T_u)}{k_u} = \frac{q_{w\,max}(T_o)}{k_o} \quad . \tag{4.5}$$

Thus a change in the wall temperature of 100 K, which satisfies the condition of the wall temperature change being small (Equation 4.4), results in the maximum heat flux being decreased by the factor

occurred, the maximum heat flux and the time for quenching (t_q) were not affected.

$$\frac{q_{w\,max}(T_o)}{q_{w\,max}(T_u)} = \frac{k_o}{k_u} = 0.79 \quad .$$

The value of $q_{w\,max}(T_u)$ was found to vary linearly with q_c (cf. Equation 4.1). Substituting this result into Equation 4.5 gives

$$q_{w\,max}(T_o) = C_1 \frac{k_o}{k_u} q_c \quad .$$

Since the wall is assumed to be at the initial temperature, this may by written as

$$q_{w\,max}(T_w) = C_1 \frac{k_w}{k_u} q_c \tag{4.6}$$

By using Equation 4.6 the effect of the wall temperature may be determined.

As noted above, the time scale for quenching is also dependent on the wall temperature. The change in the time required for quenching can be obtained by considering the effect of the wall temperature on the diffusion of heat to the wall. The thermal diffusivity of the gas at the wall and the quenching distance give the characteristic time for quenching as:

$$t_q(T_w) \sim \frac{\delta^2(T_w)}{\alpha_w} \quad .$$

If it is assumed that the quenching distance is not affected by the thermal boundary layer (which corresponds to Equation 4.4 being satisfied), then the time for quenching, as defined in Chapter 3, may be written as

$$t_q(T_w) \sim \frac{\delta^2}{\alpha_w} \quad .$$

Thus we may write

$$\frac{t_q(T_w)}{t_q(T_u)} \approx \frac{\alpha_u}{\alpha_w} \quad . \tag{4.7}$$

In the absence of a thermal boundary layer the time for quenching was found to be linearly proportional to t_c (see Equation 4.2),

$$t_q(T_u) = C_2 t_c \quad . \tag{4.2}$$

Combining 4.7 and 4.2 gives

$$t_q(T_w) = C_2 \frac{\alpha_u}{\alpha_w} t_c \quad . \tag{4.8}$$

Using Equation 4.8, the effect of the wall temperature on the time required for quenching may be determined.

In summary, the effect of the thermal boundary layer on the heat transfer may by approximated as follows. The heat transfer to the wall in the absence of a thermal boundary layer is determined for the pressure at which quenching occurs, p_q, and with the wall at the temperature of the unburnt gases, T_u. This will be denoted as $q_w(T_u;t)$. With the wall at a different temperature, T_o, the heat flux as a function of time may be obtained from

$$q_w(T_w;t) = \frac{k_w}{k_u} q_w(T_u; \frac{\alpha_u}{\alpha_w} t) \quad . \tag{4.9}$$

In the next chapter, the numerical and the experimental results will be compared, and it will be shown that the above relation provides good agreement.

CHAPTER 5

COMPARISON OF EXPERIMENTAL AND NUMERICAL RESULTS

In this chapter, the experimental results are compared with the experimental work of others and the numerical calculations of this study. The experimental results will first be compared with the numerical results, accounting for the effects of thermal boundary layers. Similarities will then be shown to exist between the maximum heat flux and the quenching distance.

5.1 EXPERIMENTAL RESULTS AND MODELING

As previously discussed, the experimental conditions and the numerical calculations differed by the value of their wall temperatures. In the experiment, the wall temperature was approximately constant, differing only slightly from the initial wall temperature. As the pressure within the experimental apparatus increased, the gases underwent compression heating, causing a thermal boundary layer to develop between the wall and the unburnt gases. In order to avoid difficulties in modeling the unsteady boundary layer, the small temperature difference across the thermal boundary layer was neglected in the numerical calculations by choosing a wall temperature equal to the unburnt gas temperature (see Chapter 4). In order to be consistent, the pressure variation was neglected during quenching.

The effect of the thermal boundary layer during quenching was discussed in section 4.4. To include this effect it was found that the heat flux during quenching should be modified by the ratio of the thermal conductivities across the thermal boundary layer with the time scale modified by the ratio of the thermal diffusivities across the boundary layer; i.e.

$$q_w(T_w;t) = \frac{k_u}{k_w} q_w\left(T_u;t\frac{\alpha_w}{\alpha_u}\right) \quad . \tag{4.9}$$

It will be shown that the above relation accounts for the observed trends in the heat flux and in the time scale.

From Equation 4.9, the maximum heat flux and the time for quenching are functions of the wall temperature:

$$\left.\begin{aligned} \frac{q_{w\,max}(T_w)}{q_c} &= \frac{k_u}{k_w}\left[\frac{q_{w\,max}(T_u)}{q_c}\right] \\ \frac{t_q(T_w)}{t_c} &= \frac{\alpha_w}{\alpha_u}\left[\frac{t_q(T_u)}{t_c}\right] \end{aligned}\right\} \quad (5.1)$$

Using the gas property variation derived in Appendix E, and the values of $q_{w\,max}(T_u)$ and $t_q(T_u)$ as calculated using the one step kinetics model (Equations 4.1 and 4.2), Equation 5.1 is in agreement with the correlation of the experimental results (Equation 3.1 and 3.2) to within 15 %. Thus the pressure scaling applied to the data in Chapter 3 to account for trends in the heat flux appears to properly include the effect of the thermal boundary layer on the heat flux. The nondimensional results obtained by using Equation 4.9 to correlate the data are in excellent agreement with the data presented in Figures D.15 to D.28.

With the interpretation presented above, the starred quantities t^* and q^* as defined in Equation 3.3, and the values for t^*_q and $q^*_{w_{max}}$ presented in Table 3.2, are now the calculated time and heat flux corrected for the effects of the thermal boundary layer. In other words, t^* and q^* can be interpreted as representing hypothetical values which would result if the wall was at the temperature of the unburnt gases, T_u†. The variations of t^*_q and $q^*_{w_{max}}$ with pressure are shown in Figures 5.1 and 5.2 for the experimental results (from Figures 3.3 and 3.5), for the pressure scaled experimental results (from Figures 3.8 and 3.9), and for the one step kinetics model (from Figures 4.2 and 4.3). From Figures 5.1 and 5.2 it is seen that the scaling proposed for the effect of the thermal boundary

† In the models discussed in Chapter 4, the wall tremperature was equal to T_u, and thus $t = t^*$ and $q = q^*$.

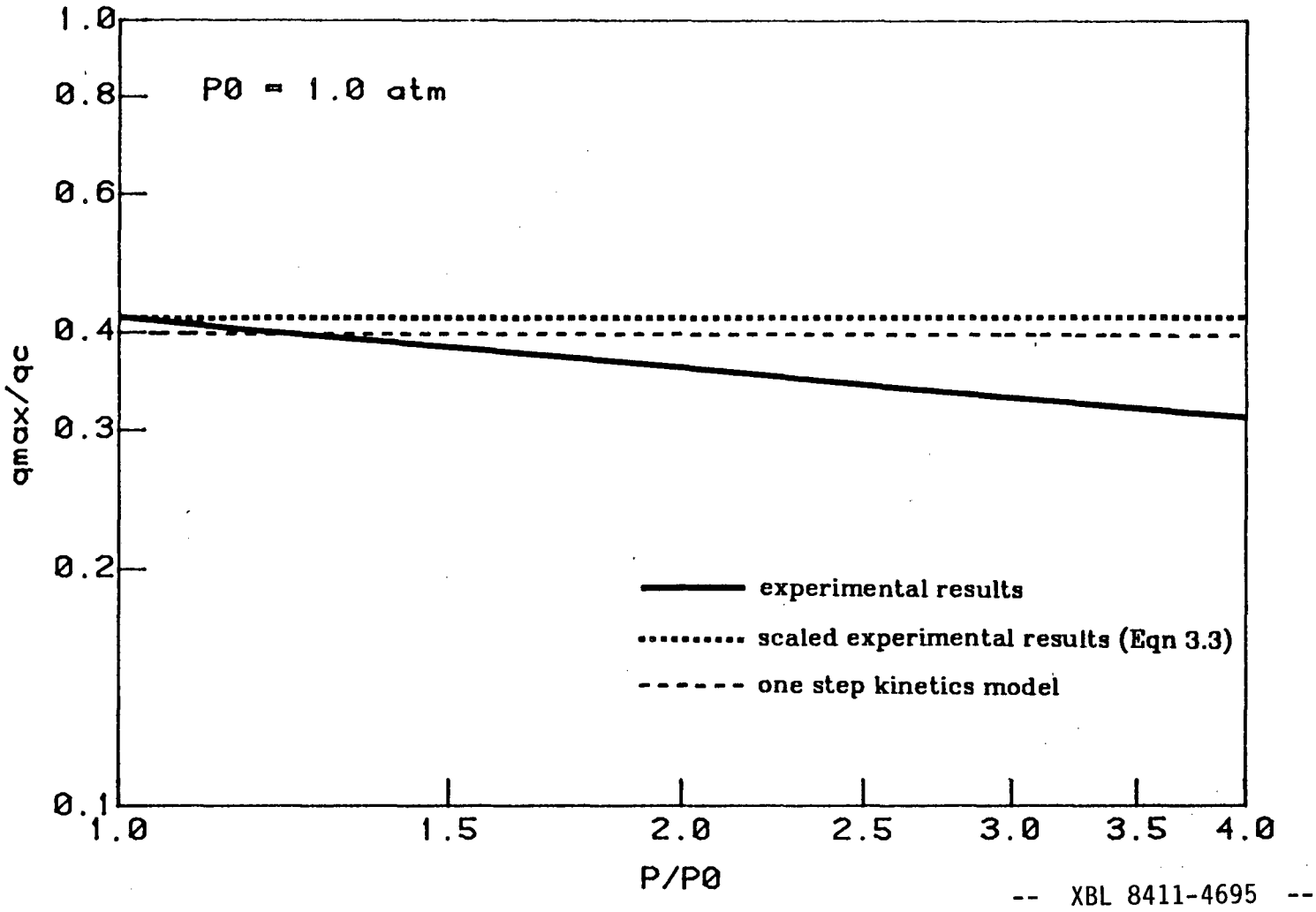

Figure 5.1 Comparison of experimental results, pressure scaled experimental results (Eqn 3.3), and one step kinetics model - maximum wall heat flux vs. pressure.

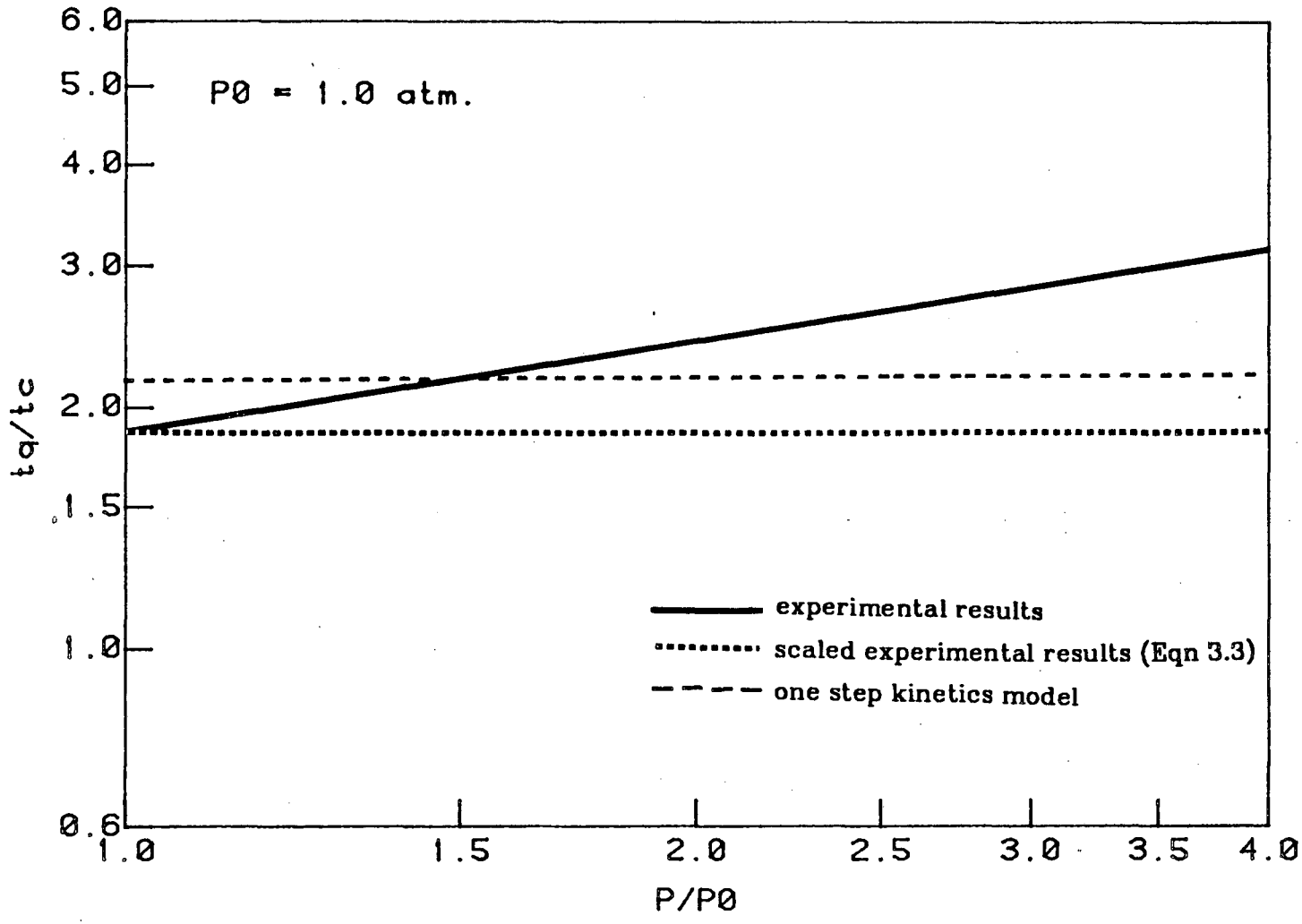

-- XBL 8411-4696 --

Figure 5.2 Comparison of experimental results, pressure scaled experimental results (Eqn 3.3), and one step kinetics model - time for quenching vs. pressure.

layer yields good agreement between the numerical results and the experimental results. The agreement between experiment and model are better seen in Figure 5.3, in which the range of results, in the form of heat flux versus time are superimposed. The two set of data agree to within the experimental uncertainty, approximately 8%.

Using the integral method, the variation of the heat flux with respect to P and φ are the same as those obtained from the other calculations, and the pressure scaled experiment results. Recall that the ignition temperature (see Equation C.21) was chosed to give the best agreement with the experimental data and the other models. As discussed in section 4.3, the integral method compared best with the one step kinetics model for a dimensionless ignition temperature of ϑ_{ig} = 0.70. In Figure 5.4, the results of the integral method are shown with the pressure scaled experimental results. Excellent agreement between the integral method and the pressure scaled experimental results is obtained for a ϑ_{ig} of 0.70. Thus the integral method, with ϑ_{ig} = 0.70, predicts the measured heat flux nearly as well as the one step kinetics model. In addition, the value of ϑ_{ig} which agreed best with the other results corresponds to a reaction zone thickness which is approximately the same as the minimum approach distance of the flame (quench distance). This is consistent with the results from the other calculations.

5.2 COMPARISONS WITH OTHER RESULTS

5.2.1 HEAT TRANSFER EXPERIMENTS

Measurements of the steady state heat transfer from one dimensional porous burner butane flames have been made by Yamazaki & Ikai (1971), who also successfully modeled the heat transfer using a thermal model of flame propagation. Their results for the heat transfer rate ($\frac{q_w}{q_c}$) are from 5 to 10 times

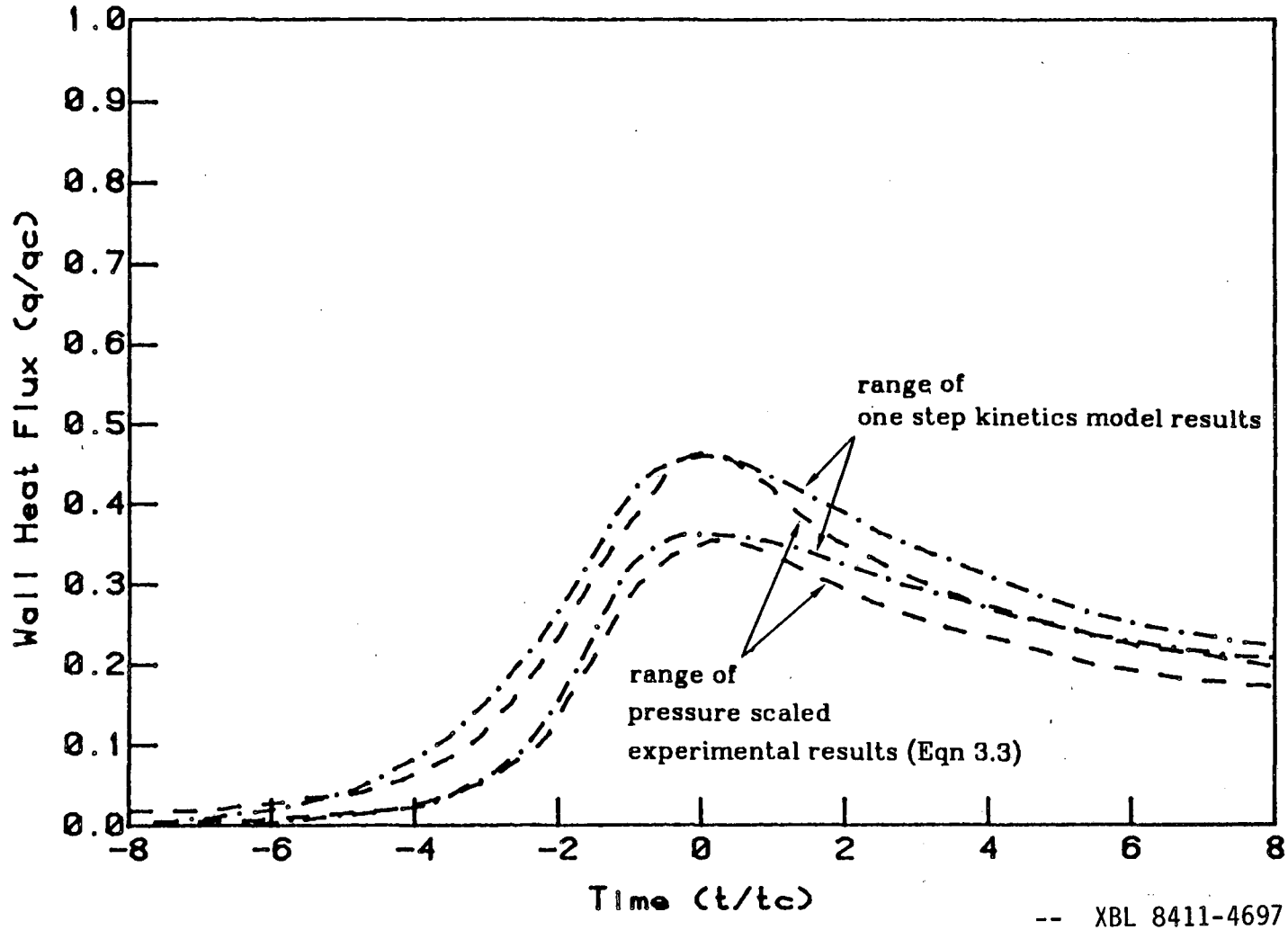

-- XBL 8411-4697 --

Figure 5.3 Comparison of pressure scaled experimental results (Eqn 3.3) and one step kinetics model - wall heat flux vs. time.

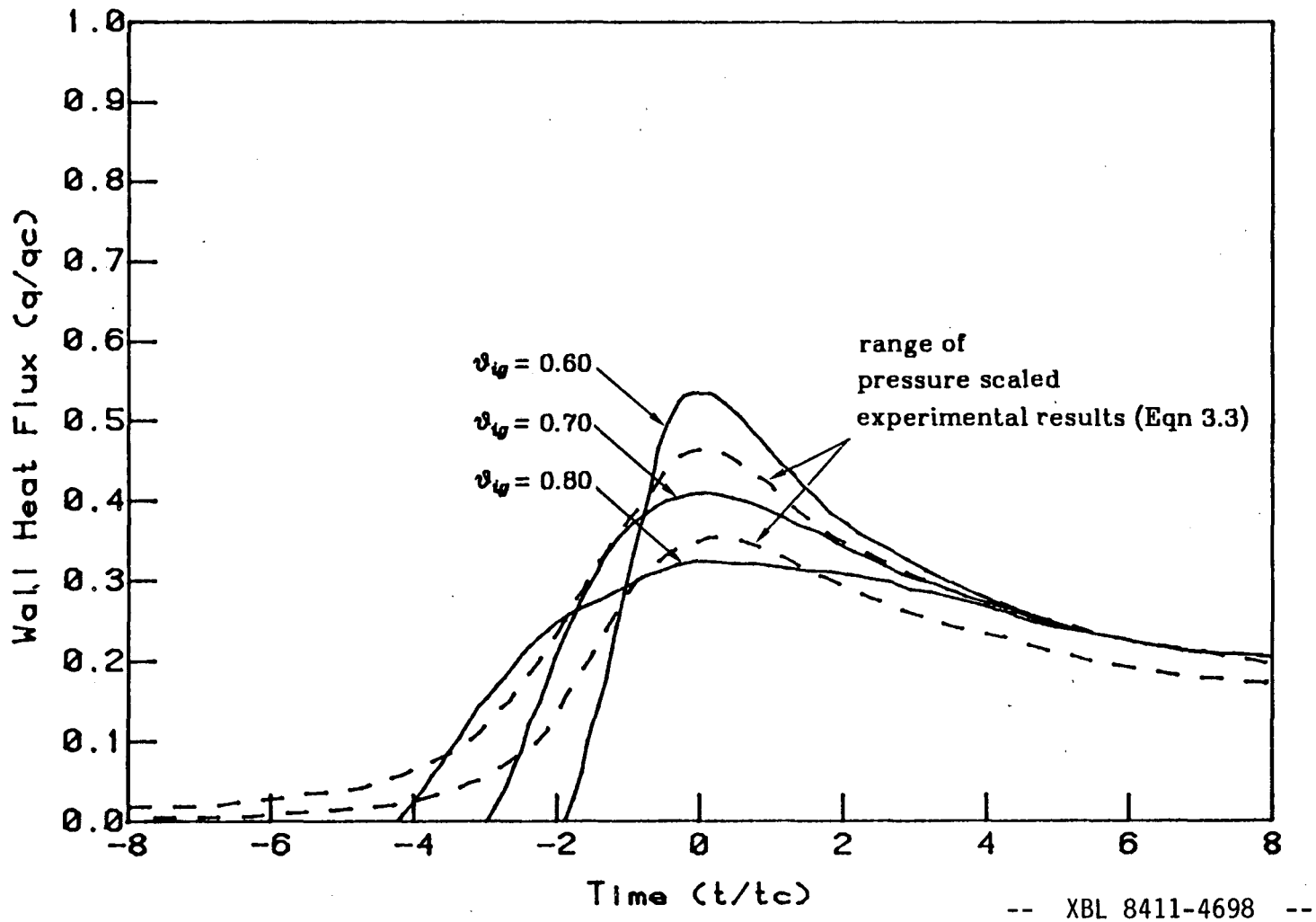

Figure 5.4 Comparison of pressure scaled experimental results (Eqn 3.3) and integral model - wall heat flux vs. time.

less than the values which were measured in the present study. Thus it appears that the heat transfer during unsteady one dimensional flame quenching is much greater than that for one dimensional flames on porous burners. While there are great differences between the heat flux for the two cases, it is noted that the porous burner has wall blowing, which differs significantly from the present problem, which has an impermeable wall.

Unsteady heat transfer measurements during flame quenching have been made under a variety of conditions. These include experiments in shock tubes [Keiper & Spurk, 1981 ; Heperkan, 1980], combustion chambers [Woodard, 1982 ; Isshiki & Nishiwaki, 1974], and internal combustion engines [Annand, 1963 ; Alkidas & Meyer, 1979]. Only the experiments of Isshiki & Nishiwaki are directly comparable to those of Chapter 3. In their study, measurements were made of one dimensional hydrogen-oxygen flames in as apparatus with instrumentation similar to that of this study.

An approximate analytic solution for the heat flux was obtained by Isshiki & Nishiwaki assuming

$$k = k_o \left(\frac{T}{T_o} \right) \quad .$$

The maximum heat flux was found to be given by (see Appendix F)

$$q_{w\,max}(T_o) = \frac{2k_o \Delta T_f}{\left(p_o \alpha_o t_f\right)^{1/2}} \left(\frac{p_q}{p_o} \right)^{1/2} \quad , \tag{F.6}$$

where the subscript i refers to the initial state ($T = T_o$, $p = p_o$), and t_f *is the total time required* for *quenching*, as determined from wall temperature measurements†. The value for t_f was obtained from measurements of the (variable) wall temperature. The agreement between the experimental values of the maximum heat flux and the maximum value obtained from Equation F.6 was quite

† The time t_f is not to be confused with t_q, defined in Chapter 3, which is the time required for the heat flux to rise from 50% to 100% of its maximum value

good (see Figure 5.5).

In order to simplify the comparison of the work of Isshiki & Nishiwaki with the present study, the characteristic heat flux from Equation (E.19), q_c, and the characteristic time from Equation (E.18), t_c, are substituted into Equation F.6 to give

$$\frac{q_{w\,max}(T_w)}{q_c}\left[\frac{t_f\,(T_w)}{t_c}\right]^{1/2} = constant \quad , \tag{F.7}$$

where the notation T_w has been used for T_o.

In the present study, it is predicted that the maximum heat flux and time for quenching are given by

$$\frac{q_{w\,max}(T_w)}{q_c} = C_1\frac{k_w}{k_u} \tag{4.6}$$

$$\frac{t_q\,(T_w)}{t_c} = C_2\frac{\alpha_u}{\alpha_w} \quad . \tag{4.8}$$

Equations 4.6 and 4.8 may be combined to give

$$\frac{q_{w\,max}(T_w)}{q_c}\left[\frac{t_q\,(T_w)}{t_c}\right]^{1/2} = C_1 C_2^{1/2}\left[\frac{k_w\rho_w c_{p\,w}}{k_u\rho_u c_{p\,u}}\right]^{1/2} \quad .$$

The time t_f was defined as the time for quenching to occur, while t_q was the time required for the wall heat flux to rise from 50% to 100% of its maximum value. From the experimental data, we have that

$$t_q\,(T_w) \approx \frac{t_f\,(T_w)}{2} \quad .$$

Over the range of conditions considered in this study, $\left[\frac{k_w\rho_w c_{p\,w}}{k_u\rho_u c_{p\,u}}\right]^{1/2}$ varied by less than 4%. Thus the above relation for the maximum heat flux is in the form:

$$\frac{q_{w\,max}(T_w)}{q_c}\left[\frac{t_f\,(T_w)}{t_c}\right]^{1/2} \approx constant \tag{5.2}$$

which is the same as the result of Isshiki & Nishiwaki (Equation F.7).

Isshiki & Nishiwaki showed that Equation F.6 successfully correlated the maximum heat flux on the basis of the experimentally determined time

required for quenching, t_f (see Figure 5.5). The results of this work (Equation 4.6 and 4.8) reduce to the result of Isshiki & Nishiwaki, and more importantly provide a basis for correlating the time and heat flux independently. In addition, the results of the present study provide a method for incorporating the effects of thermal boundary layers on the heat flux.

5.2.2 THE RELATIONSHIP OF THE HEAT FLUX TO THE QUENCHING DISTANCE

Methods for measuring the quenching distance include: optical measurements of the closest approach of a flame, standoff distances of porous burner flames, measurements of the minimum gap through which a flame can propagate, and igniting the mixture across a narrow gap. Only the first of these methods measures quenching for a one dimensional flame and it is a difficult measurement to make.

In the analysis that follows it will be shown that the the quenching distance is related to the maximum heat flux during quenching, and thus correlations of the quenching distance may be useful in predicing the maximum heat flux during quenching.

The maximum wall heat flux is given by

$$q_{w\,max}(T_w) = -k_w \left.\frac{\partial T}{\partial x}\right|_{w,max} \quad , \tag{5.3}$$

where $q_{w\,max}(T_w)$ is the maximum flux with a wall temperature of T_w. A characteristic distance for quenching, d, is obtained from:

$$\left.\frac{\partial T}{\partial x}\right|_{w,max} \equiv -\frac{\Delta T_f}{\delta_T} \quad . \tag{5.4}$$

Where ΔT_f is the the temperature difference across the flame, and the distance, δ_T, is a characteristic distance for the quenching process†. This distance is not

† Recall from section 4.4 that the value of the maximum temperature gradient at the wall is insensitive to the wall temperature for values of $T_u - T_w \ll \Delta T_f$.

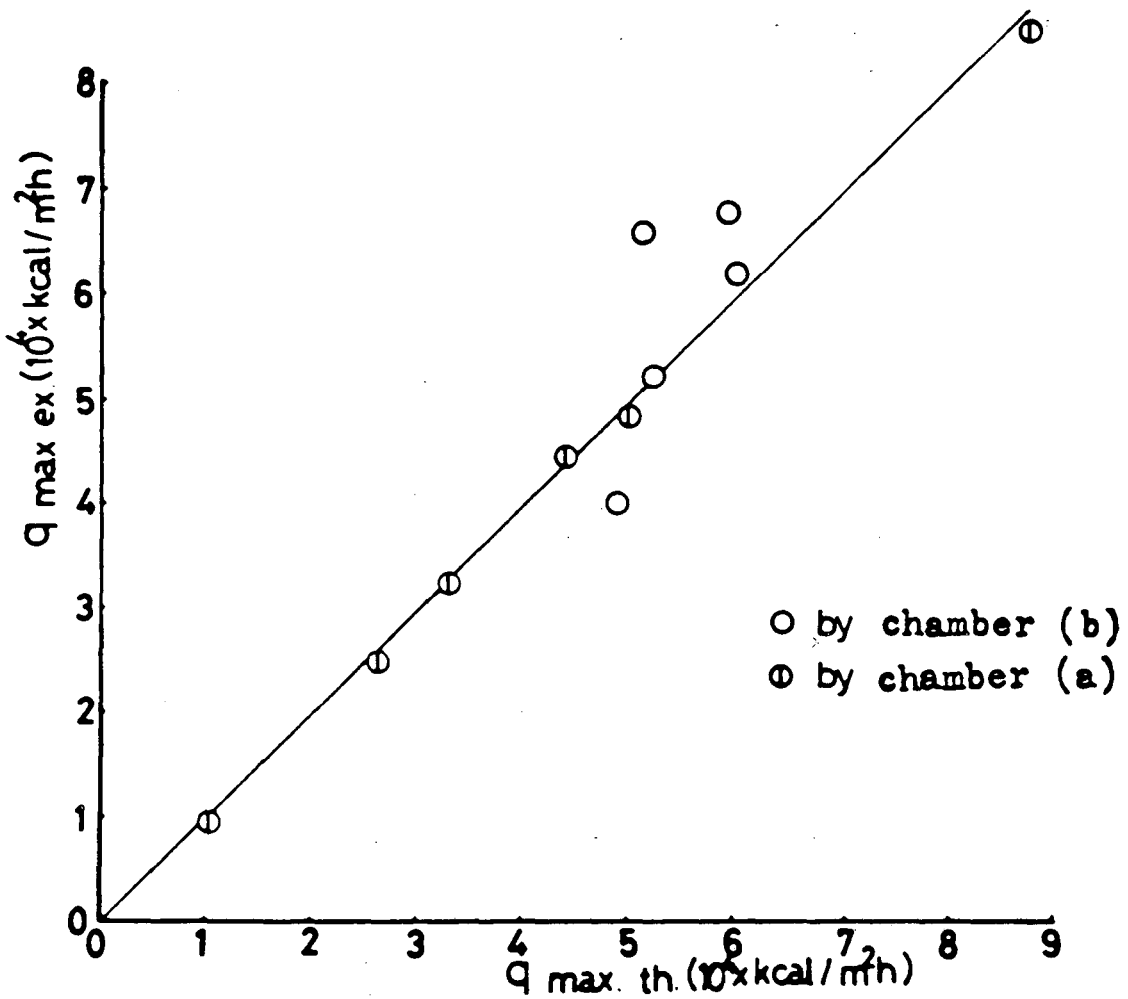

-- XBL 8411-4699 --

Figure 5.5 Results of Isshiki & Nishiwaki

the same as quenching distances that are measured in ignition studies. However, since the ignition and quenching processes are both known to be controlled by thermal effects it is felt that there should be a correlation between the distance defined in Equation 5.4, and that obtained from measurements in ignition studies.

From Equations 5.3 and 5.4 we obtain

$$\frac{S_u \delta_T}{\alpha_u} = \frac{S_u \left[\dfrac{\Delta T_f k_w}{q_{w\,\max}(T_w)} \right]}{\left[\dfrac{k_u}{\rho_u c_{p_u}} \right]}$$

$$= \frac{q_c}{q_{w\,\max}(T_w)} \frac{k_w}{k_u} \quad , \tag{5.5}$$

where

$$q_c \equiv \rho_u S_u c_{p_u} \Delta T_f \quad . \tag{E.19}$$

S_u is the laminar flame speed, and α_u is the thermal diffusivity of the unburnt gas. The Peclet number for quenching, based on the properties of the unburnt gas is defined as:

$$Pe_u = \rho_u S_u \frac{c_{pu}}{k_u} \delta_T = \frac{S_u \delta_T}{\alpha_u} \quad . \tag{5.6}$$

Where dg is the quenching distance as determined from Equation 5.4. Taking this to be the value determined from the temperature profile in Equation 5.4, Equations 5.5 and 5.6 give:

$$Pe_u = \frac{q_c}{q_{w\,\max}(T_w)} \frac{k_w}{k_u} \tag{5.7}$$

From experimental and theoretical studies of both steady two dimensional and unsteady one dimensional quenching, the Peclet number for the quenching distance is shown to be a function of the kinetics constants for the fuel used. Depending on the nature of the analysis, the important parameter is shown to

be the Peclet number for the quenching distance based on either the unburnt gas properties [Kurkov, 1967 ; Ishikawa, 1978], or on the burnt gas properties [Westbrook, et.al., 1981 ; Furguson & Keck, 1977]. It was found in this study that the distance defined in Equation 5.4 correlates as the Peclet number based on the unburnt gas properties.

In the one step kinetics model, with $T_w = T_u$, it was predicted that $q_{w\,max}(T_u) = 0.40 q_c$ (cf. Equation 4.1). Using this result, 5.7 reduces to

$$Pe_u = 2.50 \quad . \tag{5.8}$$

From the experimental results, we have

$$\frac{q_{w\,max}(T_w)}{q_c} = 0.42 \left[\frac{p_q}{p_o}\right]^{-0.209} \quad , \tag{3.1}$$

and from the properties of gas mixtures near room temperature (Appendix E),

$$\frac{k_u}{k_w} = \left[\frac{T_u}{T_w}\right]^{0.881} \quad .$$

Assuming adiabatic compression of the gas far from the wall,

$$\frac{k_u}{k_w} = \left[\frac{p_q}{p_o}\right]^{\frac{\gamma-1}{\gamma}(0.881)} = \left[\frac{p_q}{p_o}\right]^{0.291} \quad , \tag{5.9}$$

and the Peclet number using Equation 5.7, 5.8 and 5.9 is:

$$Pe_u = 2.38 \quad .$$

This value is within 5% of the numerically determined value (Equation 5.8). Thus, as in section 4.4, the effect of the thermal boundary layer is again seen to be properly accounted for by considering the variation of the thermal properties of the reactant through the thermal boundary layer.

The nondimensional maximum heat flux during unsteady flame quenching has been shown to be equal to the Peclet number for the quenching distance (Equation 5.7). In addition, it has been shown that the experimental results and the numerical results both predict the same constant value for the Peclet number. Based on these results, it appears that it should be possible to utilize

correlations of the Peclet for the quenching distance in predicting the maximum value of the unsteady heat flux.

CHAPTER 6

CONCLUSIONS AND RECOMMENDATIONS

6.1 CONCLUSIONS

6.1.1 EXPERIMENTAL RESULTS

Measurements have been made of the heat transfer to a wall during the quenching of a premixed, methane-air flame. The geometry of the interaction of the flame with the wall was essentially one dimensional, and the flame was laminar prior to quenching. The experiments were preformed over a range of pressures from 1 to 4 atmospheres and over a range of equivalence ratios from 0.7 to 1.2.

1) From the comparison of bare platinum, coated platinum, and nickel gauges, it may be concluded that the measurements made for this study were independent of the gauge material. Since catalytic effects were not observed, they were either:

    a) not important due to the low temperature (320 °K) of the platinum surface,

    b) not present due to degradation of the platinum surface from repeated use, or

    c) were less than the experimental uncertainty of 8%.

2) The data were successfully correlated on the basis of the heat release rate in a steady, laminar flame. This incorporated the effects of the equivalence ratio and the pressure.

3) There is a very strong connection between the experimental maximum heat flux and the experimental values of the quenching distance. It may be pos-

sible to use these results in conjunction with measurements of the quenching distance for other fuels to infer the corresponding heat fluxes.

6.1.2 EXPERIMENTAL AND NUMERICAL RESULTS

For the range of experimental conditions covered, a comparison of the experimental results and the numerical calculations yields the following:

1) Omitting the effect of the thermal boundary layers at the wall increases the maximum heat flux and decreases the time required for quenching to occur.

2) If the temperature difference across the thermal boundary layer is much less than the temperature difference across the flame, an approximate method for incorporating the effects of the thermal boundary layer may be used (Equation 4.9).

3) The changes in the heat flux and in the time required for quenching due to the thermal boundary layer are proportional to the thermal conductivity of the gas evaluated at the wall temperature. In addition, for wall temperatures near the unburnt gas temperature, the total heat transferred to the wall is found to be insensitive to the wall temperature.

4) A one dimensional finite difference model with one step Arrhenius kinetics predicts the heat transfer to an accuracy of 15%.

5) Integral equations may be used to predict the heat transfer to the wall if the Arrhenius temperature dependence of the reaction rate is replaced by an ignition temperature. The one dimensional integral species and energy equations, in conjunction with one step ignition temperature kinetics, predict the heat transfer nearly as well as the one step kinetics, finite difference model. For methane air flames at pressures varying from one to four atmospheres, and equivalence ratios varying from 0.70 to 1.20, the

integral method gives good results for the heat transfer during quenching for an ignition temperature T_{ig} given by

$$T_{ig} = T_b - 0.70(\Delta T_f) \quad ,$$

where T_b is the burnt gas, or flame temperature, and ΔT_f is the temperature rise across the flame.

5) The integral model provides a good estimate of the heat transfer during quenching with only a modest computational effort.

6) Although the integral equations, with ignition temperature kinetics, are much less complete than the other two formulations, they do incorporate the essential transport phenomena and kinetics. Specifically, a comparison of the results of the integral model with the experimental results indicates that the thermal diffusivity and the chemical reaction rate of combustion are the dominant processes which determine the heat flux during quenching.

6.2 RECOMMENDATIONS FOR FURTHER RESEARCH

For flame quenching under at nearly constant pressure, the effects of equivalence ratio and pressure on the unsteady heat transfer were shown to be the same as the effects on steady laminar flames. The experimental range of conditions was actually quite narrow when one considers the broad range of conditions that exist in practical systems. In particular, the pressures tested were several times less than those encountered in internal combustion engines. Furthermore, the flow field was laminar and one dimensional. The following recommendations are therefore made which should help expand the knowledge of the quenching process and thereby increase our understanding of the performance of practical systems.

Experiments should be performed with one dimensional laminar flames at

elevated pressures. The important kinetics mechanisms change with pressure: those which are important at several atmospheres are not the same as those which are important at one atmosphere. Since the kinetics do change, modifications would have to be made to the one step kinetics models.

More complex hydrocarbons should be used. Methane produces much less soot than do heavier fuels. As a result, radiation heat transfer should be more important with heavier fuels.

Two dimensional turbulent flows should be studied. Constant volume combustion chambers can be modified so that these effects are present. Experiments of this type are inherently more complex, since velocity measurements near the wall must be made in order to characterize the flow conditions.

In the modeling of quenching in flows which are multidimensional, the integral approach with ignition temperature kinetics may still prove to be useful, since the quenching seems to be insensitive to the actual form of the kinetics used.

APPENDIX A

DETERMINATION OF THE WALL HEAT FLUX FROM THE WALL TEMPERATURE VARIATION

For a semi-infinite slab with constant properties and a specified wall temperature variation, the wall heat flux is given by [Carslaw & Jaeger, 1948]

$$q_w(t) = \left[\frac{k_s \rho_s c_{p_s}}{\pi}\right]^{1/2} \int_0^t \frac{dT_w(\lambda)}{d\lambda} \frac{d\lambda}{\sqrt{t-\lambda}} \quad . \tag{A.1}$$

From the experiment, the wall temperature is known only at times that are an interval Δt apart. Defining:

$$t \equiv N\Delta\lambda \quad ;$$

and

$$\lambda_j \equiv j\Delta\lambda \quad ;$$

Equation (A.1) can be rewritten as

$$q_w(t) = \left[\frac{k_s \rho_s c_{p_s}}{\pi}\right]^{1/2} \sum_{j=0}^{N-1} \left\{ \int_{\lambda_j}^{\lambda_{j+1}} \frac{dT_w(\lambda)}{d\lambda} \frac{d\lambda}{\sqrt{t-\lambda}} \right\} \quad . \tag{A.2}$$

In order to proceed further, some assumptions must be made as to the variation of the temperature between times λ_j and λ_{j+1}. It will be assumed here that the temperature increases linearly with time, giving

$$\frac{dT_w(\lambda)}{d\lambda} = \frac{T_w(\lambda_{j+1}) - T_w(\lambda_j)}{\lambda_{j+1} - \lambda_j} \quad ; \quad \lambda_j < \lambda < \lambda_{j+1} \quad .$$

Defining:

$$T_j \equiv T_w(\lambda_j) \quad ;$$

$$\Delta T_j \equiv T_{j+1} - T_j \quad ;$$

$$\Delta\lambda \equiv \lambda_{j+1} - \lambda_j \quad ;$$

the integral in equation (A.2) therefore becomes

$$\int_{\lambda_j}^{\lambda_{j+1}} \frac{dT_w(\lambda)}{d\lambda} \frac{d\lambda}{\sqrt{t-\lambda}} \approx \frac{\Delta T_j}{\Delta\lambda} \int_{\lambda_j}^{\lambda_{j+1}} \frac{d\lambda}{\sqrt{t-\lambda}} \quad . \tag{A.3}$$

Integrating equation (A.3),

$$\approx \frac{2\Delta T_j}{\Delta\lambda}\left[\sqrt{t-\lambda_j} - \sqrt{t-\lambda_{j+1}}\right] \quad ,$$

or

$$\approx \frac{2\Delta T_j}{\sqrt{\Delta\lambda}}\left[\sqrt{N-j} - \sqrt{N-j-1}\right] \quad .$$

Thus the heat flux is given by

$$q_w(t) = 2\left(\frac{k_s \rho_s c_{p_s}}{\pi \Delta t}\right)^{1/2} \sum_{j=0}^{N-1} \left(\Delta T_j \Delta\sqrt{\tau_{N-j-1}}\right) \quad , \tag{A.4}$$

where

$$\Delta T_j = T_w(\lambda_{j+1}) - T_w(\lambda_j)$$

and

$$\Delta\sqrt{\tau_{N-j-1}} = \sqrt{N-j} - \sqrt{N-j-1} \quad .$$

Computer Program - Heat Flux From Wall Temperature

```
      Subroutine Qsolid(T,Q,reclen,period)
c
c     reclen = length of the input file
c     period = time between data points, microseconds
c
c  The temperature and the heat flux are in S.I. units.
c     T is the input file,(temp) and is one collumn wide and "reclen" long
c     Q is the ouput file, & has the temp in col. 1 and q in col.2
c  Time=0 corresponds to  J=0. Assume that T(0)=T(1), giving Q(0)=Q(1)=0.
c
      Integer reclen,period
      Real T(reclen),Q(reclen)
      Real DTemp(2000)
      Real RT(2000)
c
c  Properties of the solid (Macor)
c
      dens = 2352.
      cond = 1.675
      spht = 460.
      pi = 3.1416
      dt = period * 1.0E-6
      const = 2.0 * ((cond*dens*spht/(pi*dt))**0.5)
c
c  Compute values which are used often
c
      Do 150 J = 1, reclen-1
      DTemp(J) = T(J+1) - T(J)
      RT(J) = Sqrt(Float(J)) - Sqrt(Float(J-1))
  150 Continue
c
c  Duhamel's integral using
c
      Q(1) = 0.0
      Do 300 N = 2, reclen
      S = 0.0
      Do 200 J = 1, N-1
      S = S + DTemp(J) * RT(N-J)
  200 Continue
      Q(N) = const * S
  300 Continue
      Return
      End
```

APPENDIX B

THE GOVERNING EQUATIONS

Several forms of the conservation equations were used in the numerical work described in Chapter III. In this appendix, the derivation of these equations will be presented, starting with the most general form.

B.1 THE GENERAL EQUATIONS

As explained in Chapter II, the geometry of interest is nearly one dimensional. The appropriate governing equations are [Williams,1965] the conservation of:

mass

$$\frac{\partial \rho}{\partial t} + \frac{\partial \rho u}{\partial x} = 0 \quad , \tag{B.1}$$

momentum

$$\rho \frac{Du}{Dt} = - \frac{\partial}{\partial x}(p + \tau) \quad , \tag{B.2}$$

the energy equation in terms of the enthalpy

$$\rho \frac{Dh}{Dt} = - \frac{\partial q}{\partial x} + \frac{Dp}{Dt} - \tau \frac{\partial u}{\partial x} \quad , \tag{B.3}$$

and the conservation of species

$$\rho \frac{DY_i}{Dt} = \omega_i - \frac{\partial j_i}{\partial x} \quad ; \quad i = 1,2,...N \quad . \tag{B.4.i}$$

where N is the number of species present.

The enthalpy is given by

$$h = \sum_{i=0}^{N} Y_i h_i \quad , \tag{B.5}$$

where h_i is the enthalpy of species i. For one dimensional flow, the shear stress is given by

$$\tau = -\left(\frac{4}{3}\mu + \kappa\right)\frac{\partial u}{\partial x} \quad . \tag{B.6}$$

Expressions for the heat flux, q, and the mass flux, j_i, will be derived using the following assumptions:

1) The dominant mechanism of species diffusion is by gradients of concentration, which may be represented by a term analogous to Fickian diffusion for binary mixtures. Thus the Soret, Dufour, and pressure gradient mechanisms are neglected.

2) Radiant heat transfer is neglected.

3) The pressure far from the wall is uniform.

4) Depending on the model, the species production term will either take an Arrhenius form, or an ignition temperature form (cf. Eqn C.1 and C.24).

Assumption 1) allows the mass flux of species i to be written as

$$j_i = -\rho D_i \frac{\partial Y_i}{\partial x} \tag{B.7}$$

and assumptions 2) gives

$$q = -k\frac{\partial T}{\partial x} + \sum_{i=0}^{N} j_i h_i \quad ,$$

or, using B.7,

$$q = -k\frac{\partial T}{\partial x} - \rho\sum_{i=0}^{N} h_i D_i \frac{\partial Y_i}{\partial x} \quad . \tag{B.8}$$

From assumption 3),

$$\frac{\partial p}{\partial x} \approx 0 \quad ,$$

and thus

$$\frac{Dp}{Dt} \approx \frac{dp}{dt} \quad .$$

The production term, ω_i, is different in each of the three models used in Chapter IV. The details of the form of ω_i are presented in Appendix C.

B.2 MASS TRANSFORMATION

If the transformation is made to the mass coordinates, then the continuity equation (B.1) is satisfied identically. This proved to be useful when used in conjunction with the integral method, since no informations was needed in the physical coordinates, and because the number of equations was reduced.

The mass coordinates, (ψ,t), are defined by

$$\frac{\partial \psi}{\partial x} = \frac{\rho}{\rho_r} \quad , \qquad \text{(B.9)}$$
$$\frac{\partial \psi}{\partial t} = -\frac{\rho u}{\rho_r} \quad .$$

In the (ψ,t) coordinate system, the time derivative becomes

$$\left.\frac{\partial}{\partial t}\right|_x = \left.\frac{\partial}{\partial t}\right|_\psi + \left.\frac{\partial \psi}{\partial t}\frac{\partial}{\partial \psi}\right|_t$$
$$= \left.\frac{\partial}{\partial t}\right|_\psi - \left.\frac{\rho u}{\rho_r}\frac{\partial}{\partial \psi}\right|_t \quad ,$$

and the spatial derivative becomes

$$\left.\frac{\partial}{\partial x}\right|_t = \left.\frac{\rho}{\rho_r}\frac{\partial}{\partial \psi}\right|_t \quad .$$

The substantial derivative, $\frac{D}{Dt}$, then becomes

$$\frac{D}{Dt} \equiv \left.\frac{\partial}{\partial t}\right|_x + u\left.\frac{\partial}{\partial x}\right|_t$$
$$= \left.\frac{\partial}{\partial t}\right|_\psi \quad .$$

APPENDIX C

NUMERICAL MODELS

The three numerical models used differed mainly by assumptions of the kinetics of methane-air combustion. The three models will be referred to here as "detailed kinetics", "one step kinetics", and "integral method" models.

C.1 DETAILED KINETICS

Calculations involving a detailed description of the kinetics of methane - air combustion were preformed using the computer program HCT [Lund, 1978].

Assumptions concerning the transport processes are outlined in Appendix B. Information on the kinetics was compiled from current work concerning the combustion of methane, involving 16 chemical species and 46 chemical reactions [Westbrook, et al, 1981].

All chemical reactions were considered to be elementary reactions, and as such the reaction rate is given by

$$\omega_k = f_k(T)\prod_i^N C_i \quad . \tag{C.1}$$

where

$$f_k(T) = A_k T^{b_k} \exp\left[-\frac{E_k}{RT}\right] \quad . \tag{C.2}$$

N is the number of species, and k is the reaction number.

Incorporated in the program HCT are modifications to C.1 and C.2 to aid in the efficiency of integrating the governing equations. The details of these modifications is given in Lund (1978). A list of the chemical reactions considered, and rate constants used, is given in Table C.1.

Table C.1
Table of Reaction Rates for
Detailed Kinetic Model of Methane-Air Combustion.
Rates in cgs units, $k = A\,T^n \exp(-E_a/RT)$

	Reaction	Forward rate log A	Forward rate n	Forward rate E_a	Reverse rate log A	Reverse rate n	Reverse rate E_a
1.	$H+O_2 \rightarrow O+OH$	14.27	0	16.79	13.17	0	0.68
2.	$H_2+O \rightarrow H+OH$	10.26	1	8.90	9.92	1	6.95
3.	$H_2O+O \rightarrow OH+OH$	13.53	0	18.35	12.50	0	1.10
4.	$H_2O+H \rightarrow H_2+OH$	13.98	0	20.30	13.34	0	5.15
5.	$H_2O_2+OH \rightarrow H_2O+HO_2$	13.00	0	1.80	13.45	0	32.79
6.	$H_2O+M \rightarrow H+OH+M$	16.34	0	105.00	23.15	-2	0.00
7.	$H+O_2+M \rightarrow HO_2+M$	15.22	0	-1.00	15.36	0	45.90
8.	$HO_2+O \rightarrow OH+O_2$	13.70	0	1.00	13.81	0	56.61
9.	$HO_2+H \rightarrow OH+OH$	14.40	0	1.90	13.08	0	40.10
10.	$HO_2+H \rightarrow H_2+O_2$	13.40	0	0.70	13.74	0	57.80
11.	$HO_2+OH \rightarrow H_2O+O_2$	13.70	0	1.00	14.80	0	73.86
12.	$H_2O_2+O_2 \rightarrow HO_2+HO_2$	13.60	0	42.64	13.00	0	1.00
13.	$H_2O_2+M \rightarrow OH+OH+M$	17.08	0	45.50	14.96	0	-5.07
14.	$H_2O_2+H \rightarrow HO_2+H_2$	12.23	0	3.75	11.86	0	18.70
15.	$O+H+M \rightarrow OH+M$	16.00	0	0.00	19.90	-1	103.72
16.	$O_2+M \rightarrow O+O+M$	15.71	0	115.00	15.67	-0.28	0.00
17.	$H_2+M \rightarrow H+H+M$	14.34	0	96.00	15.48	0	0.00
18.	$CO+OH \rightarrow CO_2+H$	7.11	1.3	-0.77	9.15	1.3	21.58
19.	$CO+HO_2 \rightarrow CO_2+OH$	14.18	0	23.65	15.23	0	85.50
20.	$CO+O+M \rightarrow CO_2+M$	15.77	0	4.10	21.74	-1	131.78
21.	$CO_2+O \rightarrow CO+O_2$	12.44	0	43.83	11.50	0	37.60
22.	$HCO+OH \rightarrow CO+H_2O$	14.00	0	0.00	15.45	0	105.15
23.	$HCO+M \rightarrow H+CO+M$	14.16	0	19.00	11.70	1	1.55
24.	$HCO+H \rightarrow CO+H_2$	14.30	0	0.00	15.12	0	90.00
25.	$HCO+O \rightarrow CO+OH$	14.00	0	0.00	14.46	0	87.90
26.	$HCO+HO_2 \rightarrow CH_2O+O_2$	14.00	0	3.00	15.56	0	46.04
27.	$HCO+O_2 \rightarrow CO+HO_2$	12.60	0	7.00	12.95	0	39.29
28.	$CH_2O+M \rightarrow HCO+H+M$	16.52	0	81.00	11.15	1	-11.77
29.	$CH_2O+OH \rightarrow HCO+H_2O$	12.88	0	0.17	12.41	0	29.99
30.	$CH_2O+H \rightarrow HCO+H_2$	14.52	0	10.50	13.42	0	25.17
31.	$CH_2O+O \rightarrow HCO+OH$	13.70	0	4.60	12.24	0	17.17

Table C.1 (Continued)
Table of Reaction Rates for
Detailed Kinetic Model of Methane-Air Combustion.
Rates in cgs units, $k = A\,T^n \exp(-E_a/RT)$

	Reaction	Forward rate log A	Forward rate n	Forward rate E_a	Reverse rate log A	Reverse rate n	Reverse rate E_a
32.	$CH_2O+HO_2 \rightarrow HCO+H_2O_2$	12.00	0	8.00	11.04	0	6.59
33.	$CH_4+M \rightarrow CH_3+H+M$	17.15	0	88.40	11.45	1	-19.52
34.	$CH_4+H \rightarrow CH_3+H_2$	14.10	0	11.90	12.68	0	11.43
35.	$CH_4+OH \rightarrow CH_3+H_2O$	3.54	3.08	2.00	2.76	3.08	16.68
36.	$CH_4+O \rightarrow CH_3+OH$	13.20	0	9.20	11.43	0	6.64
37.	$CH_4+HO_2 \rightarrow CH_3+H_2O_2$	13.30	0	18.00	12.02	0	1.45
38.	$CH_3+HO_2 \rightarrow CH_3O+OH$	13.51	0	0.00	10.00	0	0.00
39.	$CH_3+OH \rightarrow CH_2O+H_2$	12.60	0	0.00	14.08	0	71.73
40.	$CH_3+O \rightarrow CH_2O+H$	14.11	0	2.00	15.23	0	71.63
41.	$CH_3+O_2 \rightarrow CH_3O+O$	13.68	0	29.00	14.48	0	0.73
42.	$CH_2O+CH_3 \rightarrow CH_4+HCO$	10.00	0.5	6.00	10.32	0.5	21.14
43.	$CH_3+HCO \rightarrow CH_4+CO$	11.48	0.5	0.00	13.71	0.5	90.47
44.	$CH_3+HO_2 \rightarrow CH_4+O_2$	12.00	0	0.40	13.88	0	58.59
45.	$CH_3O+M \rightarrow CH_2O+H+M$	13.70	0	21.00	9.00	1	-2.56
46.	$CH_3O+O_2 \rightarrow CH_2O+HO_2$	12.00	0	6.00	11.11	0	32.17

C.2 ONE STEP KINETICS MODEL

Finite difference calculations involving a one step chemical reaction were also carried out using HCT. Again, the approximations involving transport processes outlined in section B.1.a were made. In addition, the kinetics were described by the overall reaction

$$CH_4 + 2O_2 \underset{k''}{\overset{k'}{\rightleftharpoons}} CO_2 + 2H_2O \quad . \tag{C.3}$$

Thus there are two chemical reactions (k' and k''), and five species present (CH_4, O_2, CO_2, H_2O, and inert N_2).

The reaction rates are specified as follows:

$$\omega_{k'} = A_{k'}[CH_4]^{.3}[O_2]^{1.2}\exp\left[-\frac{E_{k'}}{RT}\right]$$
$$\omega_{k''} = A_{k''}[CO_2]^{.5}[H_2O]^{1.0}\exp\left[-\frac{E_{k''}}{RT}\right] \tag{C.4}$$

where the constants A and E are chosen to give laminar flame speeds which are in agreement with experimental results [Westbrook & Dryer, 1981].

C.3 INTEGRAL METHOD

The first step in the integral method was to determine the relative importance of the terms in the energy and momentum equations, and to only keep the dominant terms. The energy equation is given by B.4, with the orders of magnitude shown below:

$$\begin{array}{ccccccc} (1) & & (2) & & (3) & & (4) \\ \rho\dfrac{Dh}{Dt} & = & -\dfrac{\partial q}{\partial x} & + & \dfrac{DP}{Dt} & - & \tau\dfrac{\partial u}{\partial x} \\ \left(\dfrac{\overline{\rho}\Delta h}{\Delta t_q}\right) & & \left(\dfrac{\Delta q}{\Delta x_q}\right) & & \left(\dfrac{dp}{dt}\Big|_q\right)^{\dagger} & & \left(\overline{\tau}\dfrac{\Delta u}{\Delta x_q}\right) \end{array} \tag{B.4}$$

The subscript q applies to the quenching event, that is,

$$\Delta(\,)_q \equiv (\,)_b - (\,)_w \quad ,$$

where $(\,)_b$ is evaluated in the burnt gases, and $(\,)_w$ is evaluated at the wall.

Normalizing to (1), we have

$$(1) \sim 1$$

$$(2) \sim \frac{\Delta q\ \Delta t_q}{\Delta x_q\ \overline{\rho}\ \Delta h}$$

$$(3) \sim \frac{\Delta t_q}{\overline{\rho}\ \Delta h}\ \frac{dp}{dt}\Big|_q$$

$$(4) \sim \overline{\tau}\frac{\Delta u\ \Delta t_q}{\Delta x_q\ \overline{\rho}\ \Delta h} \quad .$$

With the following approximations,

$$\Delta q \approx q_\infty - q_w \approx -q_{w\,\max} \approx \overline{k}\frac{\Delta T_f}{\Delta x_q}$$

$$\Delta h \approx h_\infty - h_w \approx c_p\ \Delta T_f$$

$$\Delta u \approx S_b - 0 = S_b$$

and:

$$\overline{\tau} \approx \overline{\mu}\frac{\Delta u}{\Delta x_q} \approx \frac{\overline{\mu} S_b}{\Delta x_q}$$

$$\Delta x_q \approx \Delta x_{flame} \approx \frac{\overline{\alpha}}{S_b}$$

$$\Delta t_q \approx \frac{\Delta x_{flame}}{S_b} \approx \frac{\overline{\alpha}}{{S_b}^2}$$

the terms become

$$(2) \sim \frac{\Delta q\ \Delta t_q}{\Delta x_q\ \overline{\rho}\ \Delta h} \approx \frac{\overline{k}\ \Delta T_f\ \Delta t_q}{\overline{\rho}\ c_p\ \Delta T_f\ {\Delta x_q}^2} \approx \frac{\overline{\alpha}}{S_b}\frac{1}{\Delta x_q} \approx 1$$

† Since the flow in the combustion chamber is slow (M<<1), the pressure throughout the chamber is spatially uniform. However, the volume is fixed causing the pressure to rise. At the time that quenching occurs, the pressure is rising at the rate $\frac{dp}{dt}\Big|_q$, which is determined experimentally (see section 3.3).

$$(3) \sim \frac{\Delta t_q}{\overline{\rho}\,\Delta h}\left.\frac{dp}{dt}\right|_q \approx \left(\frac{\overline{\alpha}}{S_b}\right)\frac{1}{\overline{\rho} S_b c_p \Delta T_f}\left.\frac{dp}{dt}\right|_q$$

$$(4) \sim \overline{\tau}\frac{\Delta u}{\Delta x_q}\frac{\Delta t_q}{\overline{\rho}\Delta h} \sim \frac{\overline{\mu} S_b{}^2}{\Delta x_q{}^2}\frac{\Delta t_q}{\overline{\rho} c_p \Delta T_f} \approx Pr\frac{S_b{}^2}{c_p \Delta T_f}$$

For methane - air flames

$$S_b \sim 4\,\frac{m}{sec}$$
$$c_p \sim 1000\,\frac{J}{kg\,^\circ K}$$
$$\Delta T_f \sim 2000^\circ K$$
$$\overline{\alpha} \sim 10^{-5}\,\frac{m^2}{sec}$$
$$\overline{\rho} \sim .2\,\frac{kg}{m^3}$$
$$Pr \sim 1$$

and from the measurements,

$$\left.\frac{dp}{dt}\right|_{\exp} \sim 100\,\frac{atm}{sec}$$

Carrying out the calculations gives that, (3) and (4) are both much less than (1) and (2). *Thus, both the viscous dissipation term, (4), and the pressure term, (3), may be neglected so that the energy equation reduces to:*

$$\rho\frac{Dh}{Dt} = -\frac{\partial q}{\partial x} \quad , \tag{C.5}$$

with the heat flux given by B.7.

C.3.1 TRANSFORMATION TO MASS COORDINATES

If the mass transformation,

$$\frac{\partial \psi}{\partial x} = \frac{\rho}{\rho_w} \quad ; \quad \frac{\partial \psi}{\partial t} = -\frac{\rho u}{\rho_w} \tag{B.8}$$

is made, where

$$\rho_w = \frac{p_q}{RT_w} \quad ,$$

the fluid velocity will not appear explicitly in either the energy, momentum, of species equations, and thus need not be of immediate concern. The objective of

the integral method is to determine the heat flux at the wall only, so only the energy equation will be solved. The pressure has also dropped out of this formulation. This may be interpreted as meaning that the quenching process in the combustion chamber occurs at essentially constant pressure.

Introducing the transformation B.8, the energy equation (B.4) becomes

$$\frac{\partial h}{\partial t} = -\frac{1}{\rho_w}\frac{\partial q}{\partial \psi} \tag{C.6}$$

and the species equation (B.5)

$$\frac{\partial Y_i}{\partial t} = \frac{\omega_i}{\rho} - \frac{1}{\rho_w}\frac{\partial j_i}{\partial \psi} \quad , \tag{C.7}$$

while the heat and mass fluxes are given from B.5 and B.6, by

$$q = -\frac{k\rho}{\rho_w}\frac{\partial T}{\partial \psi} - \sum h_i D_i \frac{\rho^2}{\rho_w}\frac{\partial Y_i}{\partial \psi} \tag{C.8}$$

$$j_i = -\frac{\rho^2 D_i}{\rho_w}\frac{\partial Y_i}{\partial \psi} \tag{C.9}$$

respectively.

The boundary conditions will be those for a constant temperature impervious wall, and for uniform conditions far from the wall:

$$T(0,t) = T_w = constant \quad ; \quad \left.\frac{\partial Y_i}{\partial \psi}\right|_w = 0 \tag{C.10}$$

$$\left.\frac{\partial}{\partial \psi}\right|_{\psi\to\infty} = 0 \quad .$$

C.3.2 REACTION MECHANISM AND TRANSPORT PROPERTY ASSUMPTIONS

In this integral formulation, it will be assumed that the chemical reaction is one step, unimolecular,

$$R \rightarrow P \quad .$$

The molecular diffusivities are assumed to be equal,

$$D_i = D \tag{C.11}$$

and equal to the thermal diffusivity,

$$D = \alpha = \frac{k}{\rho c_p} \quad , \tag{C.12}$$

and the specific heat assumed to be is constant

$$c_p = constant. \tag{C.13}$$

In addition, it will be assumed that the reaction rate is given by the expression

$$\omega_R = -\rho A Y_R F(T) \tag{C.14}$$

where $F(T)$ is the step function,

$$F(T) = \begin{cases} 0 & \text{if } T<T_{ig} \\ 1 & \text{if } T>T_{ig} \end{cases} \tag{C.15}$$

By definition,

$$h = \sum h_i Y_i \tag{C.16}$$

and by assumption,

$$h_i = h_i^o + \int c_{pi} dT \tag{C.17}$$

so that

$$\frac{\partial h}{\partial t} = \sum h_i^o \frac{\partial Y_i}{\partial t} + c_p \frac{\partial T}{\partial t} \tag{C.18}$$

and

$$q = -\frac{k\rho}{\rho_w}\frac{\partial T}{\partial \psi} - \frac{k\rho}{c_p \rho_w}\sum h_i^o \frac{\partial Y_i}{\partial \psi} \quad . \tag{C.19}$$

In addition, multiplying the species equation (B.16) by h_i, and summing over i, gives

$$\sum h_i^o \frac{\partial Y_i}{\partial t} = \frac{1}{\rho}\sum \omega_i h_i^o + \frac{k}{c_p \rho_w^2}\sum h_i^o \frac{\partial Y_i}{\partial \psi} \tag{C.20}$$

Given C.16 to C.19, the energy equation (B.15) becomes

$$\frac{\partial T}{\partial t} = \frac{\partial}{\partial \psi}\left(\frac{k\rho}{\rho_w c_p}\right)\frac{\partial T}{\partial \psi} - \frac{\sum \omega_i h_i^o}{\rho c_p} \tag{C.21}$$

Defining

$$\sum \omega_i h_i^o = \omega_R h_R^o + \omega_p h_p^o \equiv -\omega \Delta h^o \quad ,$$

and

$$\theta = \frac{c_p (T_b - T)}{\Delta h^o} = \frac{T_b - T}{\Delta T_f} \tag{C.22}$$

The system of equations becomes

$$\frac{\partial \theta}{\partial t} = \frac{\partial}{\partial \psi}\left(\frac{k\rho}{\rho_w c_p}\frac{\partial \theta}{\partial \psi}\right) + \frac{\omega}{\rho} \tag{C.23}$$

$$\frac{\partial Y_R}{\partial t} = -\frac{\omega}{\rho} + \frac{\partial}{\partial \psi}\left(\frac{k\rho}{c_p \rho_w{}^2}\frac{\partial Y_R}{\partial \psi}\right) \tag{C.24}$$

The source term is

$$\omega = A Y_R F(\theta) \tag{C.25}$$

where

$$F(\theta) = \begin{cases} 0 & \text{if } \theta < \theta_{ig} \\ 1 & \text{if } \theta > \theta_{ig} \end{cases} \tag{C.26}$$

and

$$\theta_{ig} = \frac{T_b - T_{ig}}{T_b - T_w}$$

The boundary conditions for the species R are the same as those in Equation C.10, and those for the nondimensional temperature, θ, become:

$$\theta(0,t) = 0 \quad ; \quad \theta(\infty,t) = 1 \tag{C.27}$$

C.3.3 THE INTEGRAL EQUATIONS

Defining ψ_p to be the front of the preheat region of the flame, ψ_f to be the location where $\theta = \theta_{ig}$, and ψ_b to be the location where the fuel concentration disappears, the problem may be considered to consist of four zones (Figure C.1):

1) wall to preheat zone ($0<\psi<\psi_p$);

2) preheat zone ($\psi_p<\psi<\psi_f$);

3) reaction zone ($\psi_f<\psi<\psi_b$);

4) burnt gases ($\psi_b<\psi<\infty$).

Since the pressure is assumed to be constant, the conditions in front of the flame (zone 1), and behind the flame (zone 4) will be uniform. Specifically, in front of the flame,

$$\theta = 1 \quad , \quad Y_R = 1 \quad \text{for } 0 < \psi < \psi_p$$

and behind the flame,

$$\theta = 0 \quad , \quad Y_R = 0 \quad \text{for } \psi_b < \psi < \infty$$

Integrating the energy and specie equations (C.23 and C.24) over the preheat and reaction zones, and defining

$$I_{\theta_D} \equiv \int_{\psi_p}^{\psi_f} (\theta_\infty - \theta) d\psi \tag{C.28a}$$

$$I_{\theta_R} \equiv \int_{\psi_f}^{\psi_b} (\theta_\infty - \theta) d\psi \tag{C.28b}$$

$$I_{Y_D} \equiv \int_{\psi_p}^{\psi_f} Y_D d\psi \tag{C.28c}$$

$$I_{Y_R} \equiv \int_{\psi_f}^{\psi_b} Y_R d\psi \tag{C.28d}$$

$$Q_f = \frac{k_{ig}\rho_{ig}}{\rho_w{}^2 c_p} \frac{\partial\theta}{\partial\psi}\bigg|_{\psi_f} \tag{C.29a}$$

$$Q_w = \frac{k_w}{\rho_w c_p} \frac{\partial\theta}{\partial\psi}\bigg|_{w} \tag{C.29b}$$

and

$$J_f = \frac{\rho_{ig} k_{ig}}{c_p \rho_w{}^2} \frac{\partial Y}{\partial\psi}\bigg|_{\psi_f} \tag{C.29c}$$

gives the integral equations:

$$\frac{dI_{\theta_D}}{dt} - \theta_{ig}\frac{d\psi_f}{dt} + \frac{d\psi_p}{dt} = Q_f - Q_w \tag{C.30a}$$

$$\frac{dI_{\theta_R}}{df} + \theta_{ig}\frac{d\psi_f}{dt} = -Q_f - A\, I_{Y_R} \tag{C.30b}$$

$$\frac{dI_{Y_D}}{dt} - Y_R(\psi_f)\frac{d\psi_f}{dt} + \frac{d\psi_p}{dt} = J_f \tag{C.30c}$$

$$\frac{dI_{Y_R}}{dt} + Y_R(\psi_f)\frac{d\psi_f}{dt} = -J_f - A\, I_{Y_R} \tag{C.30d}$$

Quenching will be said to begin when $\psi_p = 0$ (see Figure C.1). For $\psi_p > 0$, the flame will be assumed to be steady, and moving at the laminar flame speed. Thus, prior to quenching

$$\frac{\partial\theta}{\partial\psi}\bigg|_{w} = 0$$

$$\frac{d\psi_p}{df} = \frac{d\psi_f}{dt} = -S_u \tag{C.31}$$
$$\frac{dI_{\theta_i}}{dt} = \frac{dI_{Y_i}}{dt} = 0 \quad ; \quad i = R,D$$

and so, for a steady flame, the integral equations give

$$\begin{aligned} Q_{ws} &= 0 \\ Q_{fs} &= -S_u(1-\theta_{ig}) \\ J_{fs} &= -S_u(1-Y_F\big|_s) \\ S_u &= A I_{Y_R}\big|_s \end{aligned} \tag{C.32}$$

C.3.4 PROFILES FOR THE INTEGRAL EQUATIONS

The temperature and specie profiles are chosen to satisfy the conditions:

$$\begin{aligned} \theta(\psi_p) &= 1 \quad ; \quad Y_R(\psi_p) = 1 \\ \theta(\psi_b) &= 0 \quad ; \quad Y_R(\psi_b) = 0 \\ \frac{\partial\theta}{\partial\psi}\bigg|_{\psi_b} &= 0 \quad ; \quad \frac{\partial Y_R}{\partial\psi}\bigg|_{\psi_b} = 0 \quad ; \quad \frac{\partial Y_D}{\partial\psi}\bigg|_{\psi_p} = 0 \end{aligned} \tag{C.33}$$

with the profiles and their slopes matching at $\psi = \psi_f$.

Quenching will be assumed to start when $\psi_p = 0$, and at this time, the profiles must satisfy the steady state condtions (Equations C.31). The values for the independent variables at the start of quenching are the same as their values in the steady state flame, and are denoted by the subscript "s". Choosing profiles for the two regions, simple polynomials which satisfy the above conditions are:

$$\theta_D(\psi) = 1 - (1-\theta_{ig})\left[2\left(\frac{\psi-\psi_p}{\psi_f-\psi_p}\right) - \left(\frac{\psi-\psi_p}{\psi_f-\psi_p}\right)^2\right] + \frac{2(\psi_f-\psi_p)\theta_{ig}}{\psi_b-\psi_f}\left[-\left(\frac{\psi-\psi_p}{\psi_f-\psi_p}\right) + \left(\frac{\psi-\psi_p}{\psi_f-\psi_p}\right)^2\right]$$

$$\theta_R(\psi) = \theta_{ig}\left(\frac{\psi_b-\psi}{\psi_b-\psi_f}\right)^2$$

$$Y_D(\psi) = Y_w(t) - (Y_w(t) - Y_f(t))\left(\frac{\psi-\psi_p}{\psi_f-\psi_p}\right)^2 \tag{C.34}$$

$$Y_R(\psi) = Y_f(t)\left[1 - 3\left(\frac{\psi-\psi_f}{\psi_b-\psi_f}\right)^2 + 2\left(\frac{\psi-\psi_f}{\psi_b-\psi_f}\right)^3\right]$$

$$+ 2\frac{\psi_b-\psi_f}{\psi_f-\psi_p}(Y_w(t)-Y_f(t))\left[-\left(\frac{\psi-\psi_f}{\psi_b-\psi_f}\right) + 2\left(\frac{\psi-\psi_f}{\psi_b-\psi_f}\right)^2 - \left(\frac{\psi-\psi_f}{\psi_b-\psi_f}\right)^3\right]$$

Substituting these profiles into the integral definitions and defining:

$$r = \frac{(\psi_f-\psi_p)}{(\psi_b-\psi_f)} \tag{C.35}$$

and

$$\beta = \frac{\alpha_{ig}}{\alpha_w}\left(\frac{\rho_{ig}}{\rho_w}\right)^2 \tag{C.36}$$

(Equations C.28), gives:

$$\begin{aligned}
I_{\theta_D} &= (\psi_f-\psi_p)\left[1 - \frac{2}{3}(1-\theta_{ig}) + r\frac{\theta_{ig}}{3}\right] \\
I_{\theta_R} &= (\psi_f-\psi_p)\frac{\theta_{ig}}{3r} \\
I_{Y_D} &= (\psi_f-\psi_p)\left[Y_W - \frac{Y_W-Y_F}{3}\right] \\
I_{Y_R} &= \frac{(\psi_f-\psi_p)}{r}\left[\frac{Y_F}{2} - \frac{Y_W-Y_F}{6r}\right]
\end{aligned} \tag{C.37}$$

$$Q_w = -2\frac{\alpha_w}{(\psi_f-\psi_p)}\left(1 - \vartheta_{ig} - r\,\vartheta_{ig}\right)$$

$$Q_f = -2\frac{\alpha_w\beta}{(\psi_f-\psi_p)}\, r\,\vartheta_{ig}$$

$$J_f = -2\frac{\alpha_w\beta}{(\psi_f-\psi_p)}(Y_w - Y_F)$$

the steady conditions (C.32) give:

$$r_s = \frac{(1-\theta_{ig})}{\theta_{ig}}$$

$$(\psi_f-\psi_p)\Big|_s = 2\frac{\beta\alpha_w}{S_u}$$

$$Y_F\Big|_s = \theta_{ig}$$

and

$$A = \frac{3}{2}\frac{S_u^2}{\beta\alpha_w}\frac{1-\vartheta_{ig}}{\vartheta_{ig}^2}$$

Chosing $(\psi_f - \psi_p)\big|_s$ as the characteristic length and $(\psi_f - \psi_p)\big|_s / S_u$ as the characteristic time gives the following dimensionless length and time variables:

$$z = \frac{\psi}{(\psi_f - \psi_p)_s} = \frac{\psi S_u}{2\beta\alpha\omega}$$

$$\tau = \frac{t S_u}{(\psi_f - \psi_p)_s} = \frac{t S_u^2}{2\beta\alpha\omega}$$

the integral model reduces to the following system of equations:

$$\begin{bmatrix} 1 - \theta_{ig} + \theta_{ig} r & 2\theta_{ig} z^2 & 0 & 0 \\ \theta_{ig}\left(3 + \frac{1}{r}\right) & -\frac{2z^2\theta_{ig}}{r^2} & 0 & 0 \\ Y_w - Y_f & 0 & 2z^2 & z^2 \\ \frac{3Y_f r(2r+1) - (Y_w - Y_f)}{r^2} & \frac{2z^2(2(Y_w - Y_f) - 3rY_f)}{r^3} & \frac{-2z^2}{r^2} & \frac{2z^2(3r+1)}{r^2} \end{bmatrix} \begin{bmatrix} \frac{dz^2}{dt} \\ \frac{dr}{dt} \\ \frac{dy_w}{dt} \\ \frac{dy_f}{dt} \end{bmatrix}$$

$$= \begin{bmatrix} 6z(q_f - q_w) \\ 6z(-q_f - \omega) \\ 3zj_f \\ 12z(-j_f - \omega) \end{bmatrix} \tag{C.38}$$

where, using Equations C.28, C.31, C.33 and C.34:

$$q_w = \frac{Q_w}{S_u} = \frac{1 - \theta_{ig}(1-r)}{z\beta}$$

$$q_f = \frac{Q_f}{S_u} = \frac{\theta_{ig} r}{z}$$

$$j_f = \frac{J_f}{S_u} = -\frac{Y_w - Y_f}{z} \quad .$$

The nondimensional heat release in the flame, from Equations C.28d, C.32, C.34 and C.35 to be:

$$\omega = \frac{A\, I_{Y_R}}{S_u} = \frac{1-\theta_{ig}}{\theta_{ig}^2} \frac{z}{2r^2}(3Y_F r + Y_f - Y_w) \quad .$$

The initial conditions are:

$$\begin{aligned} z(0) &= 1 \\ r(0) &= \frac{1-\theta_{ig}}{\theta_{ig}} \\ Y_w(0) &= 1 \\ Y_f(0) &= \theta_{ig} \quad . \end{aligned} \tag{C.39}$$

The heat flux at the wall is given by:

$$\dot{q}_w''(t) = q_w S_u \rho_w c_p \Delta T_f$$

Equations C.38, with initial conditions C.37 were integrated by using fourth order Runge-Kutta scheme.

From the initial condition and definition of r follows the relationship between the igntion temperature and the flame thickness:

$$\frac{(\psi_f - \psi_p)\Big|_s}{(\psi_b - \psi_p)\Big|_s} = 1 - \theta_{ig} \quad .$$

Thus a value of θ_{ig} of .7, which gave good agreement with the experiment and the other modeling, implies that the thickness of the reaction zone is of the same order as the size of the preheat region.

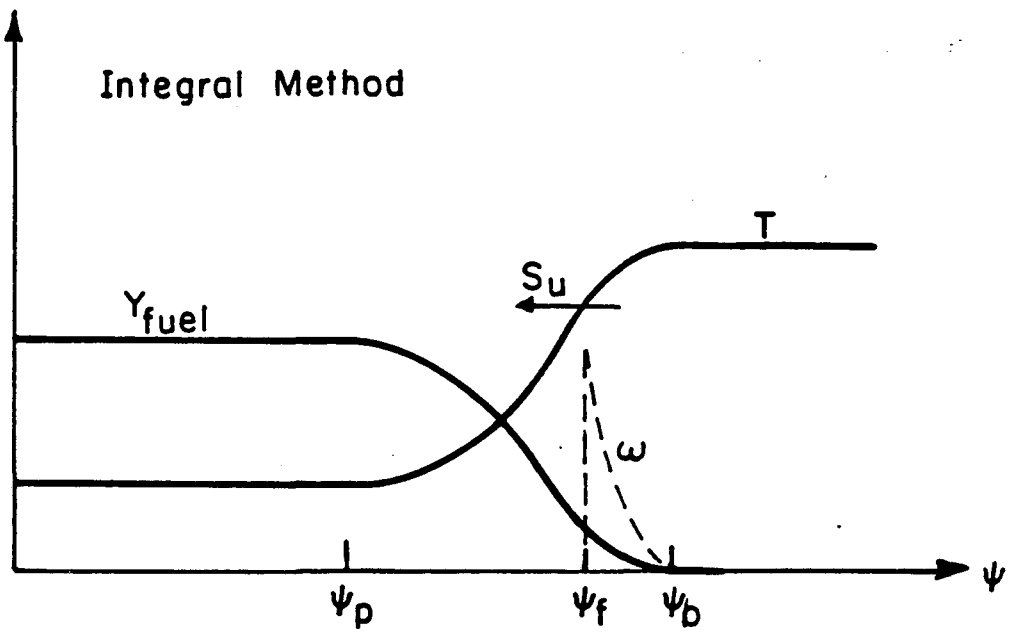

-- XBL 8411-4700 --

Figure C.1 Definitions for the variables in the integral model.

APPENDIX D

EXPERIMENTAL AND NUMERICAL DATA

Figures D.1 to D.14 - Nondimensional Experimental Data

Figures D.15 to D.28 - Corrected Nondimensional Data

Figures D.29 to D.36 - Nondimensional One Step Model Results

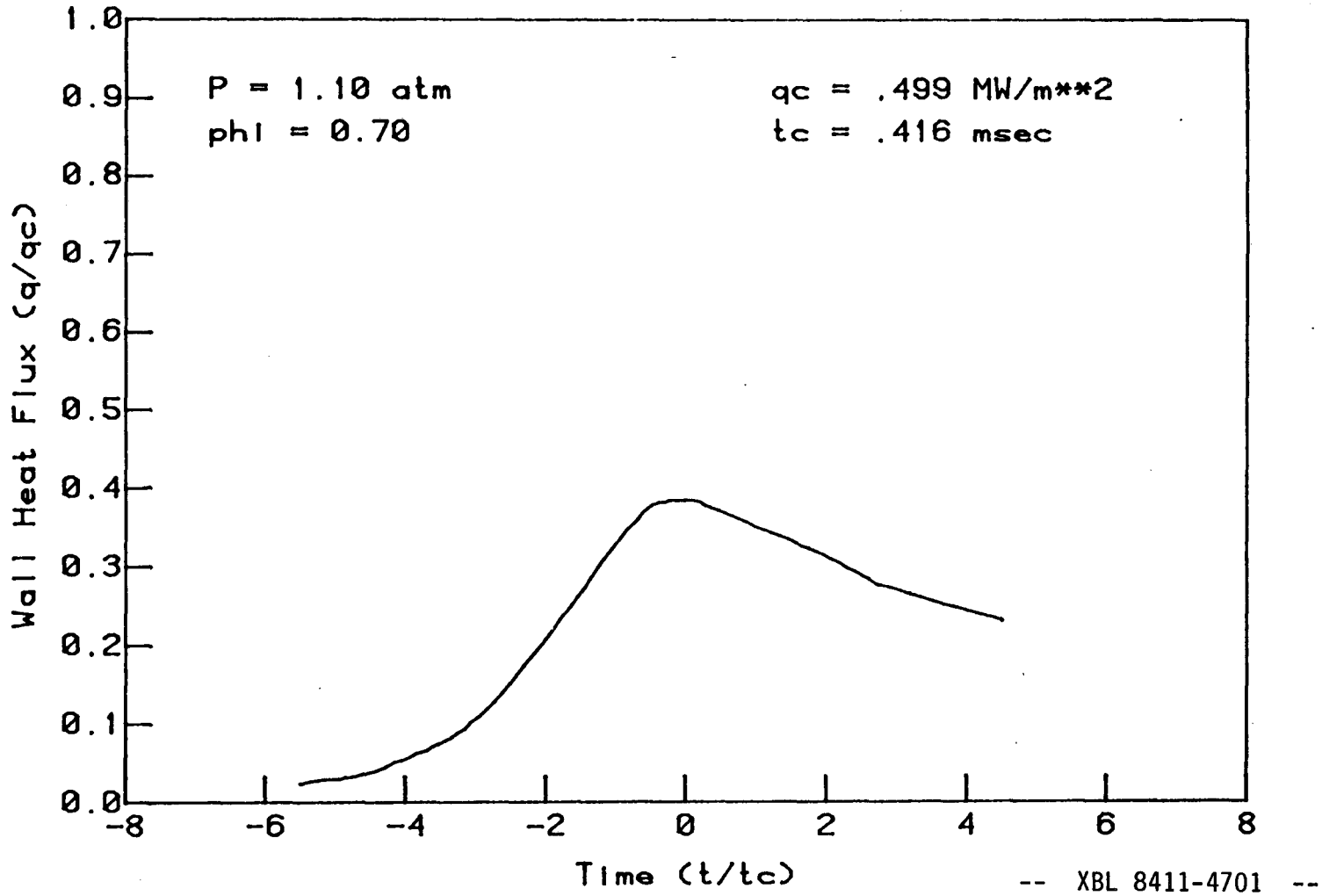

Figure D.1 Experimental results - wall heat flux vs. time - P = 1.10 atm., phi = 0.70.

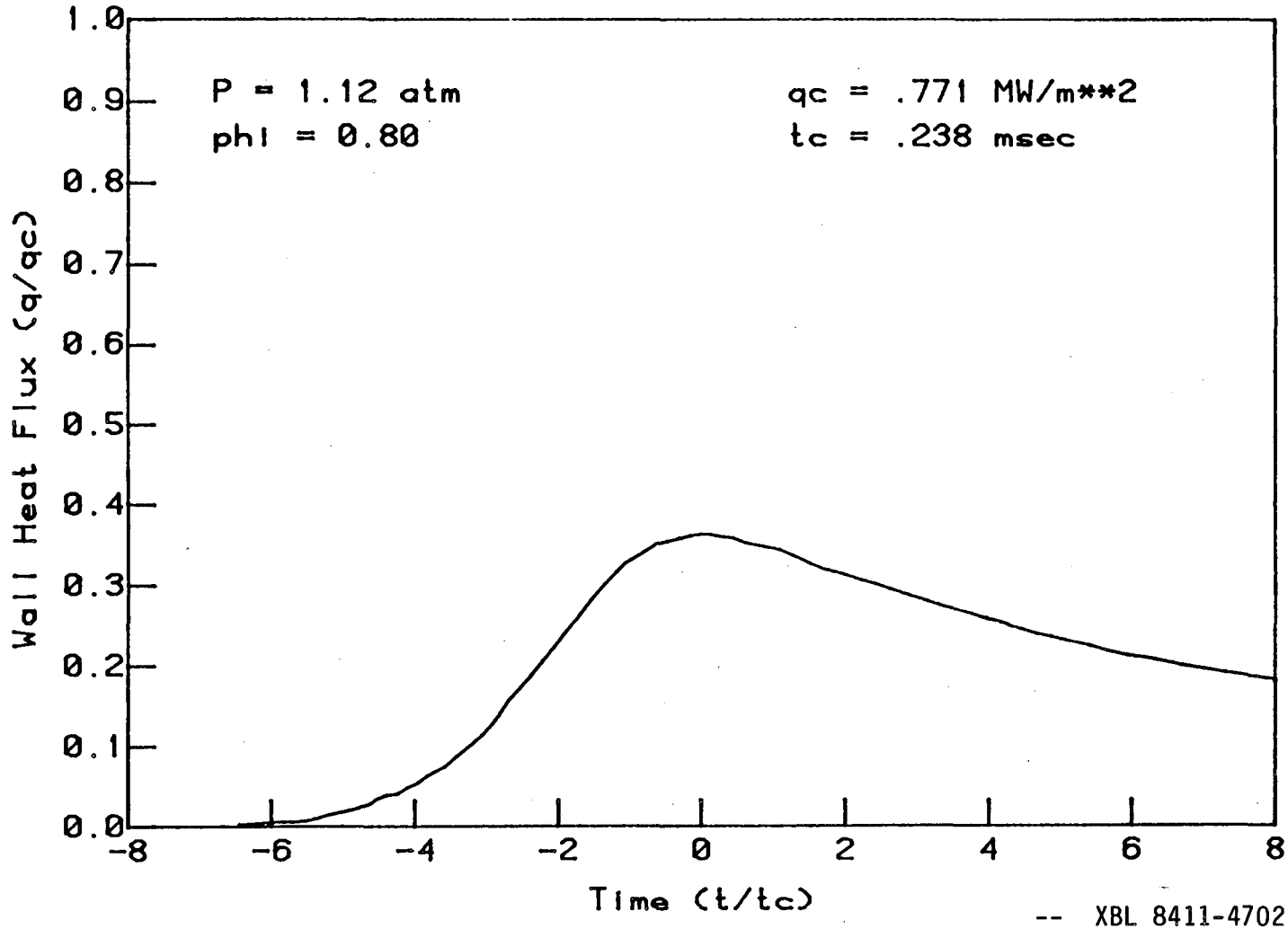

-- XBL 8411-4702 --

Figure D.2 Experimental results - wall heat flux vs. time - P = 1.12 atm., phi = 0.80.

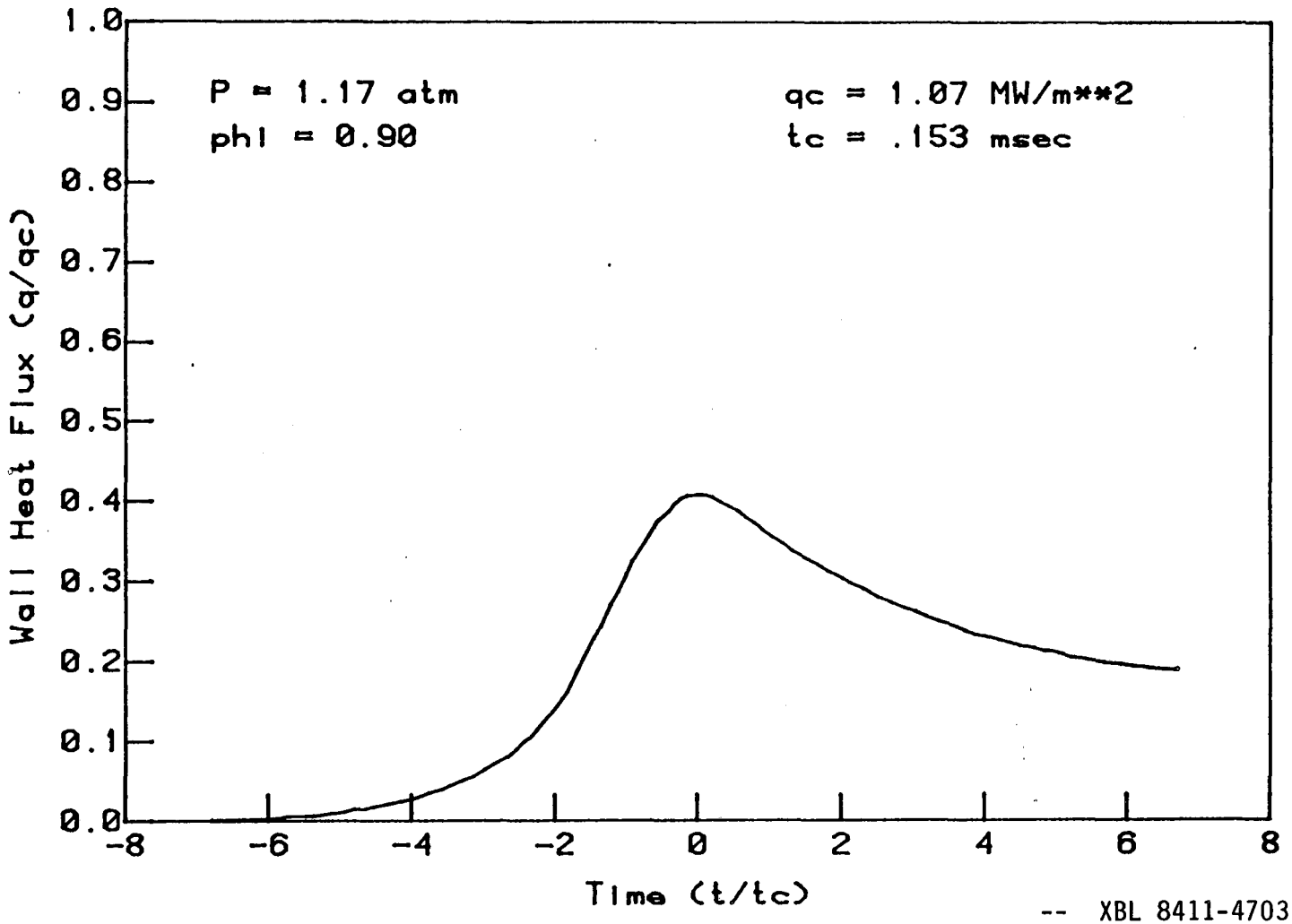

-- XBL 8411-4703 --

Figure D.3 Experimental results - wall heat flux vs. time - P = 1.17 atm., phi = 0.90.

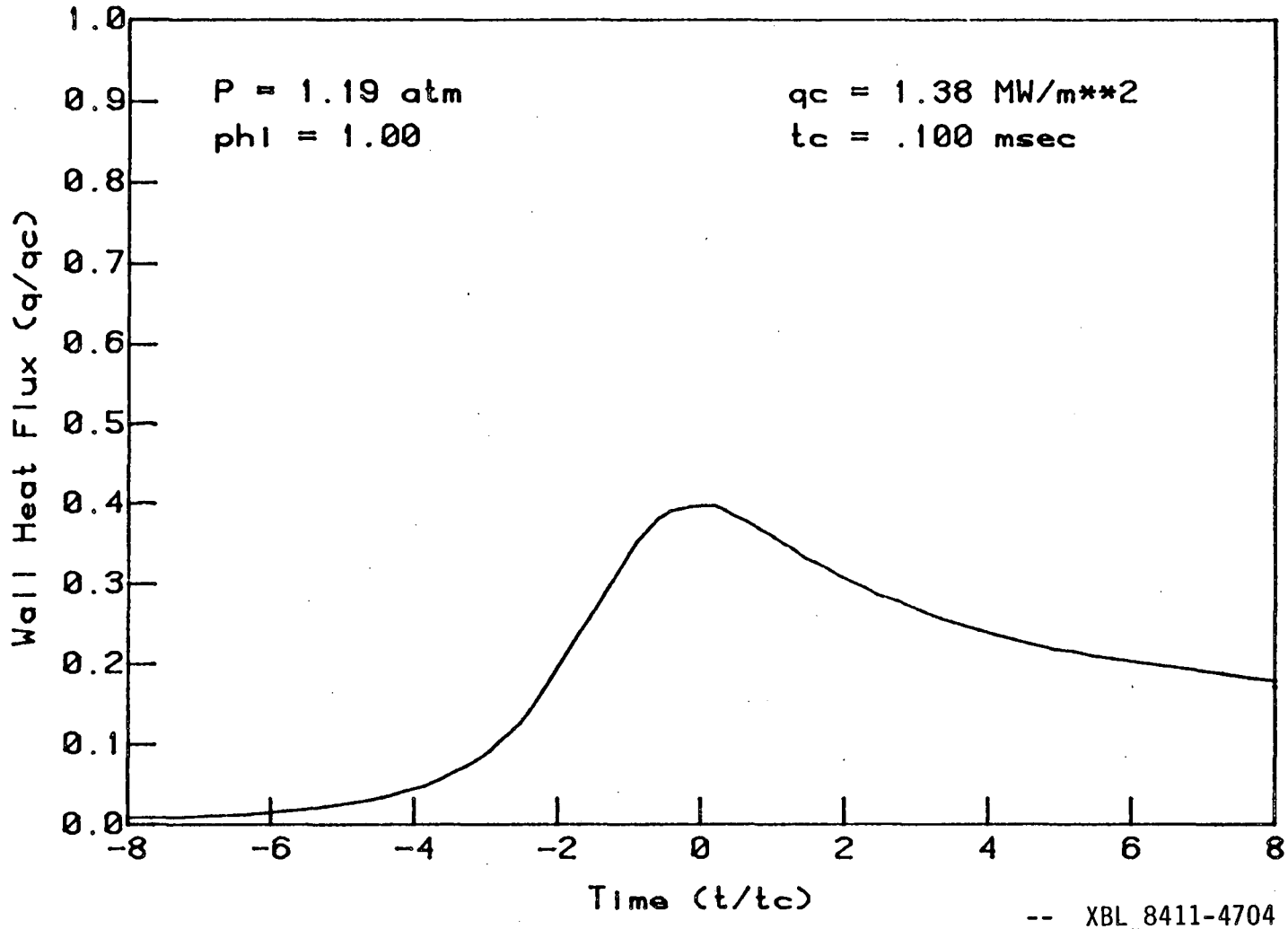

-- XBL 8411-4704 --

Figure D.4 Experimental results - wall heat flux vs. time - P = 1.19 atm., phi = 1.00.

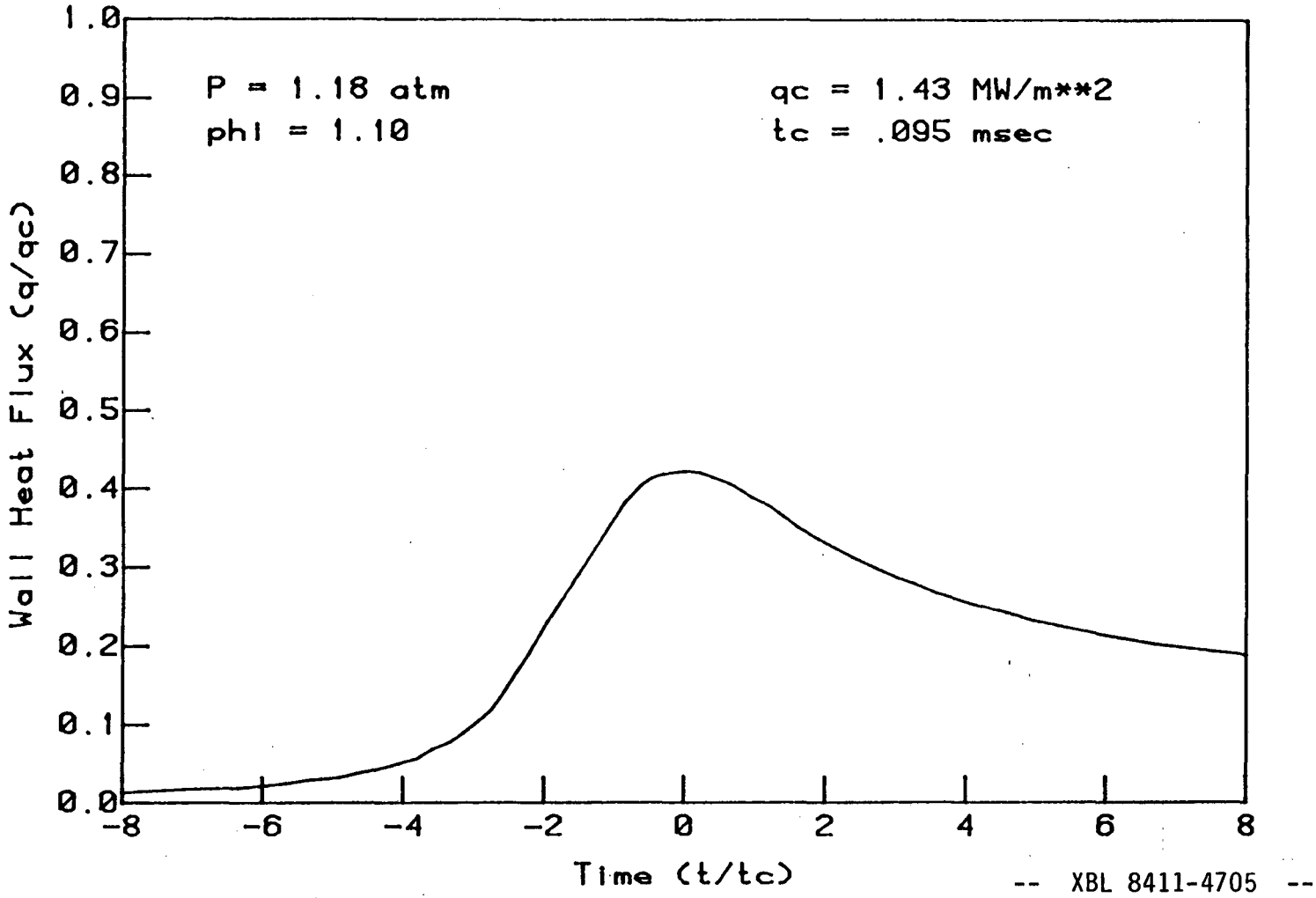

Figure D.5 Experimental results - wall heat flux vs. time - P = 1.18 atm., phi = 1.10.

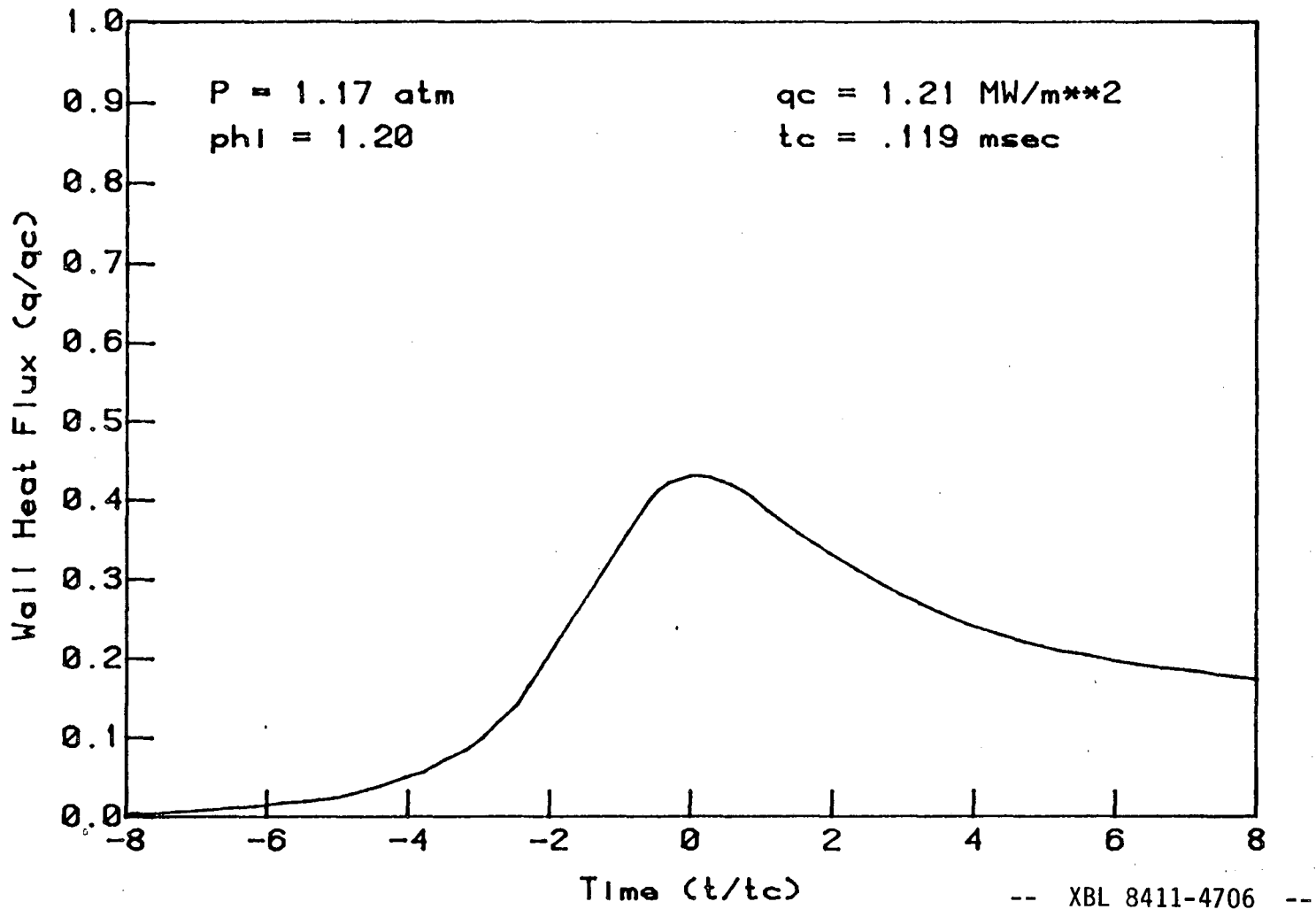

Figure D.6 Experimental results - wall heat flux vs. time - P = 1.17 atm., phi = 1.20.

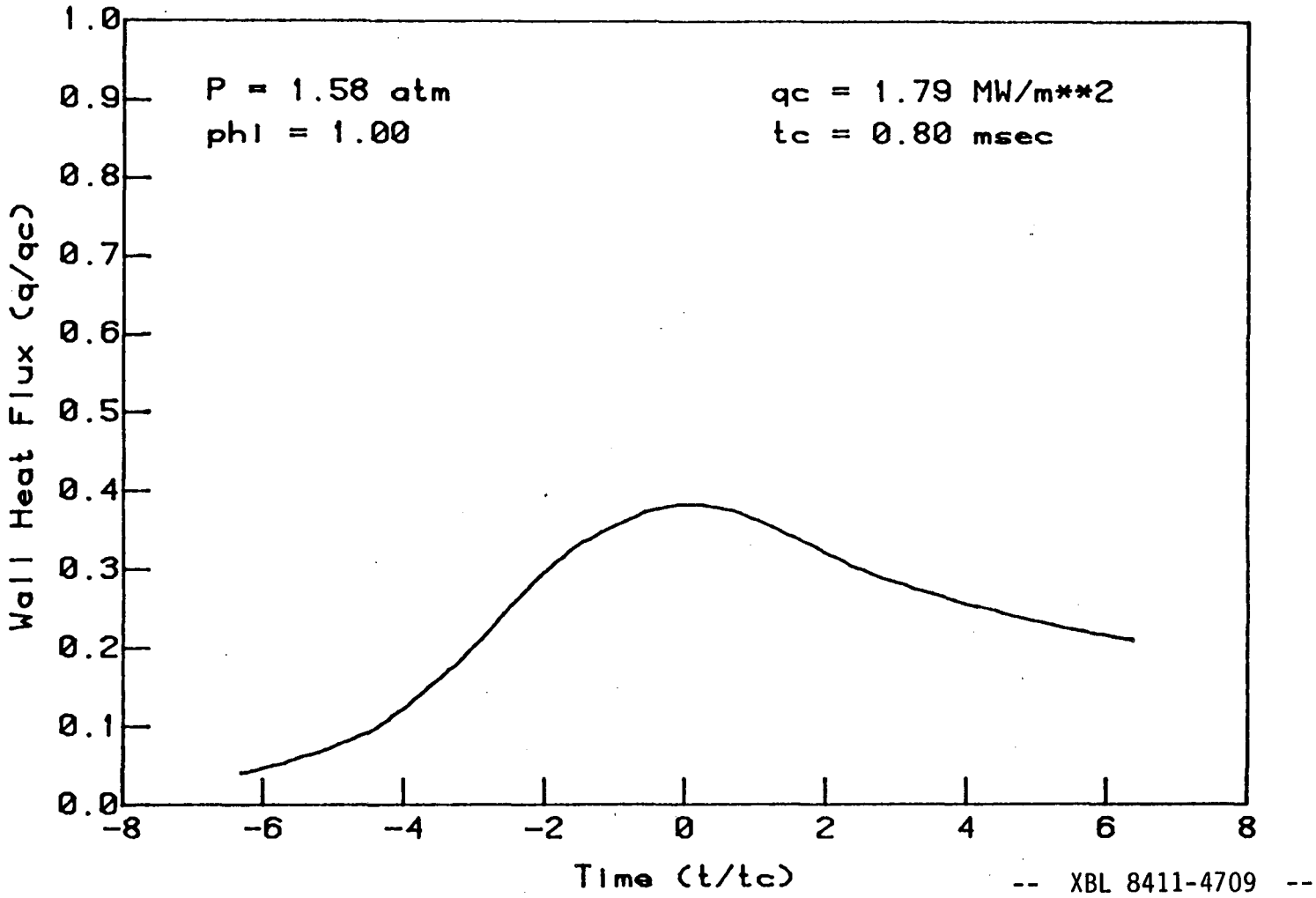

Figure D.7 Experimental results - wall heat flux vs. time - P = 1.58 atm., phi = 1.00.

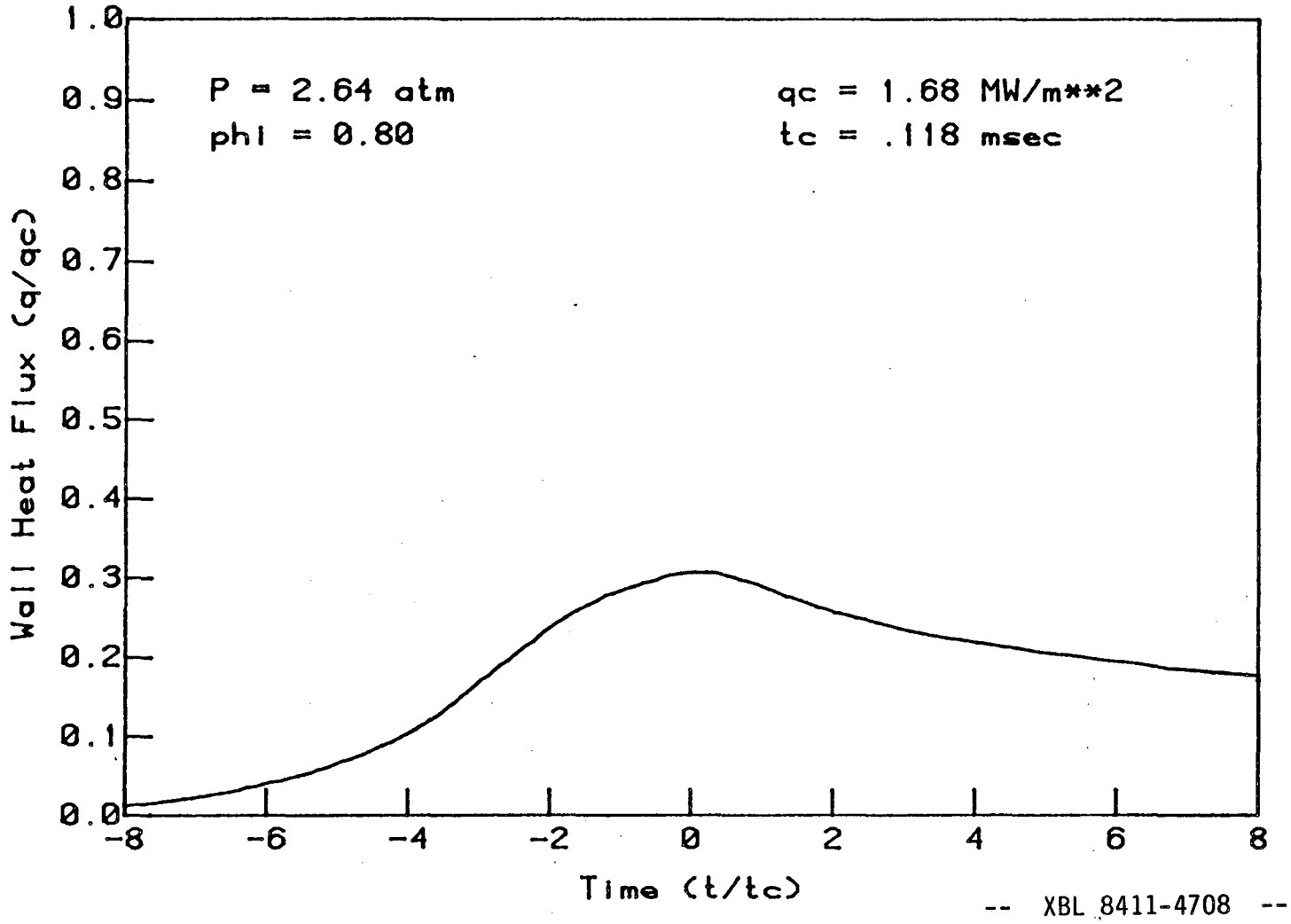

Figure D.8 Experimental results - wall heat flux vs. time - P = 2.64 atm., phi = 0.80.

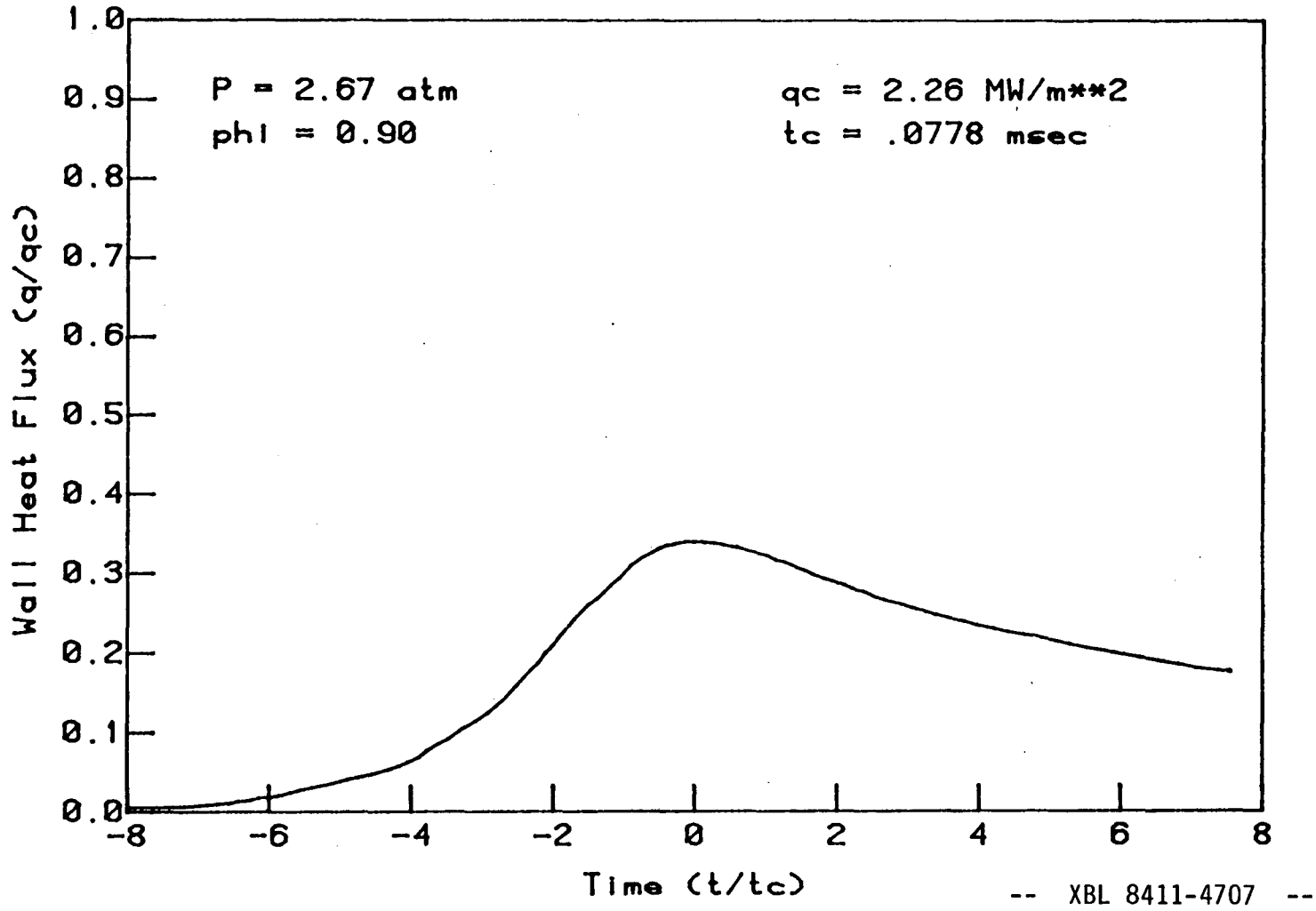

-- XBL 8411-4707 --

Figure D.9 Experimental results - wall heat flux vs. time - P = 2.67 atm., phi = 0.90.

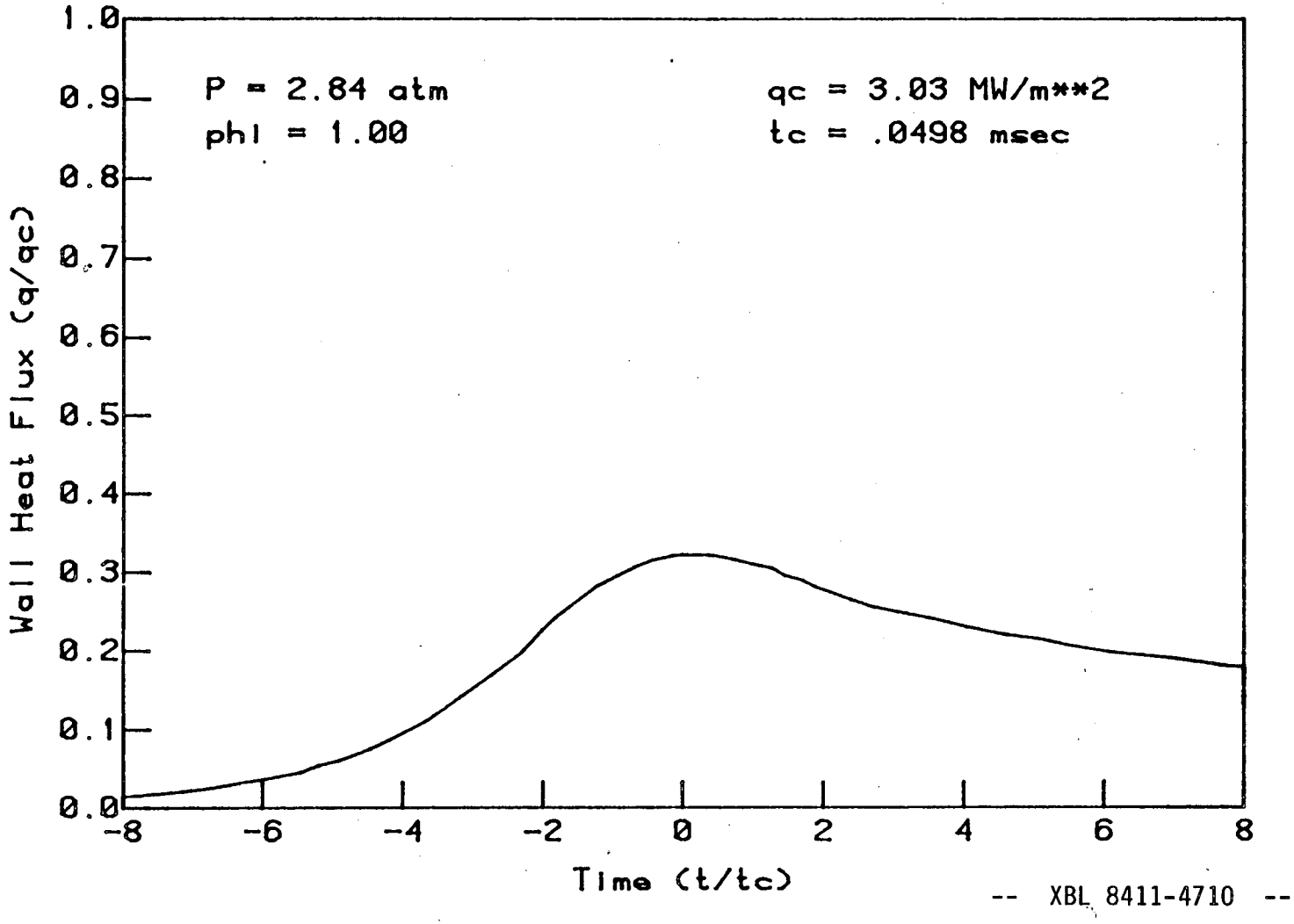

-- XBL 8411-4710 --

Figure D.10 Experimental results - wall heat flux vs. time - P = 2.84 atm., phi = 1.00.

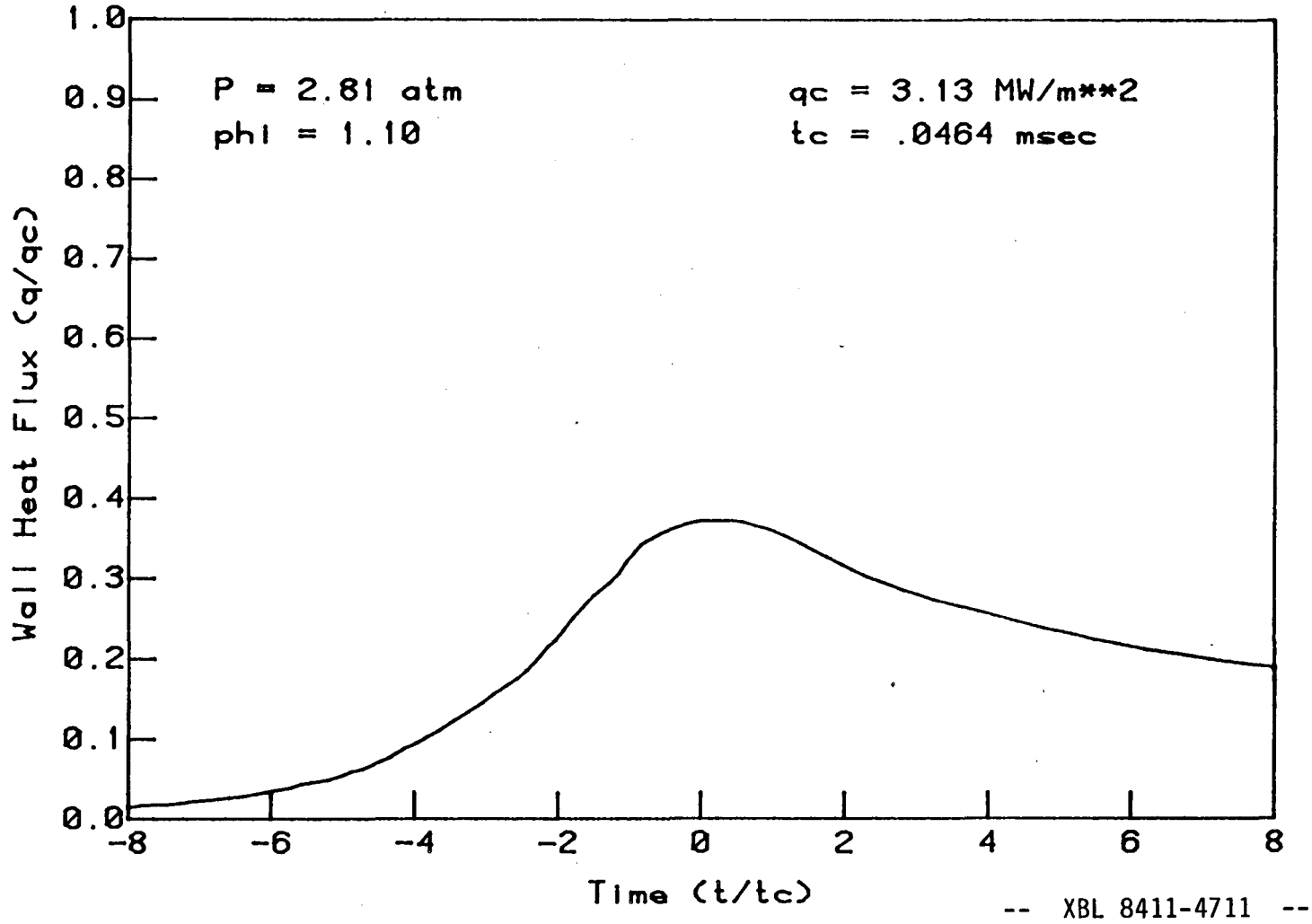

-- XBL 8411-4711 --

Figure D.11 Experimental results - wall heat flux vs. time - P = 2.81 atm., phi = 1.10.

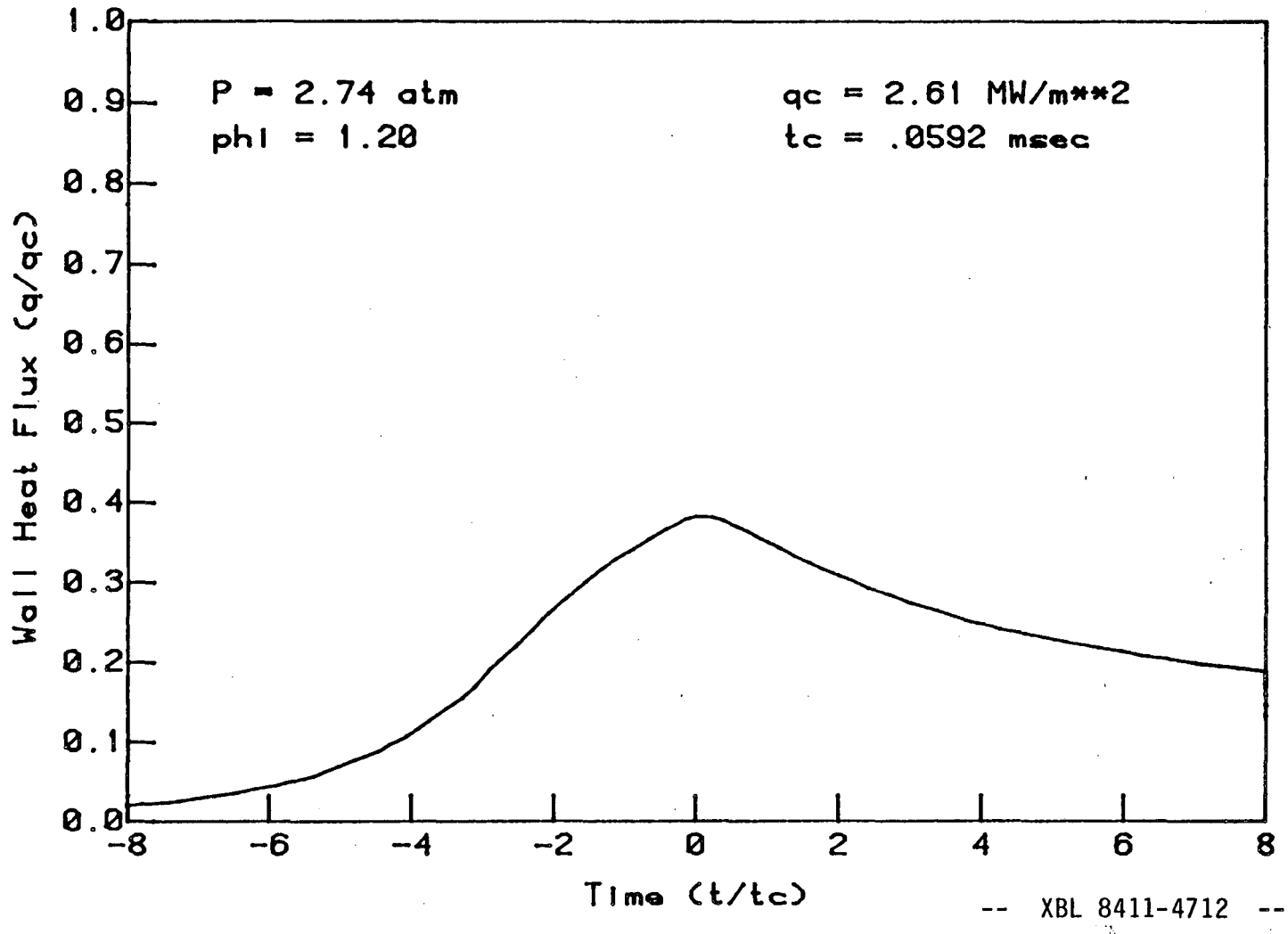

Figure D.12 Experimental results - wall heat flux vs. time - P = 2.74 atm., phi = 1.20.

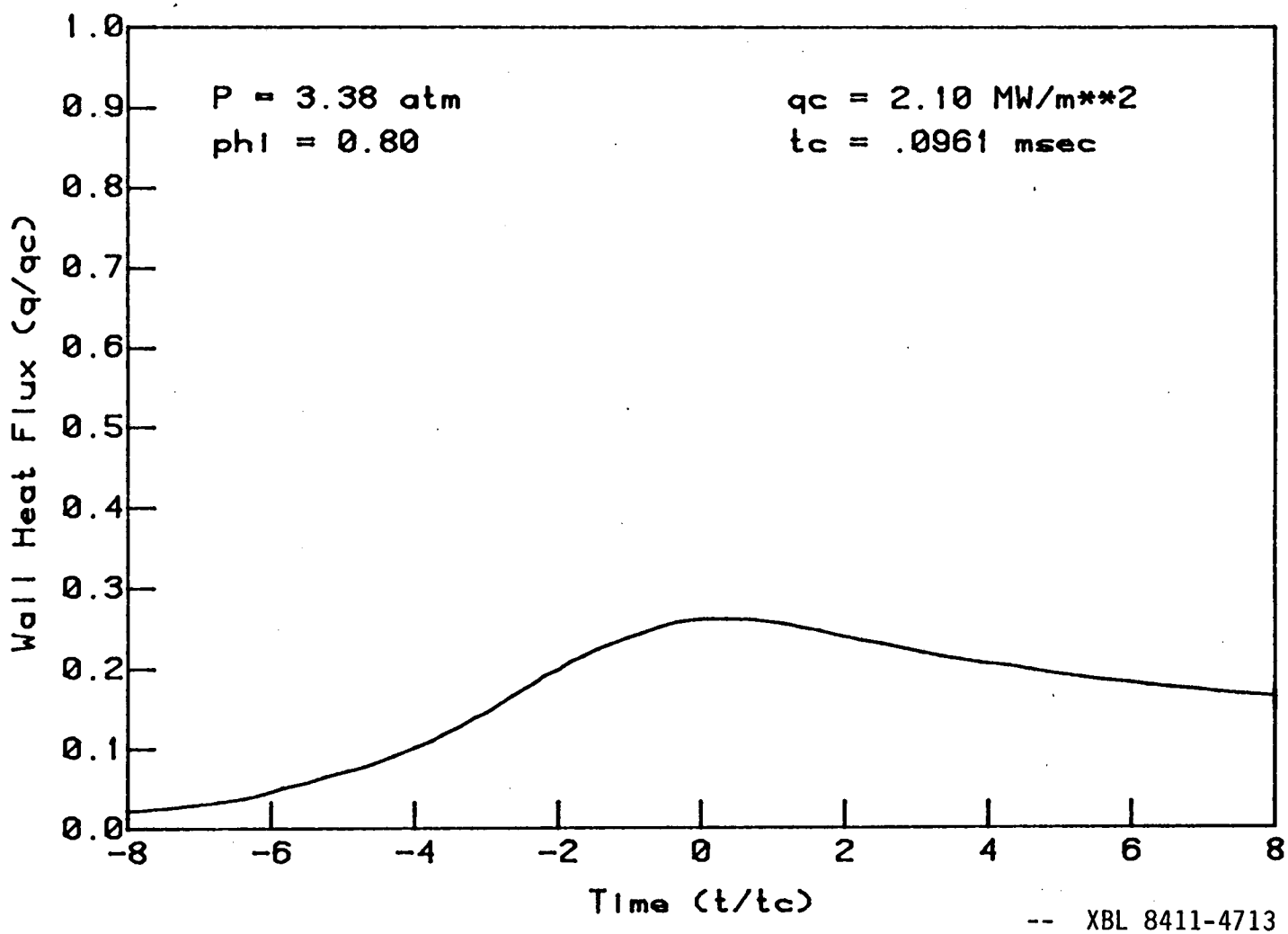

-- XBL 8411-4713 --

Figure D.13 Experimental results - wall heat flux vs. time - P = 3.38 atm., phi = 0.80.

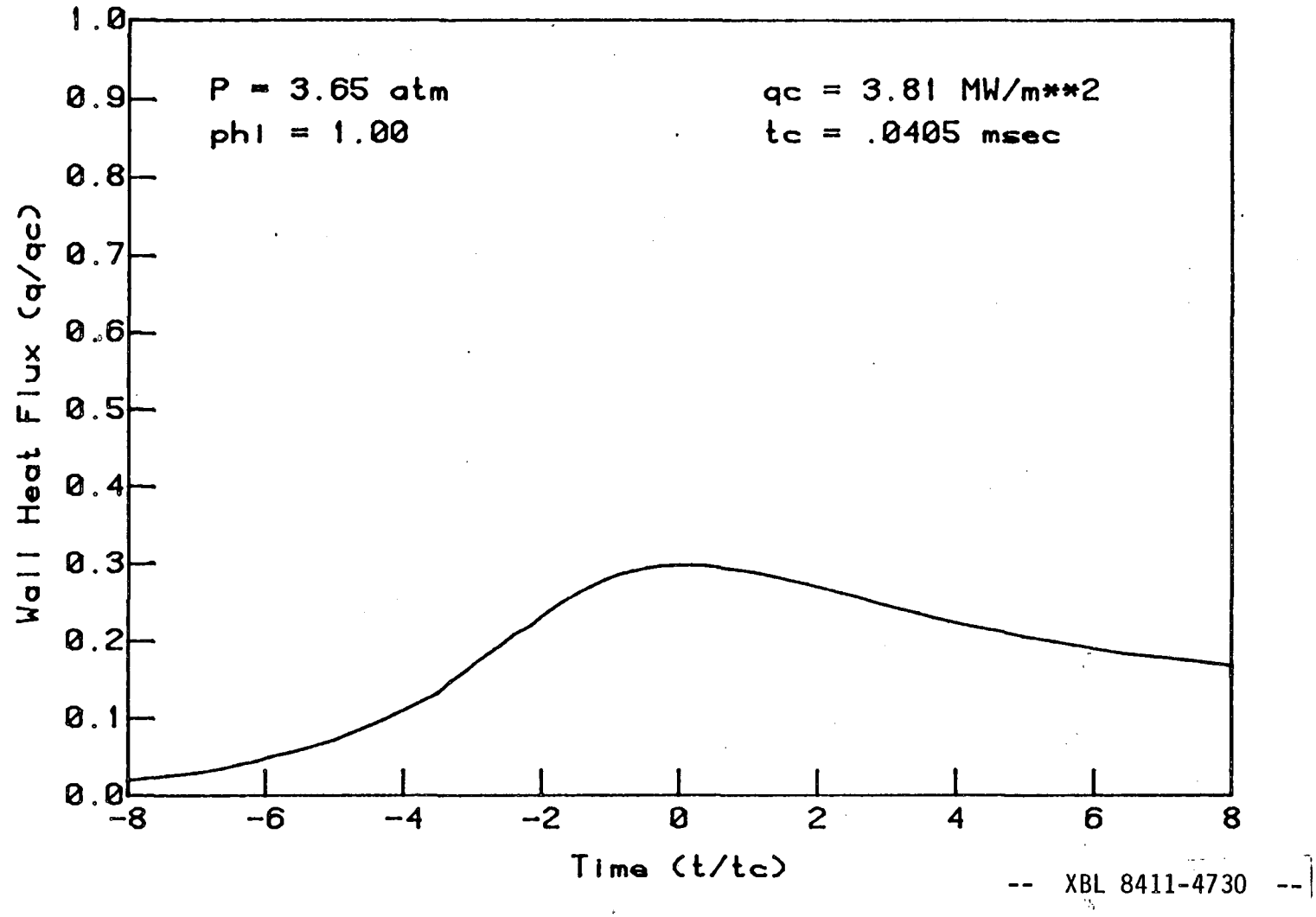

Figure D.14 Experimental results - wall heat flux vs. time - P = 3.65 atm., phi = 1.00.

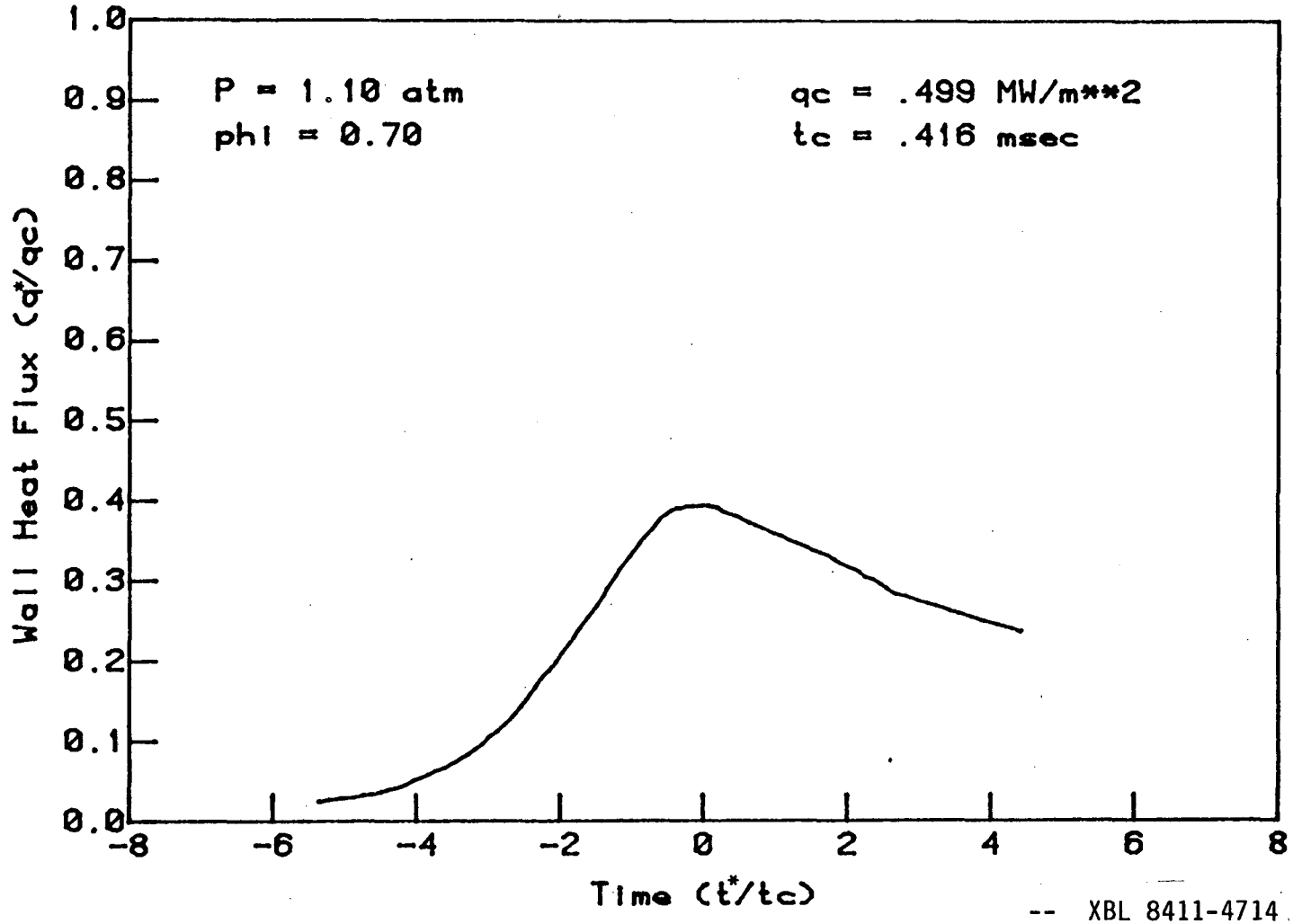

-- XBL 8411-4714 --

Figure D.15 Pressure scaled experimental results (Eqn 3.3) - wall heat flux vs. time - P = 1.10 atm., phi = 0.70.

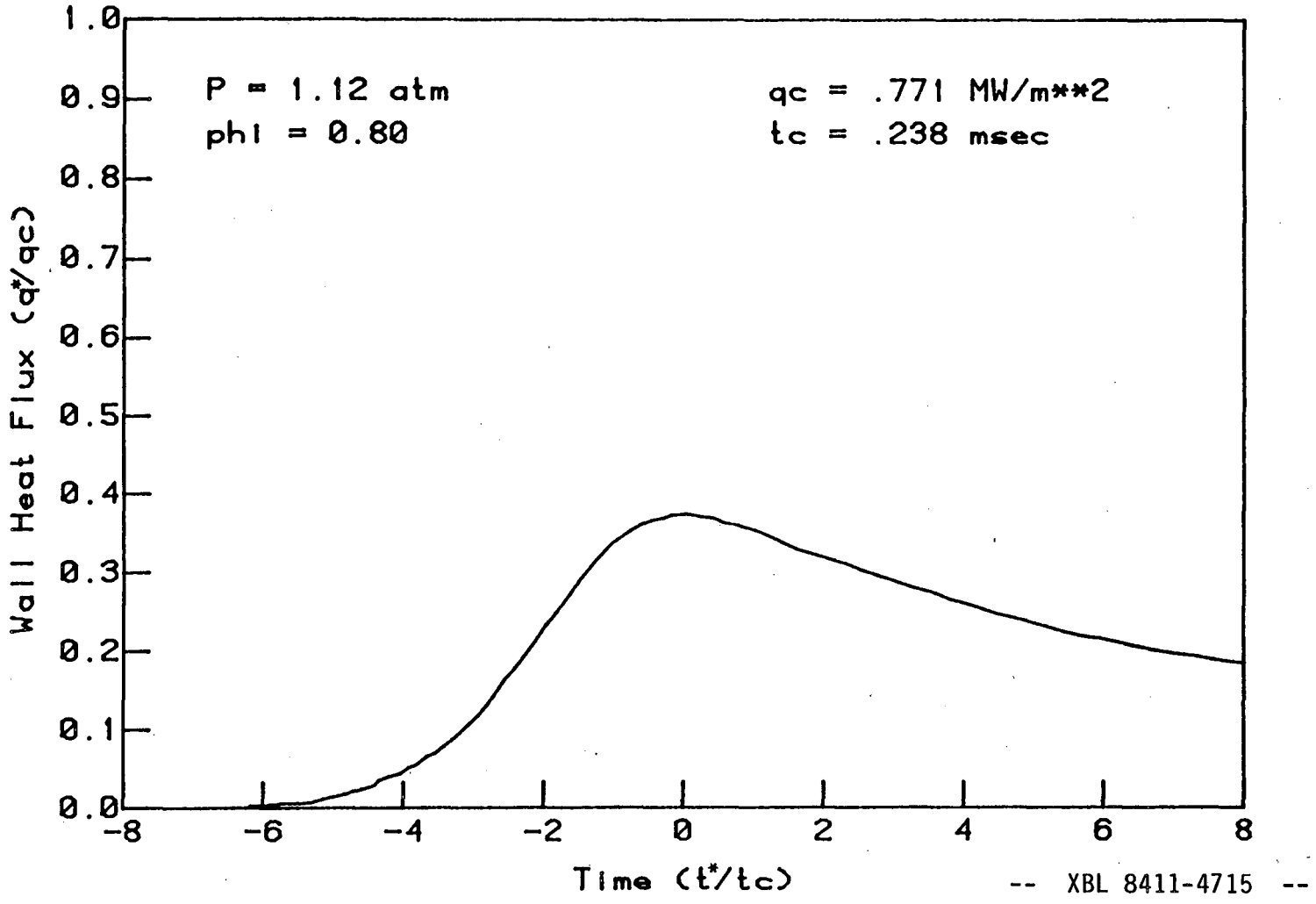

Figure D.16 Pressure scaled experimental results (Eqn 3.3) - wall heat flux vs. time - P = 1.12 atm., phi = 0.80.

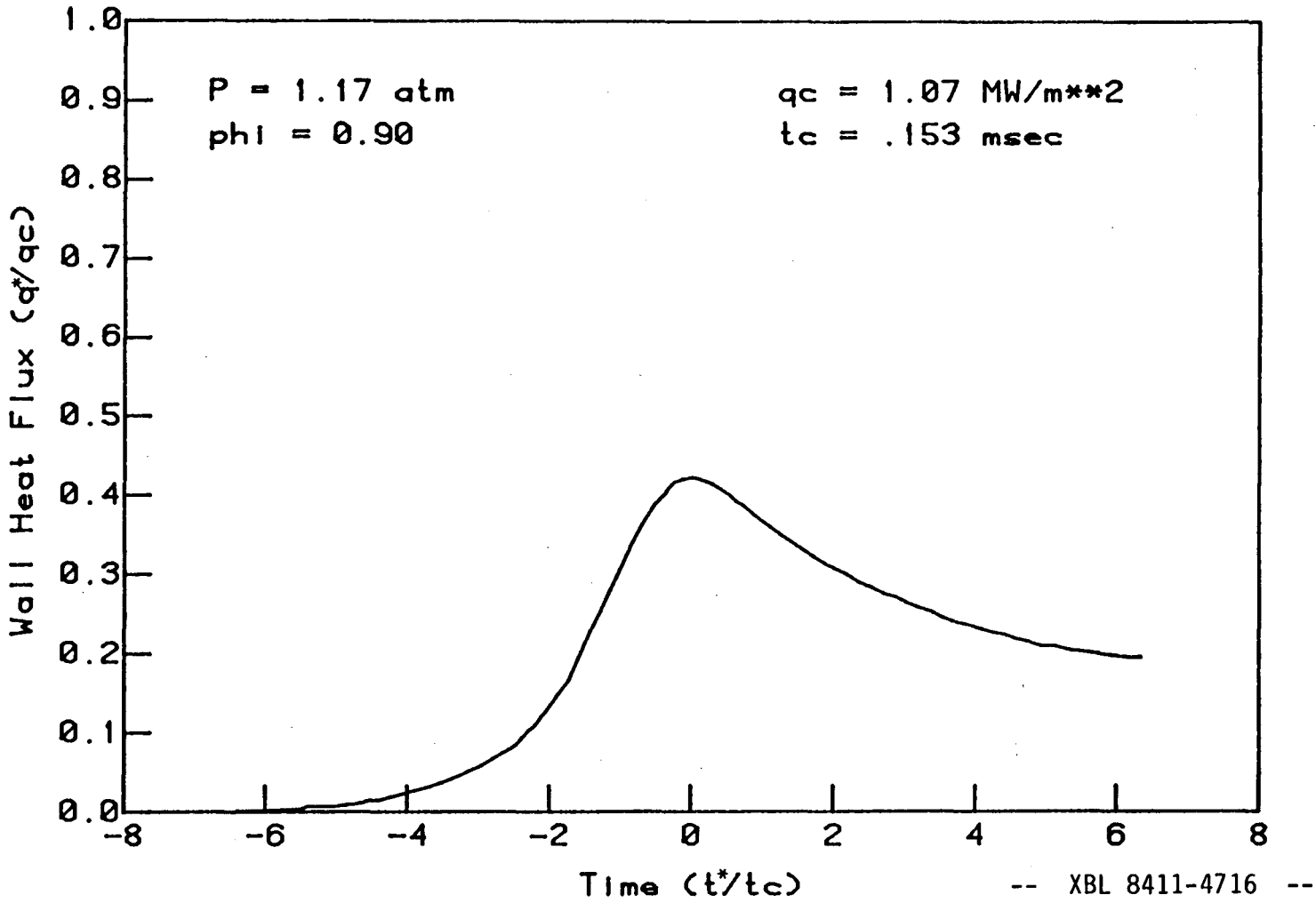

Figure D.17 Pressure scaled experimental results (Eqn 3.3) - wall heat flux vs. time - P = 1.17 atm., phi = 0.90.

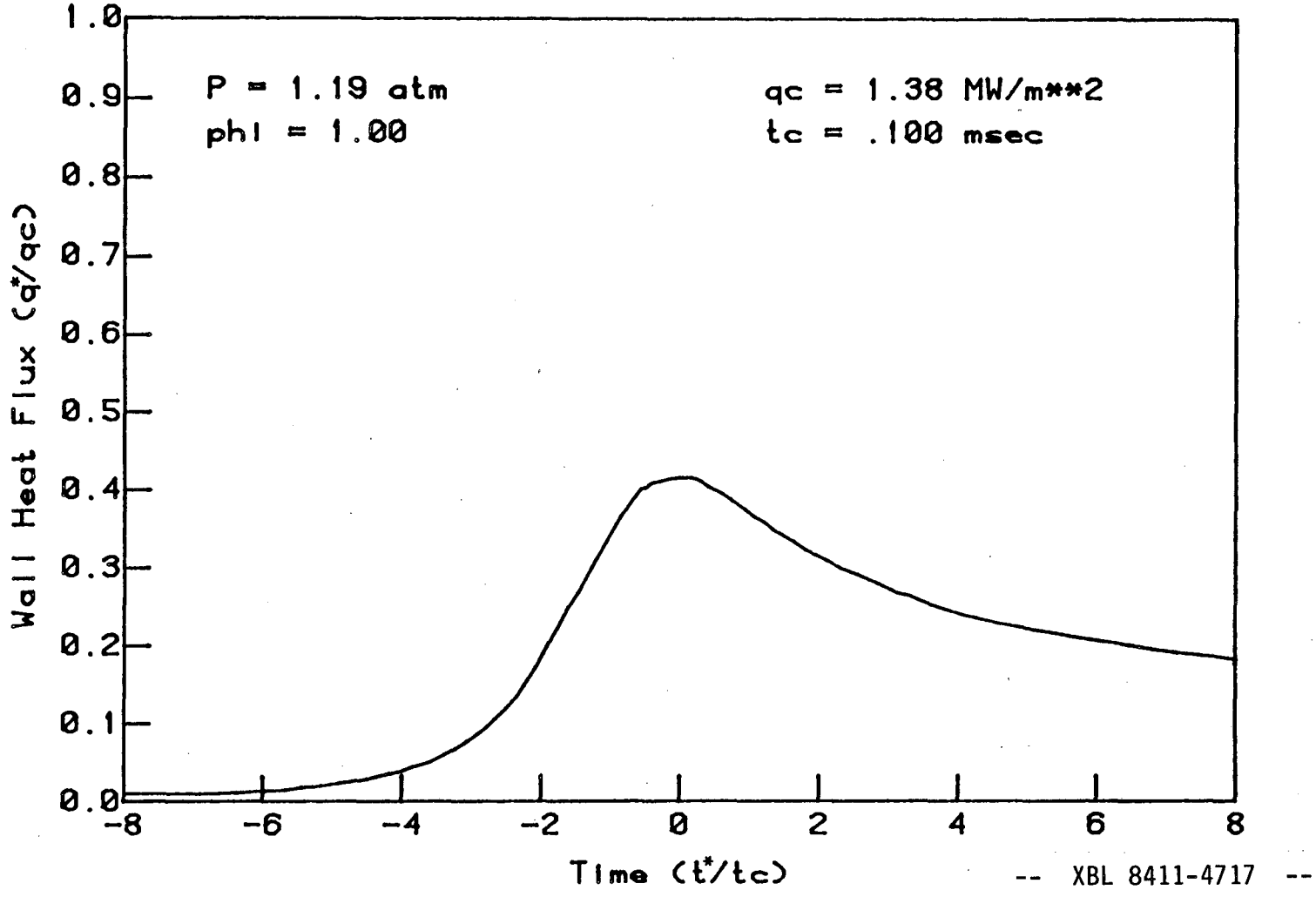

Figure D.18 Pressure scaled experimental results (Eqn 3.3) - wall heat flux vs. time - P = 1.19 atm., phi = 1.00.

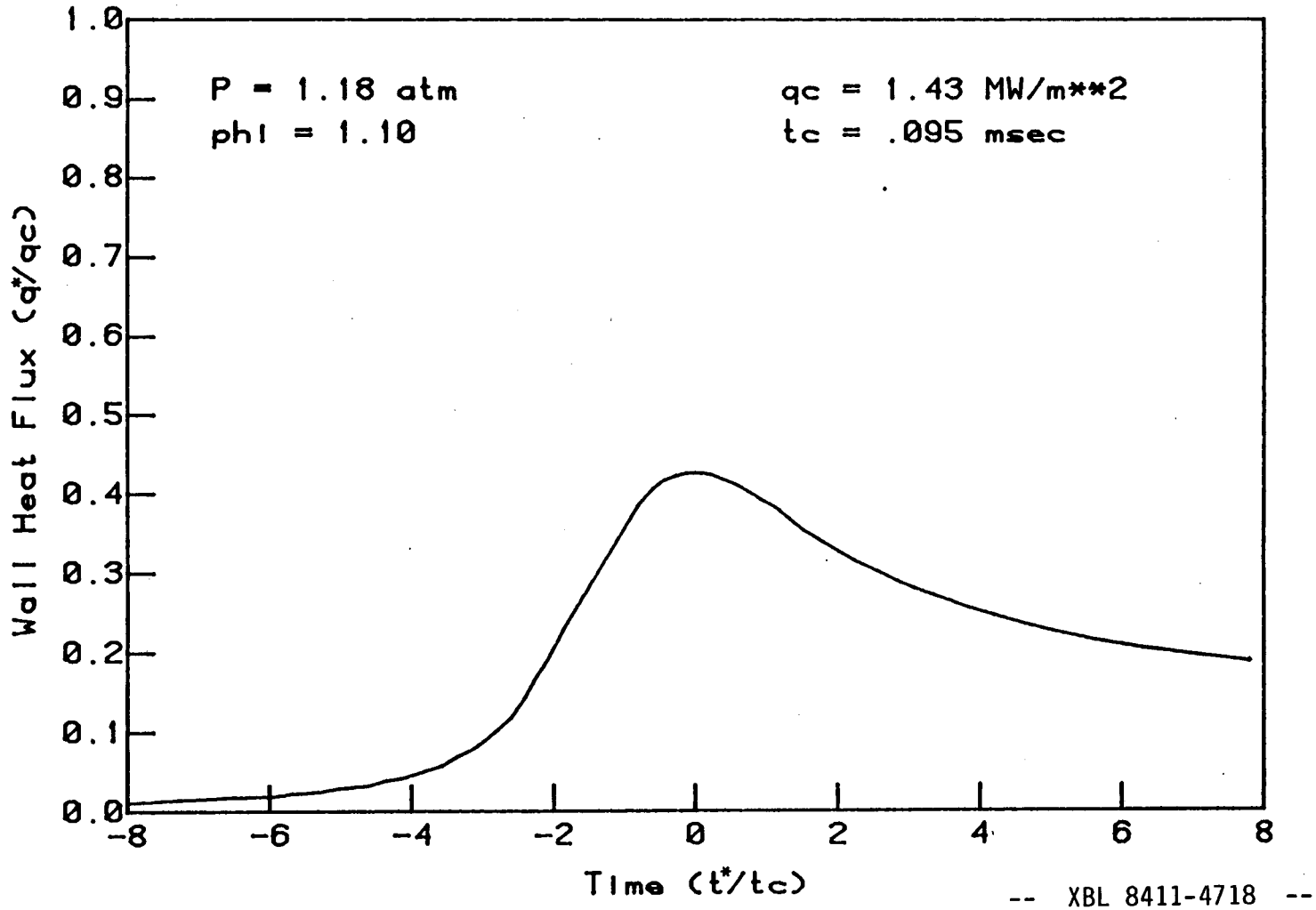

Figure D.19 Pressure scaled experimental results (Eqn 3.3) - wall heat flux vs. time - P = 1.18 atm., phi = 1.10.

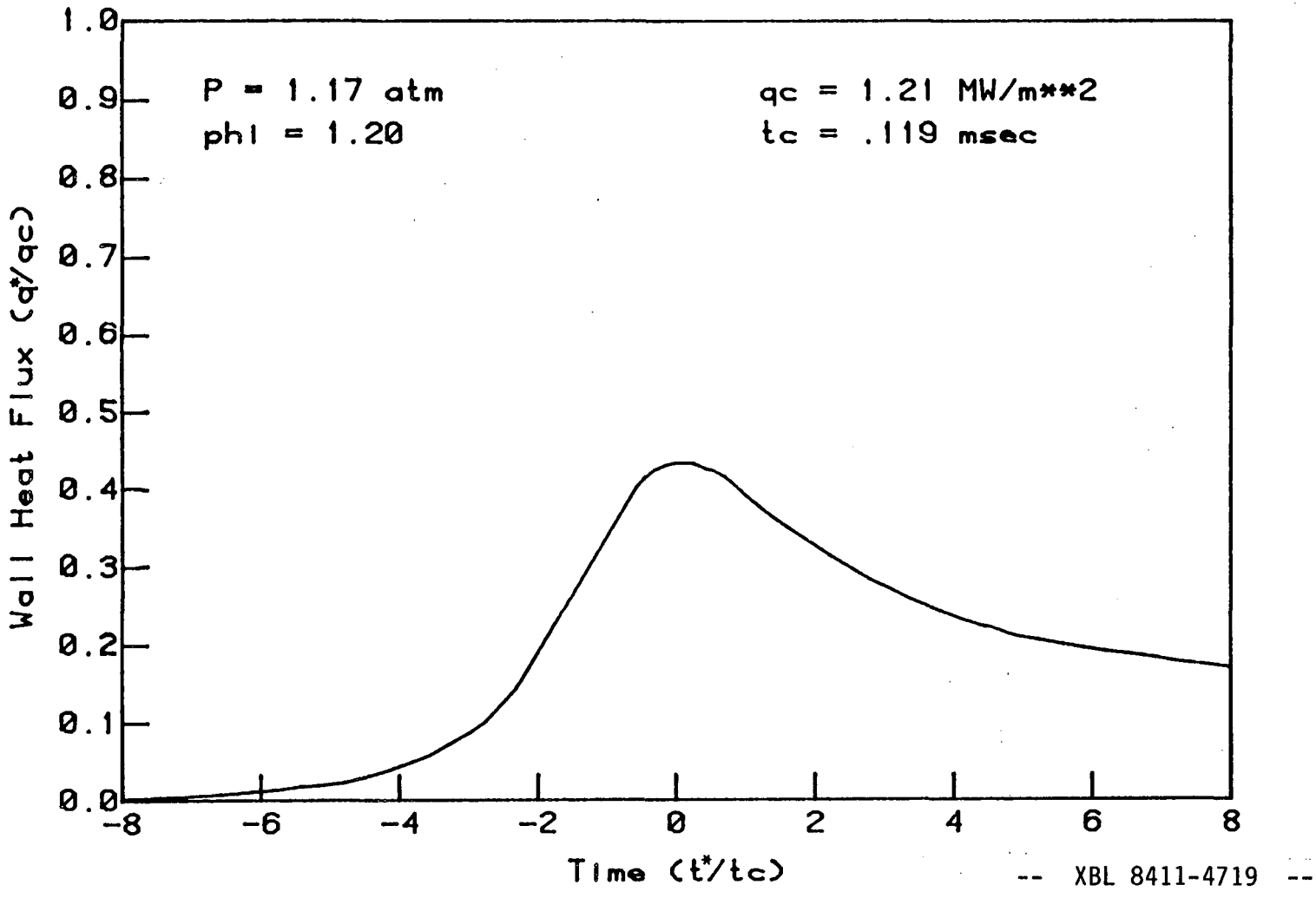

Figure D.20 Pressure scaled experimental results (Eqn 3.3) - wall heat flux vs. time - P = 1.17 atm., phi = 1.20.

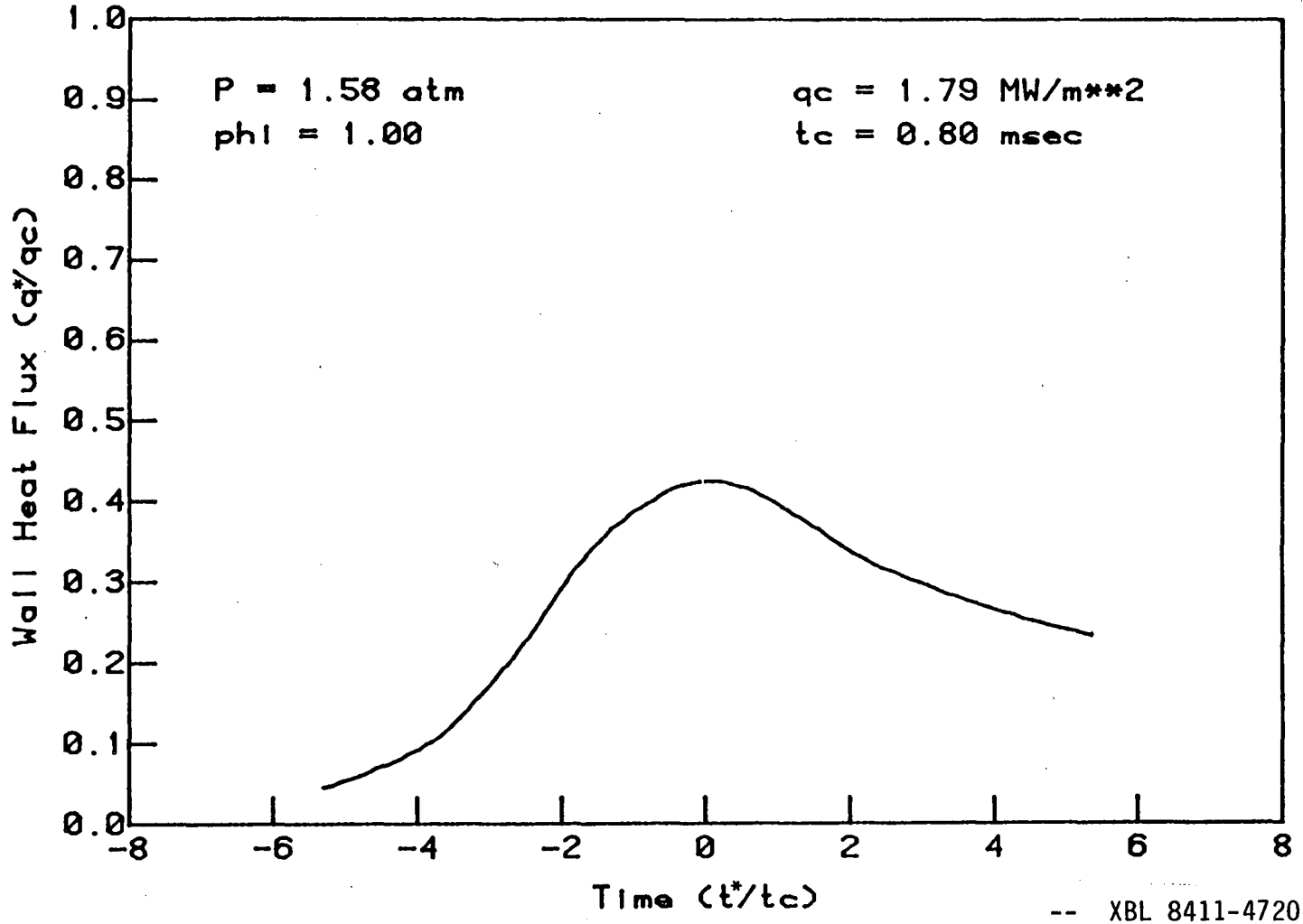

-- XBL 8411-4720 --

Figure D.21 Pressure scaled experimental results (Eqn 3.3) - wall heat flux vs. time - P = 1.58 atm., phi = 1.00.

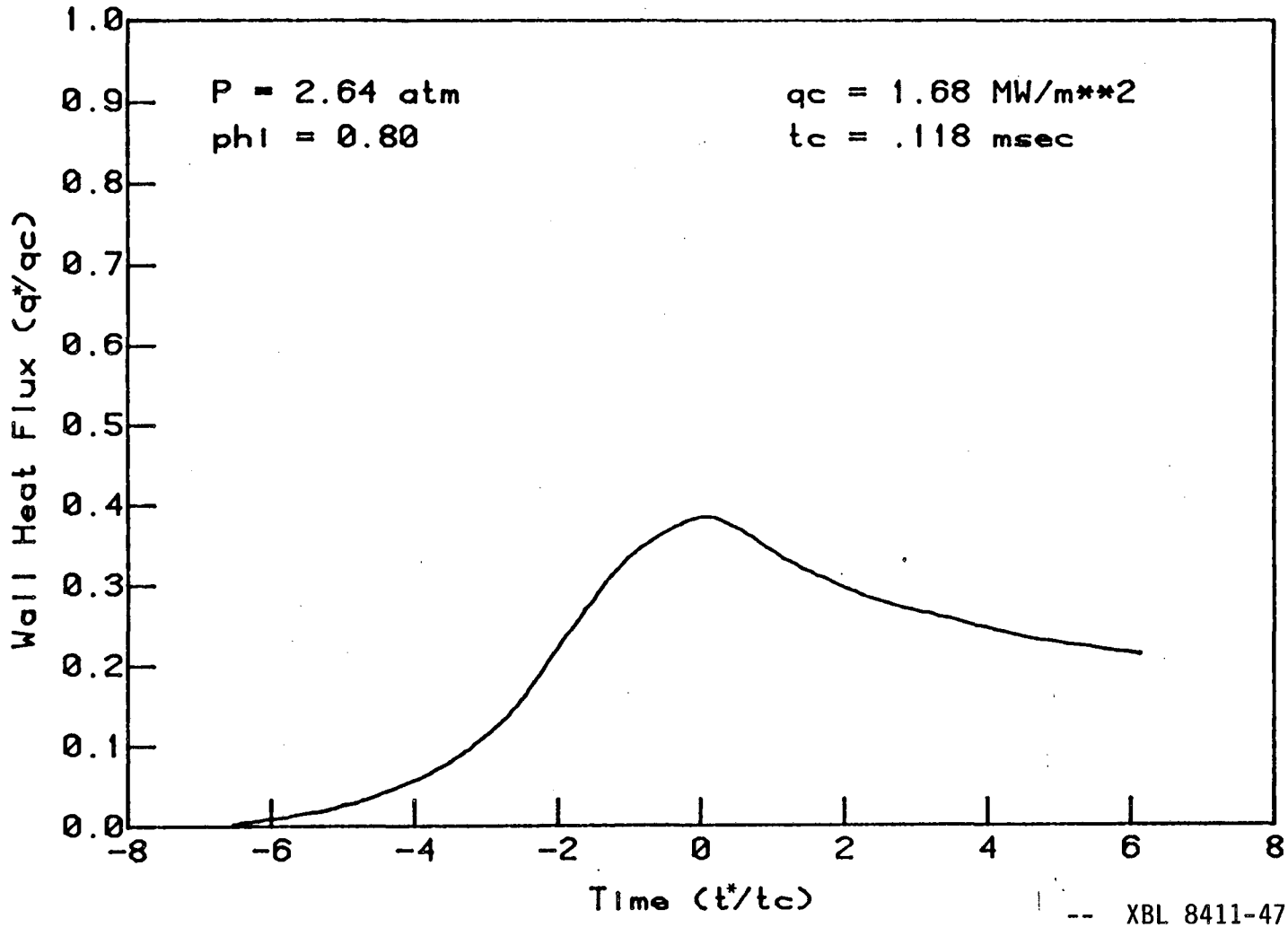

-- XBL 8411-4721 --

Figure D.22 Pressure scaled experimental results (Eqn 3.3) - wall heat flux vs. time - P = 2.64 atm., phi = 0.80.

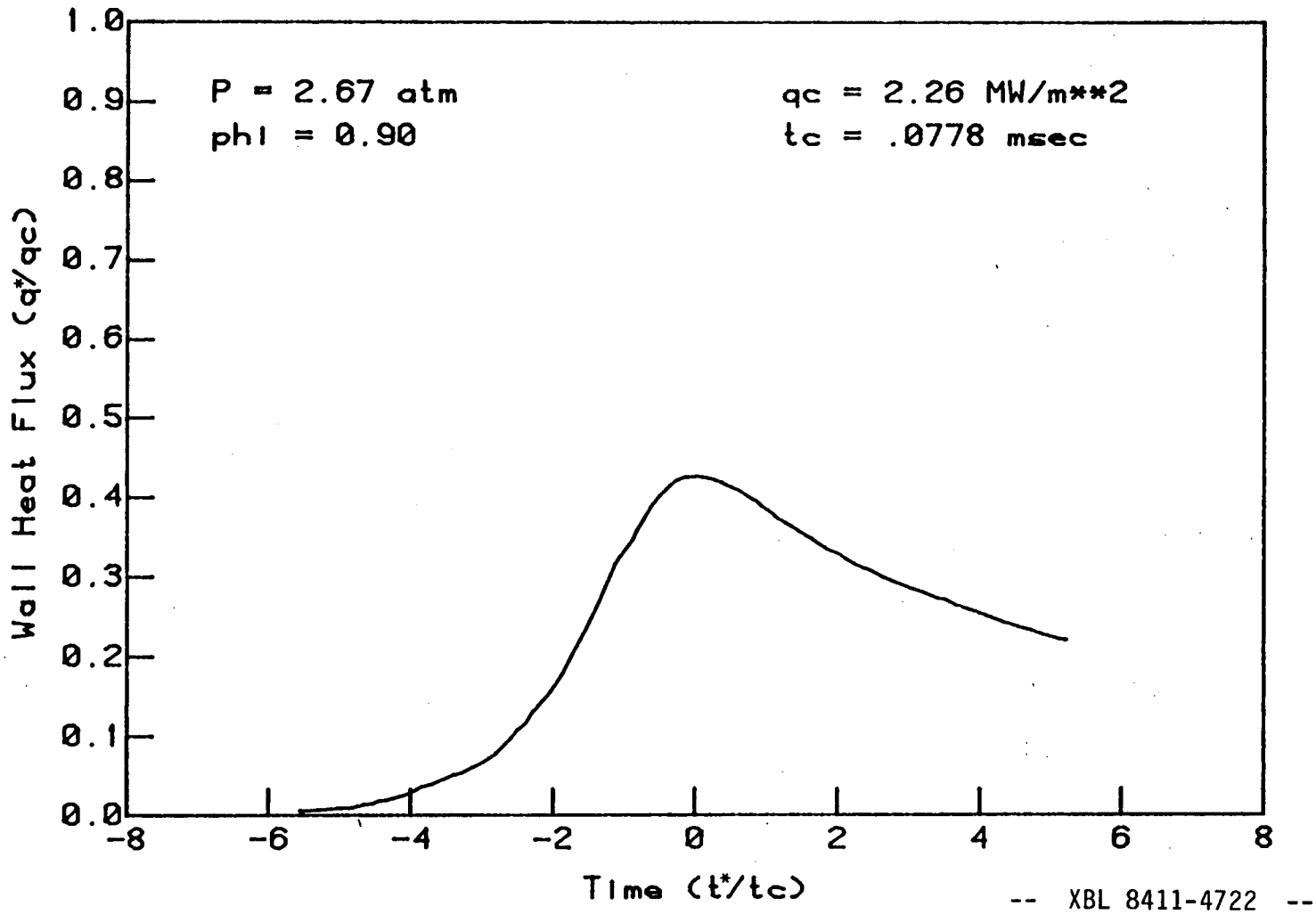

-- XBL 8411-4722 --

Figure D.23 Pressure scaled experimental results (Eqn 3.3) - wall heat flux vs. time - P = 2.67 atm., phi = 0.90.

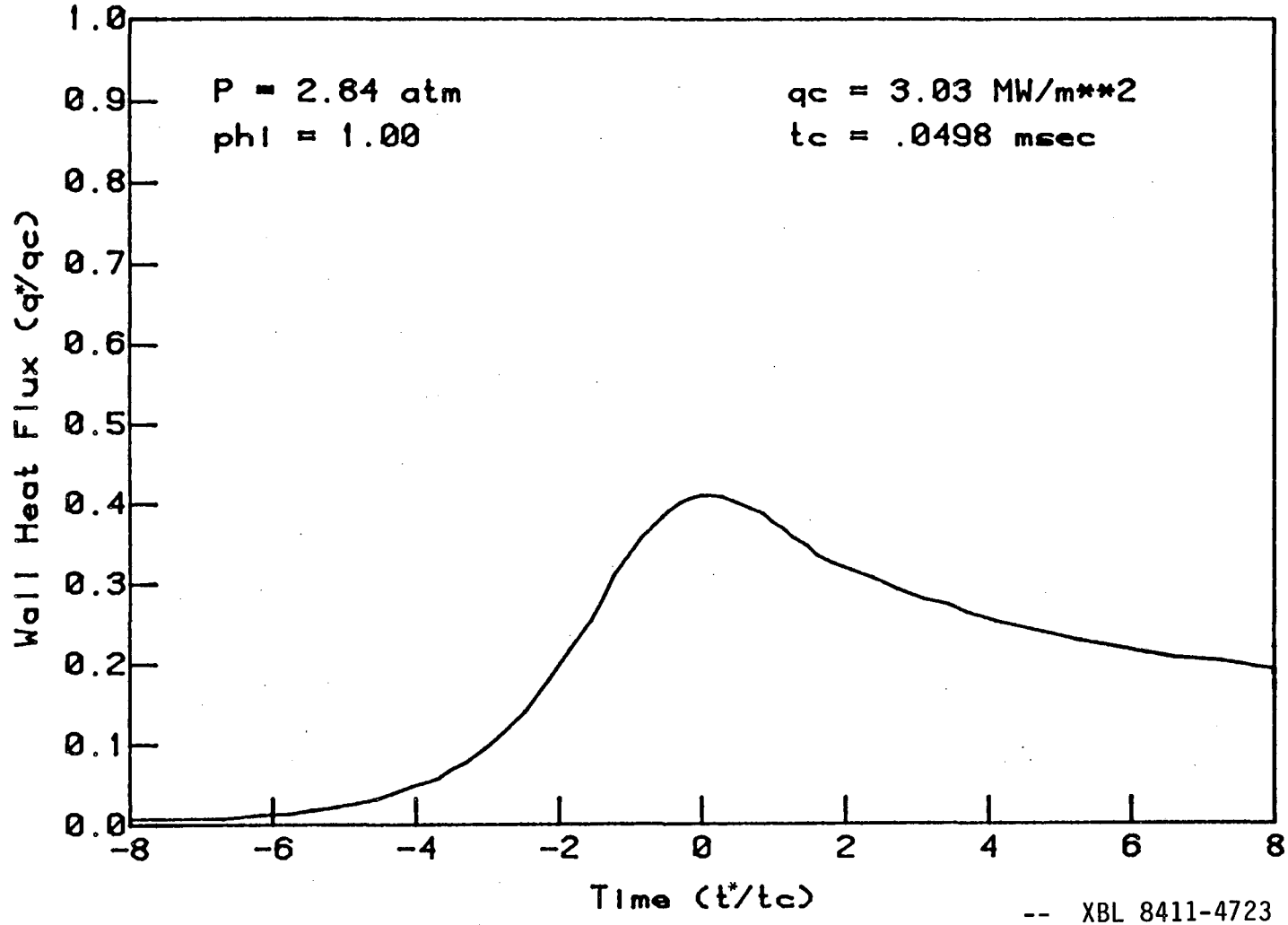

-- XBL 8411-4723 --

Figure D.24 Pressure scaled experimental results (Eqn 3.3) - wall heat flux vs. time - P = 2.84 atm., phi = 1.00.

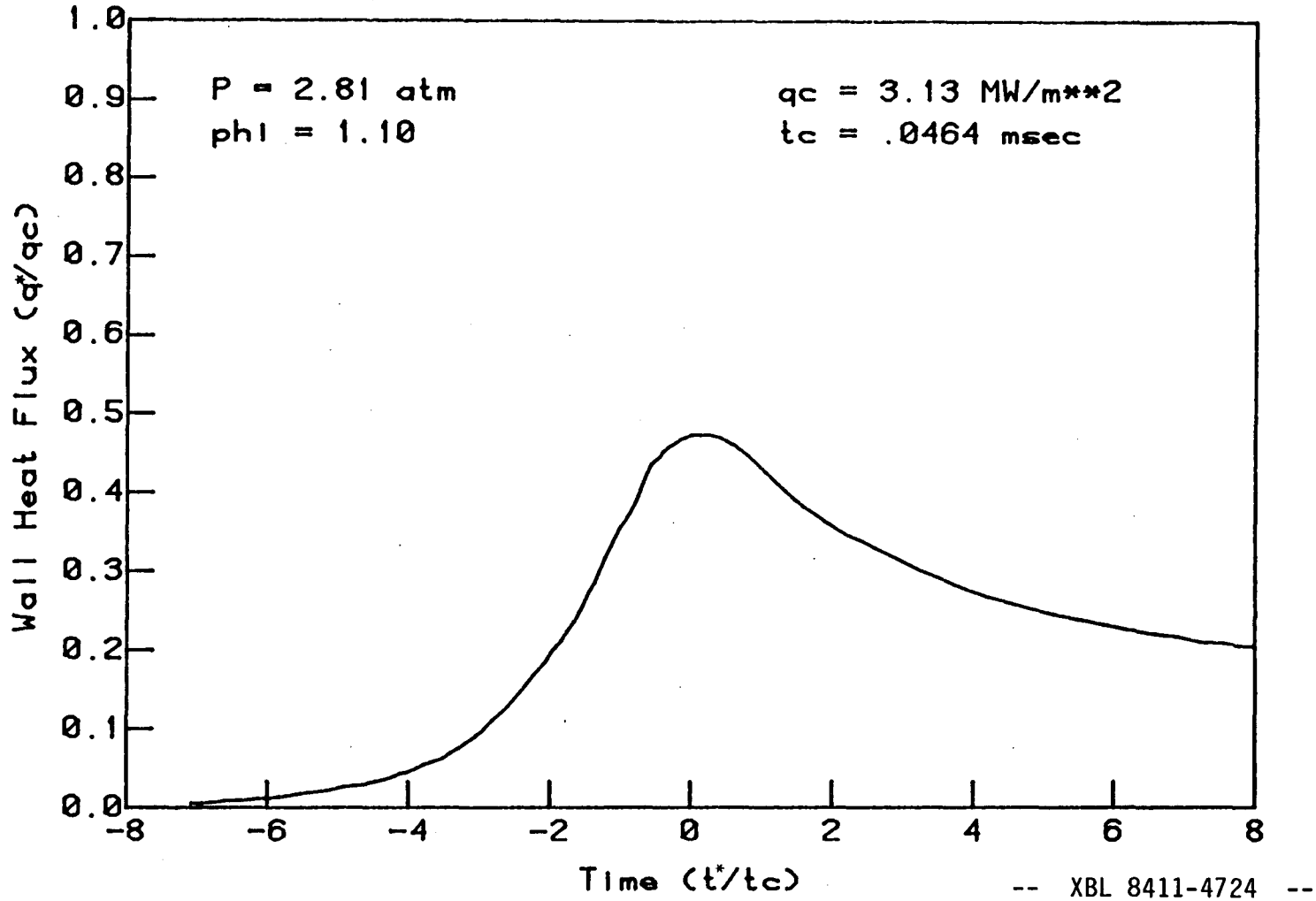

Figure D.25 Pressure scaled experimental results (Eqn 3.3) - wall heat flux vs. time - P = 2.81 atm., phi = 1.10.

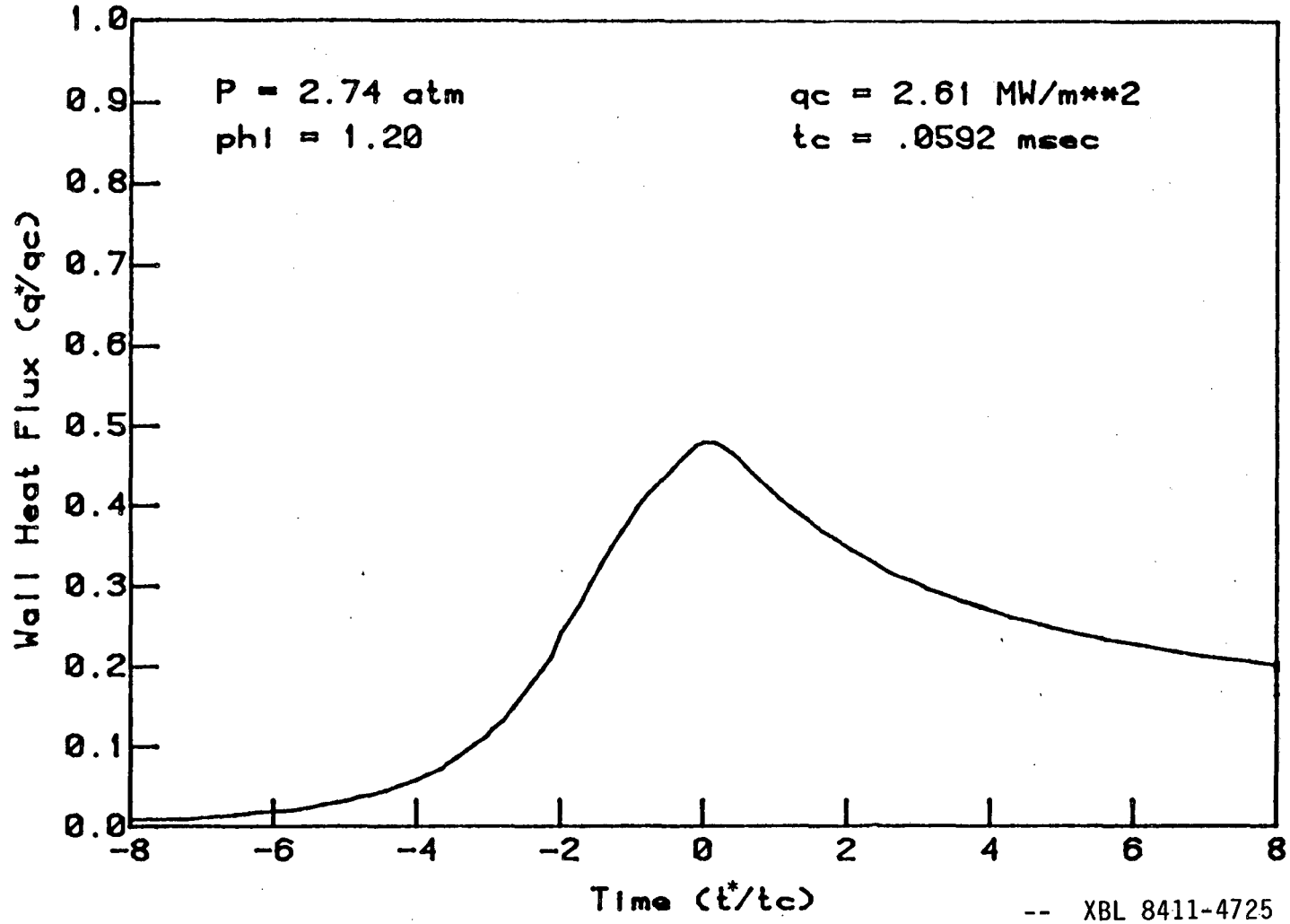

-- XBL 8411-4725 --

Figure D.26 Pressure scaled experimental results (Eqn 3.3) - wall heat flux vs. time - P = 2.74 atm., phi = 1.20.

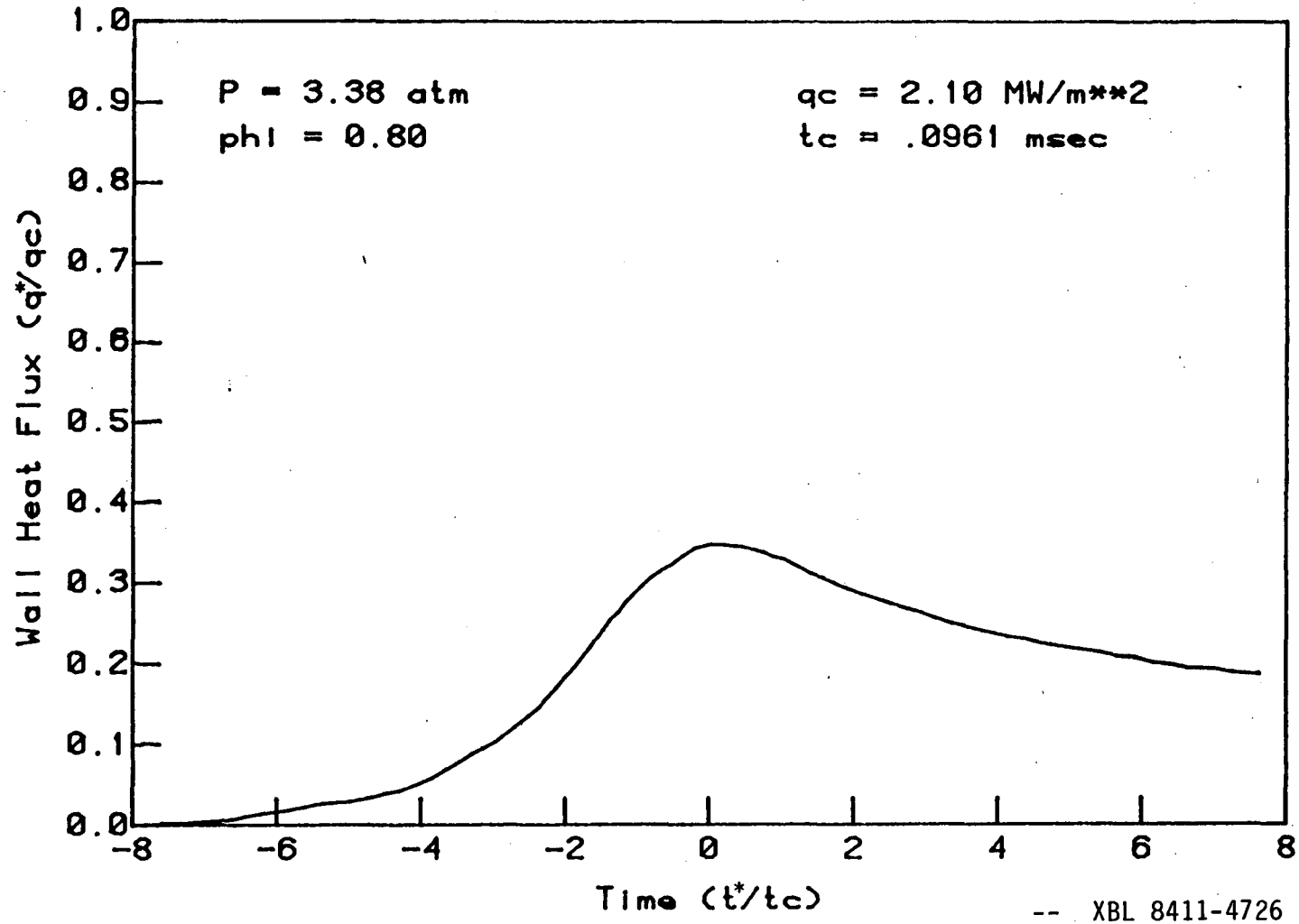

-- XBL 8411-4726 --

Figure D.27 Pressure scaled experimental results (Eqn 3.3) - wall heat flux vs. time - P = 3.38 atm., phi = 0.80.

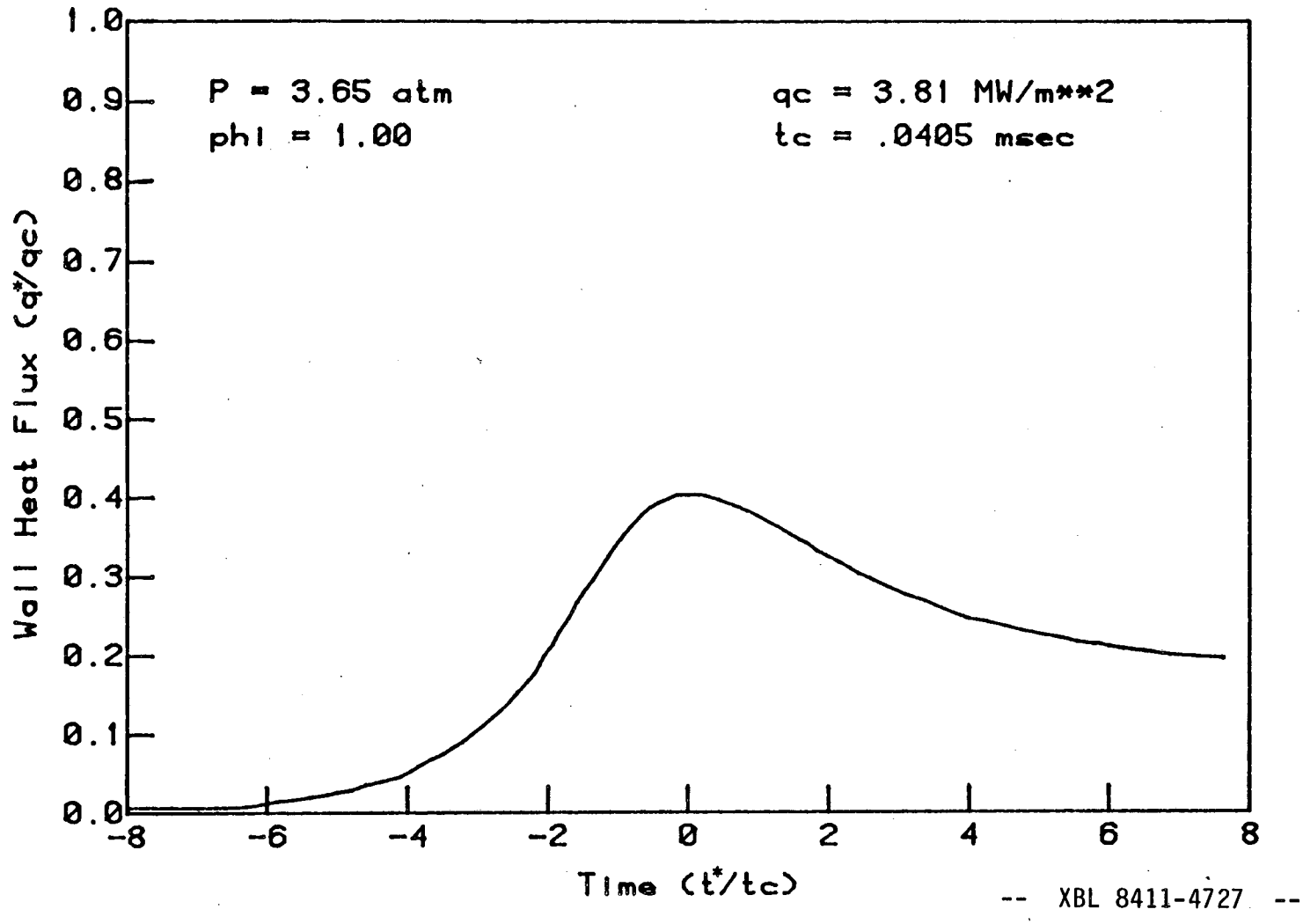

-- XBL 8411-4727 --

Figure D.28 Pressure scaled experimental results (Eqn 3.3) - wall heat flux vs. time - P = 3.65 atm., phi = 1.00.

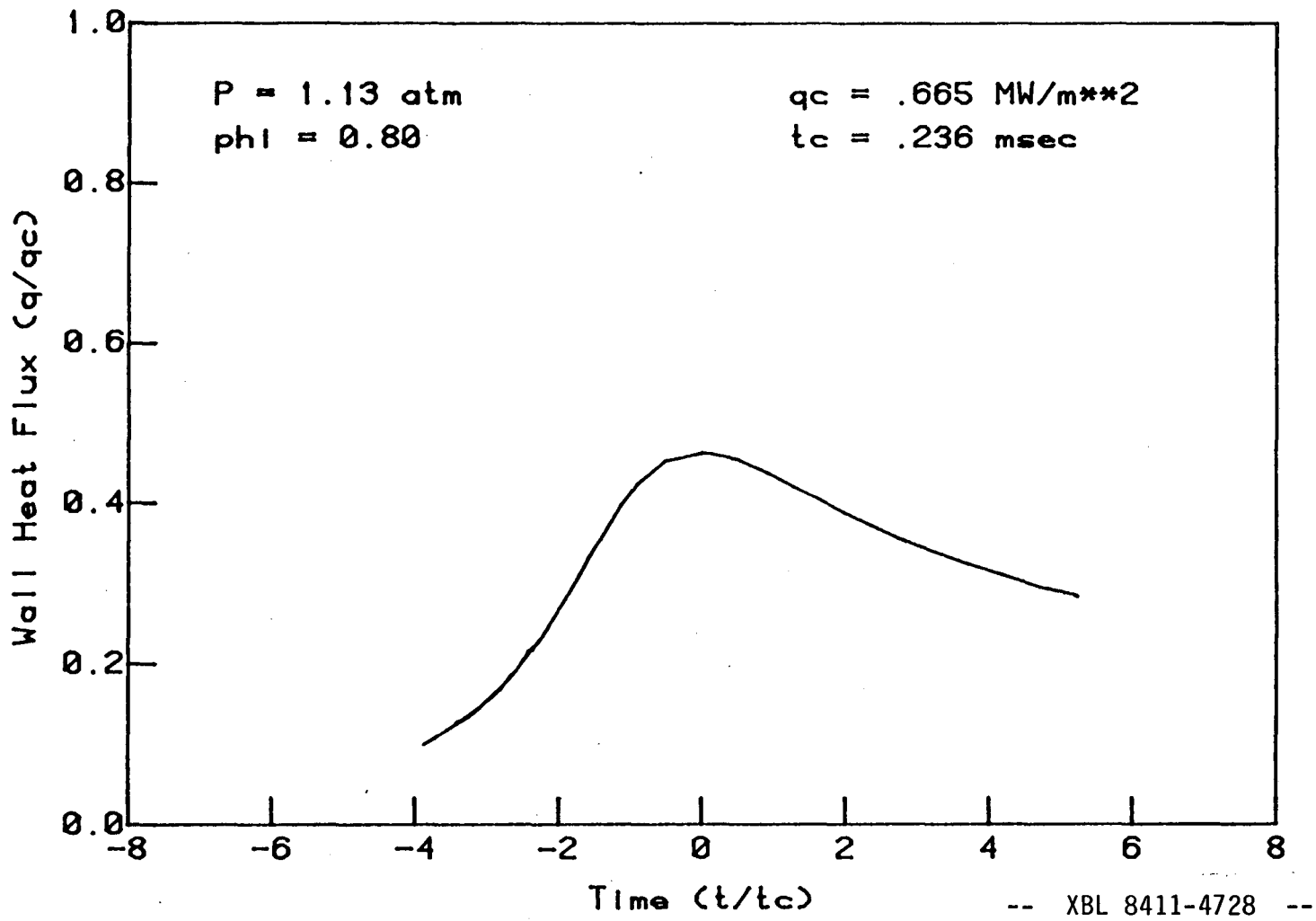

Figure D.29 One step kinetics model - wall heat flux vs. time - P = 1.13 atm., phi = 0.80.

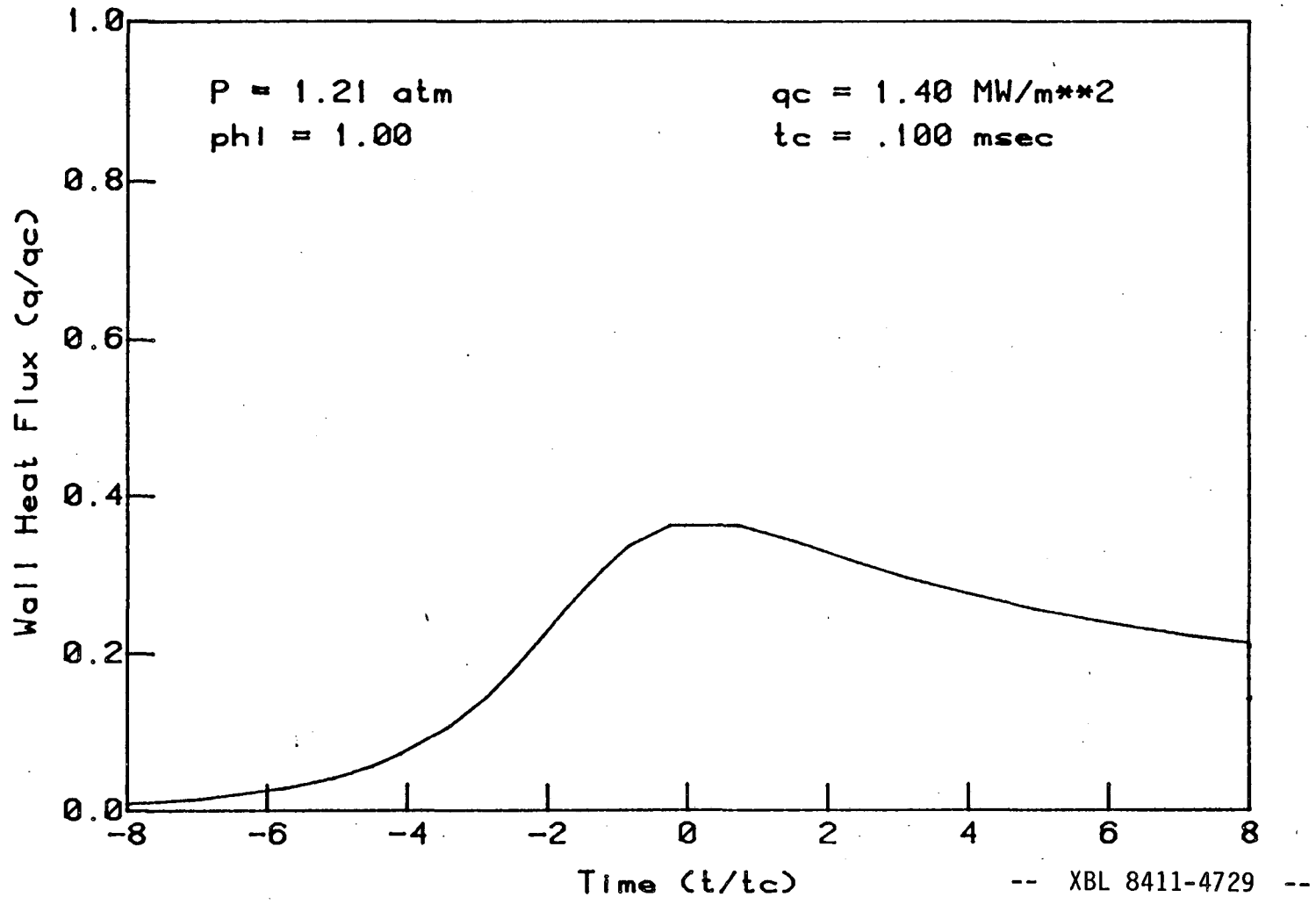

Figure D.30 One step kinetics model - wall heat flux vs. time - P = 1.21 atm., phi = 1.00.

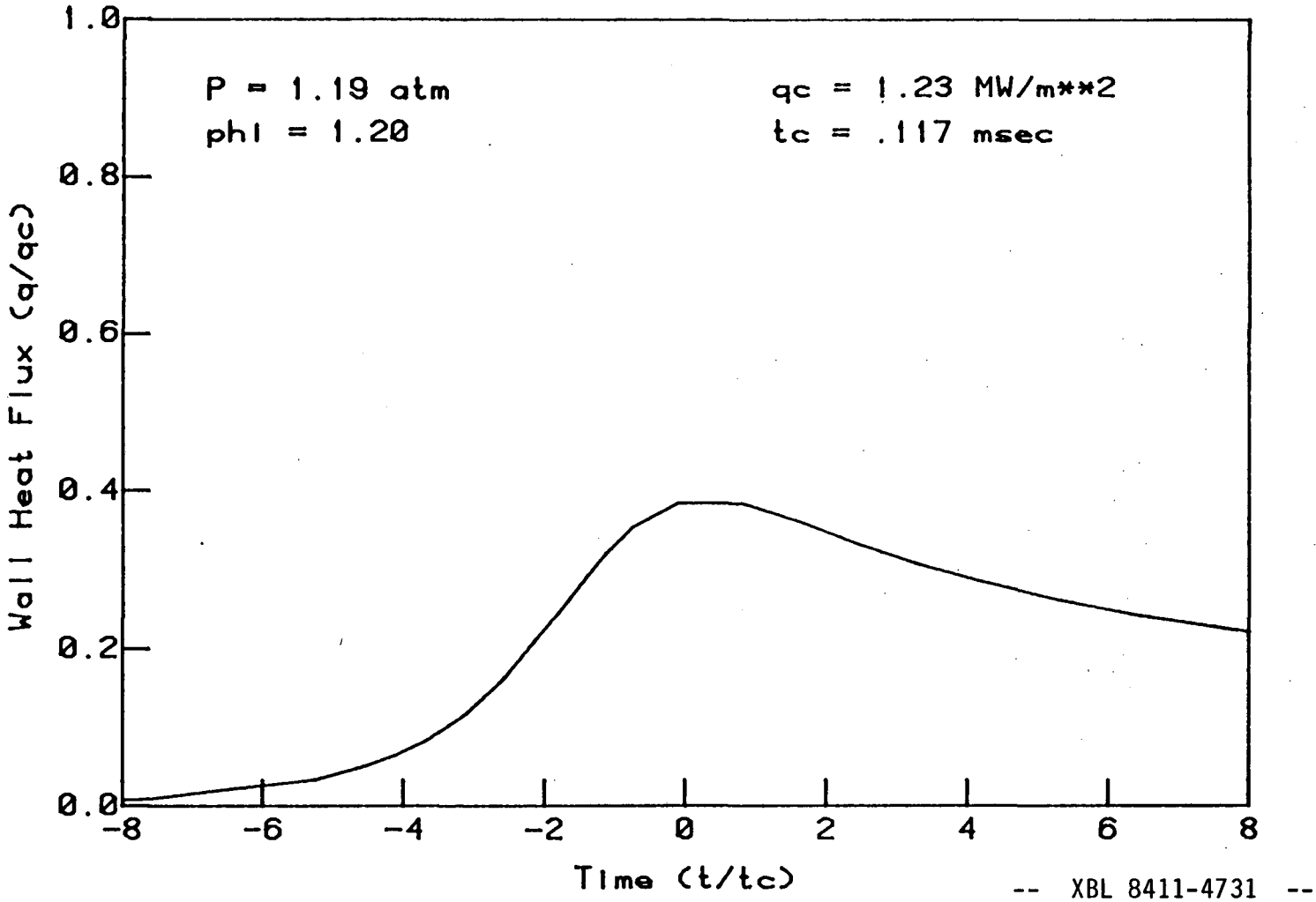

Figure D.31 One step kinetics model - wall heat flux vs. time - P = 1.19 atm., phi = 1.20.

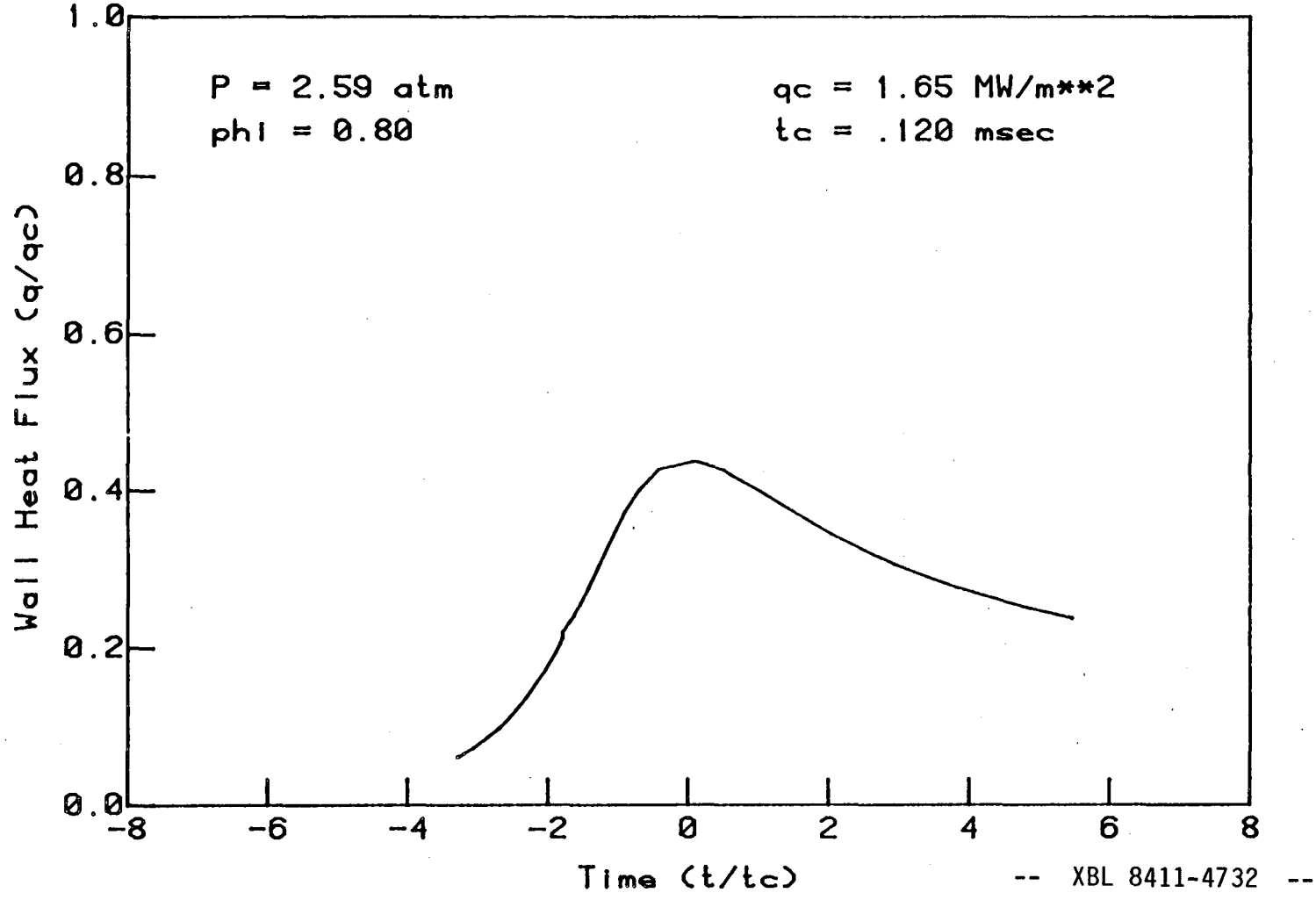

Figure D.32 One step kinetics model - wall heat flux vs. time - P = 2.59 atm., phi = 0.80

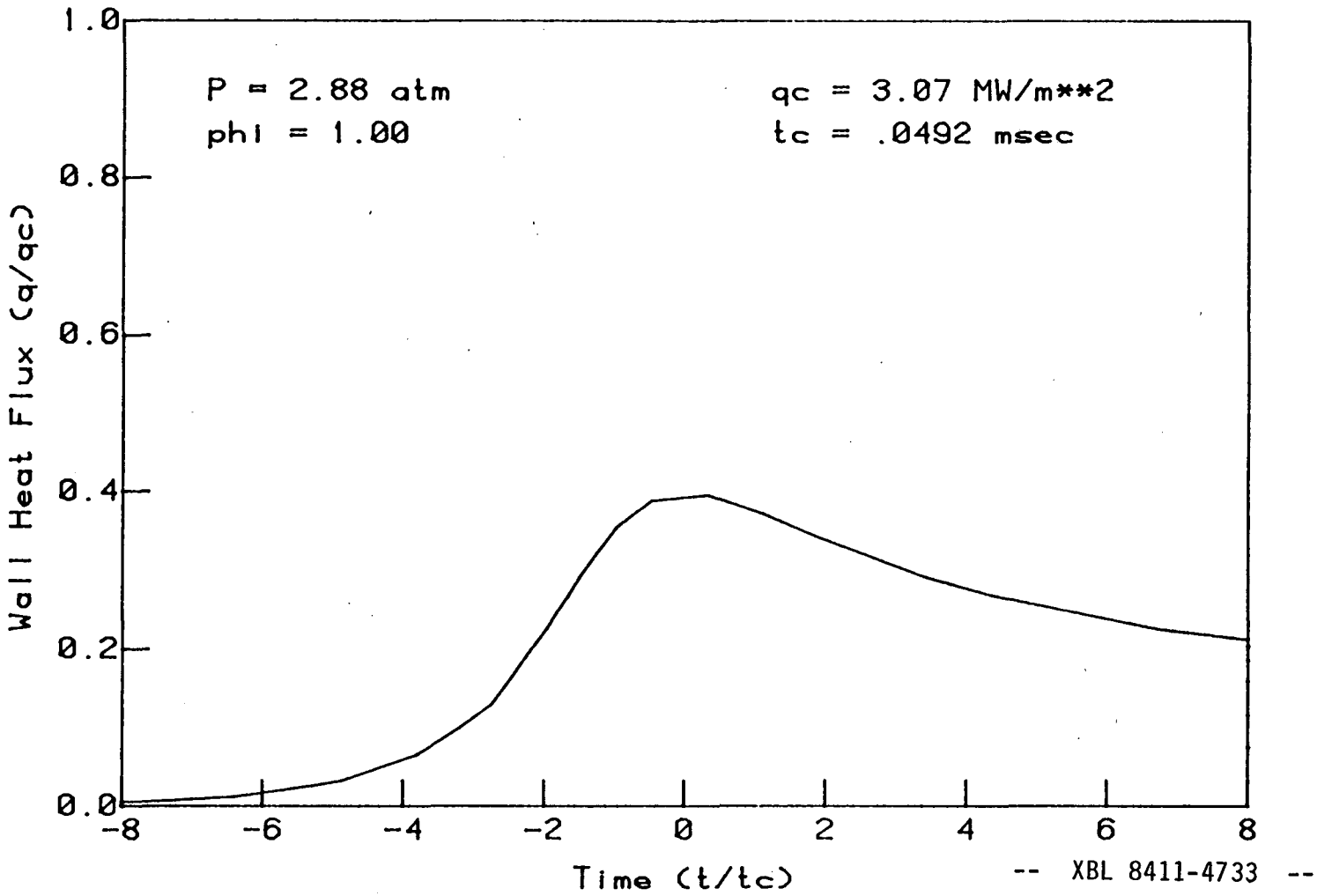

Figure D.33 One step kinetics model - wall heat flux vs. time - P = 2.88 atm., phi = 1.00.

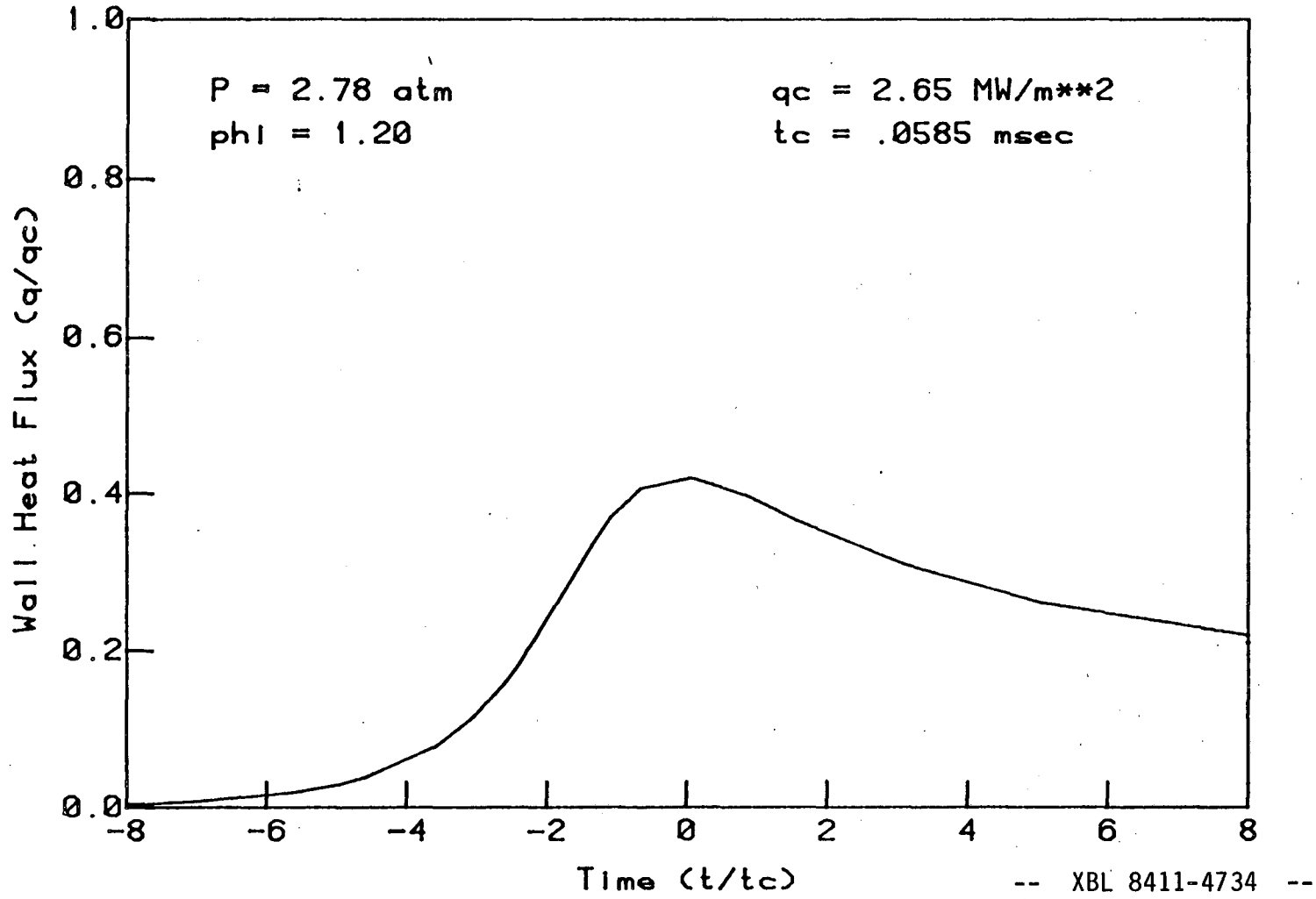

Figure D.34 One step kinetics model - wall heat flux vs. time - P = 2.78 atm., phi = 1.20.

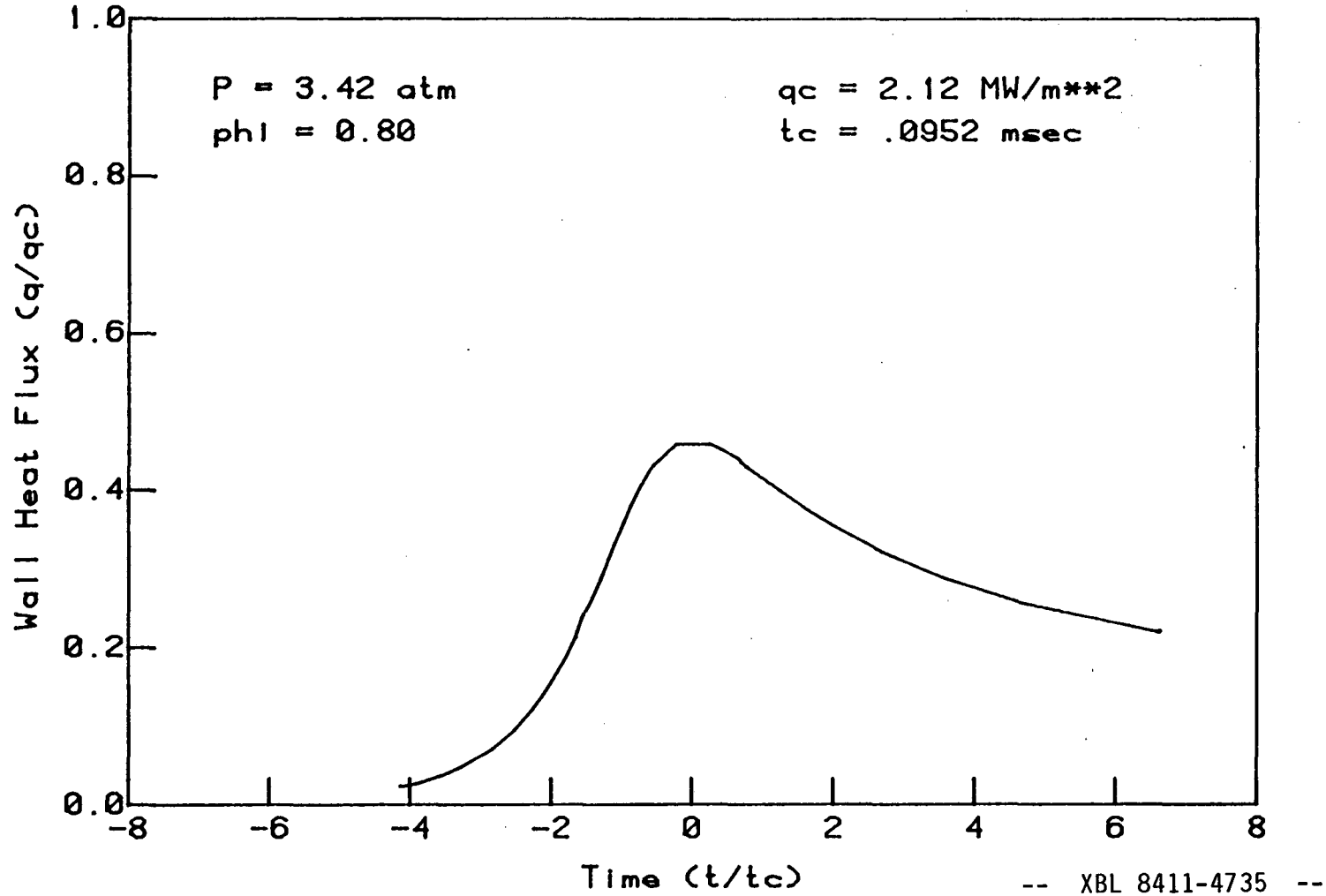

Figure D.35 One step kinetics model - wall heat flux vs. time - P = 3.42 atm., phi = 0.80.

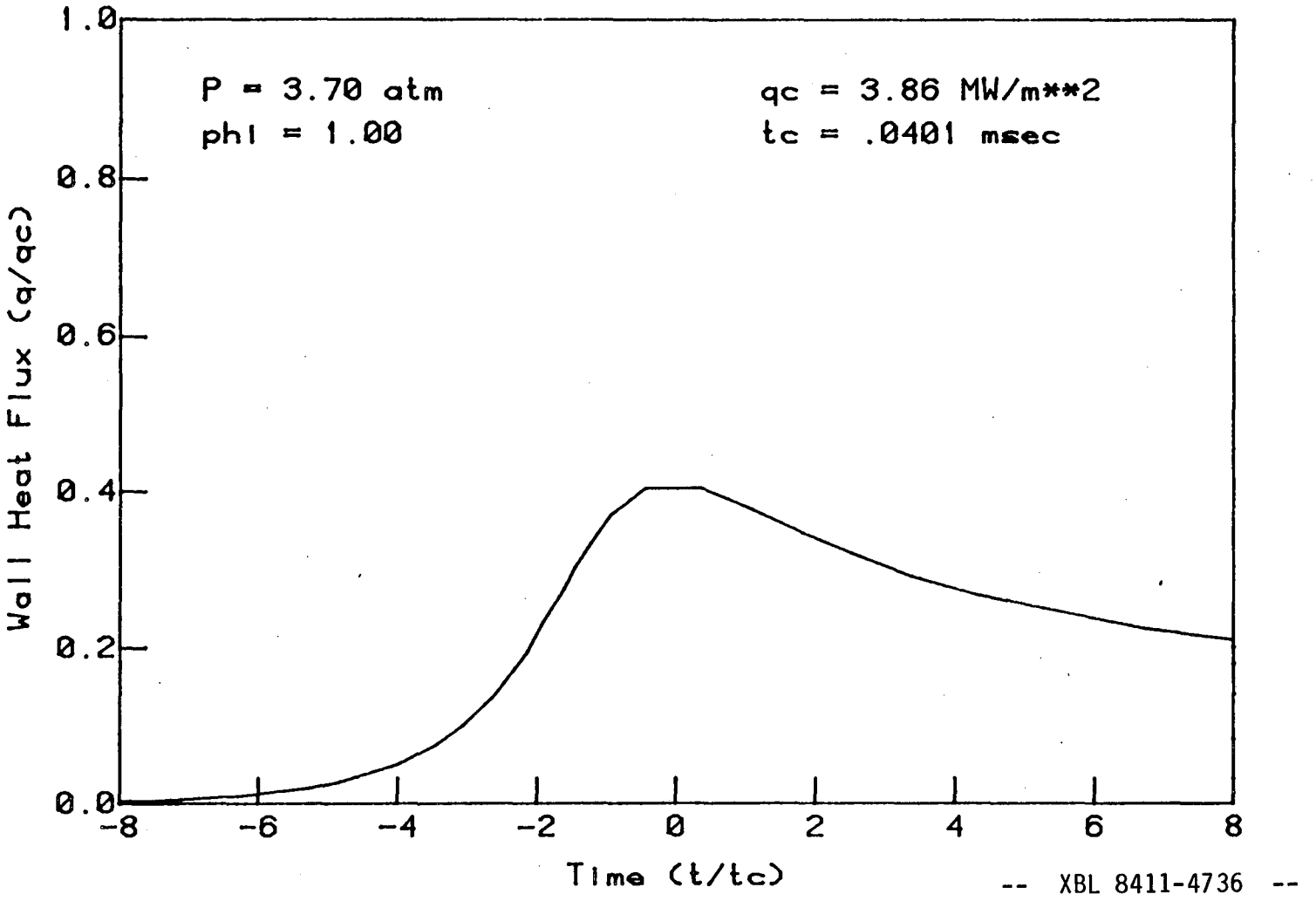

Figure D.36 One step kinetics model - wall heat flux vs. time - P = 3.70 atm., phi = 1.00.

APPENDIX E

FLUID AND FLAME PROPERTIES

E.1 FLUID PROPERTIES

The unburnt gases considered in this study were methane-air mixtures of equivalence ratio 0.70 to 1.20. The thermal conductivity, specific heat and density of these mixtures for the temperature range of 300 K to 450 K, and for pressures of 1 to 4 atmospheres were determined from by the following procedure. It was assumed that the fluid property values for both the methane and the air could be represented by equations of the form:

thermal conductivity

$$k_i = k_{oi}\left(\frac{T}{T_o}\right)^{a_{ki}} \tag{E.1}$$

specific heat

$$c_{pi} = c_{poi}\left(\frac{T}{T_o}\right)^{a_{cpi}} \tag{E.2}$$

where i = air, methane. For a reference temperature, T_o, of 300 K, and a reference pressure of, p_o, of 1 atmosphere, the constants in Equations E.1 and E.2 for pure methane and for air [Kays & Crawford, 1980], and for a stoichiometric mixture, are listed in Table E.1. The properties of the mixture were assumed to be given by the appropriate sum over the properties of the components:

$$M = \sum_i Y_i M_i \tag{E.3}$$

$$\rho = \frac{pM}{RT} \tag{E.4}$$

$$k = \sum_i k_i Y_i \tag{E.5}$$

$$c_p = \frac{1}{M}\sum_i c_{pi} M_i Y_i \tag{E.6}$$

Table E.1
Coefficients for Fluid Property Variation

	$k_o \left[\frac{W}{m°K}\right]$	a_k	$c_{p_o} \left[\frac{J}{kg°K}\right]$	a_{c_p}	$\rho_o \left[\frac{kg}{m^3}\right]$
CH_4	.0338	1.315	2262	.450	.620
Air	.0261	.812	1005	.037	1.177
$\varphi=1$	.0268	.881	1074	.090	1.127

$$k = k_o \left[\frac{T}{T_o}\right]^{a_k} \quad ; \quad c_p = c_{p_o} \left[\frac{T}{T_o}\right]^{a_{c_p}} \quad ; \quad \rho = \rho_o \left[\frac{p}{p_o}\right]\left[\frac{T_o}{T}\right]$$

The stoichiometric methane-air mass fractions are:

$$Y_{CH_4}\Big|_{st} = .0951 \quad ; \quad Y_{AIR}\Big|_{st} = .9049$$

The stoichiometric fuel-air ratio is:

$$FA_{st} = \frac{Y_{CH_4}}{Y_{AIR}}\Bigg|_{st} = .1051$$

The equivalence ratio, φ, is defined as

$$\varphi = \frac{FA}{FA_{st}}$$

so the mass fractions as a function of the equivalence ratio are

$$Y_{CH_4} = \left(1 + \left[\varphi FA_{st}\right]^{-1}\right)^{-1}$$

$$Y_{AIR} = 1 - Y_{CH_4} \tag{E.7}$$

Given the equivalence ratio, the property values for the mixture are given by Equation E.1 to E.7 and the values in Table E.1.

The ratio of specific heats, $\gamma=c_p/c_v$ does not change appreciably over the range of equivalence ratios, and is taken to be the value for stoichiometric methane-air,

$$\gamma = 1.39 \tag{E.8}$$

For isentropic compression from the initial conditions of $T = T_o$ and $p = p_o$, to the pressure p_q, the temperature of the unburnt gases is given by

$$T_u = T_o \left[\frac{p_q}{p_o}\right]^{\frac{\gamma-1}{\gamma}} \tag{E.10}$$

E.2 FLAME PROPERTIES

It has been assumed that the flame speed can be written in the form

$$S_u = F_S(\varphi)\, G(T_u, p) \tag{E.11}$$

For a stoichiometric methane-air mixtures, the experimentally determined flame speed has been taken from Bradley and Mitcheson (1976) to be

$$G(T_u, p) = .10 + 3.71\text{x}10^{-6}\, T_u^2 - 5.2\text{x}10^{-5}\, T_u^{1.5} \log_{10}(p) \quad \left[\frac{m}{sec}\right] \quad . \tag{E.12}$$

where [T] = K, and [P] = Atmos. Again assuming adiabatic compression, Equation E.10 may be substituted into Equation E.12 to give

$$G_{ad}(p) = .10 + .334p^{.571} - .27p^{.429}\log_{10}(p) \quad \left[\frac{m}{sec}\right] \quad . \tag{E.13}$$

The pressures which occurred in the experiment were in the range of one to four atmospheres. The flame speed as given from Equation E.13 can be curve fit over the smaller pressure range to give

$$G_{ad}(p) \approx .435p^{.161} \quad \left[\frac{m}{sec}\right] \tag{E.14}$$

and thus

$$S_u = .435F_S(\varphi)p^{.161} \quad \left[\frac{m}{sec}\right] \quad . \tag{E.15}$$

For the form of the function $F_S(\varphi)$ in Equation E.11, data for methane-air flames at one atmosphere was used [Andrews and Bradley, 1972]. These data are presented in Table E.2. From Equation E.14 and the information presented in Table E.2, the flame speed can be obtained over the range of pressures and

equivalence ratios encountered in the experiment.

The temperature rise across the flame, ΔT_f, was taken to be a function of equivalence ratio only,

$$\Delta T_f(\varphi) = \Delta T_f(1) F_T(\varphi) \tag{E.16}$$

where

$$\Delta T_f(1) = 1920K \tag{E.17}$$

for methane - air. The function $F_T(\varphi)$ is presented in Table E.2.

Table E.2
Dependence of Flame Speed and
Flame Temperature on Equivalence Ratio

φ	$F_S(\varphi)$	$F_T(\varphi)$
0.7	.51	.76
0.8	.67	.88
0.9	.82	.96
1.0	1.00	1.00
1.1	1.04	1.00
1.2	.93	.96

$$S_u(\varphi) = S_u(\varphi=1)\, F_S(\varphi)$$
$$\Delta T_f(\varphi) = \Delta T_f(\varphi=1)\, F_T(\varphi)$$

E.3 DERIVED QUANTITIES

The characteristic time for quenching is the same as that for a steady flame at the same pressure and unburnt gas temperature:

$$t_c = \left(\frac{\alpha}{S_u^2}\right)_{P_q, T_u} \tag{E.18}$$

The characteristic heat flux is given by the heat release rate in a steady flame:

$$q_c = (\rho S_u c_p \Delta T_f)_{P_q, T_u} \tag{E.19}$$

The values for k, ρ and c_p are determined by method outlined in section E.1. For a stoichiometric mixture, Equation E.8 may be combined with Equations E.18 and E.19 to give

$$t_c = .117\left(\frac{p_q}{p_o}\right)^{-0.819} \tag{E.20}$$

$$q_c = 1.18\left(\frac{p_q}{p_o}\right)^{0.905} \tag{E.21}$$

APPENDIX F

DERIVATION OF HEAT FLUX VS. TIME - after ISSHIKI & NISHIWAKI

Isshiki & Nishiwaki (1974) derive an analytic solution for the wall heat transfer during quenching. The following is a summary of their derivation.

Starting with the equations of continuity and energy, we have

$$\frac{\partial \rho}{\partial t} + \frac{\partial \rho u}{\partial x} = 0 \quad ,$$

$$\rho c_p \frac{DT}{Dt} = \frac{\partial}{\partial x} k \frac{\partial T}{\partial x} + \frac{Dp}{Dt} + \rho Q(x,t) \quad .$$

The source term in the energy equation, $Q(x,t)$, is a function of the reaction rates for the combustion of the fuel. In this derivation, the form of the source term will be specified in order to simplify the analysis.

The variation of the thermal properties is assumed to be of the form

$$k \sim T$$

$$c_p = constant.$$

and the pressure is assumed to be constant during quenching. The equation for the conservation of energy then becomes

$$\rho c_p \frac{Dt}{Dt} = \frac{\partial}{\partial x} k_o \frac{T}{T_o} \frac{\partial T}{\partial x} + \rho Q \quad . \tag{F.1}$$

Transforming to mass coordinates, (ψ,t), where

$$\frac{\partial \psi}{\partial x} = \frac{\rho}{\rho_o} \quad ; \quad \frac{\partial \psi}{\partial t} = -\frac{\rho u}{\rho_o}$$

and the reference state (subscript o) referring to the initial pressure and temperature, the energy equation becomes

$$\frac{\partial T}{\partial t} = \alpha_o \frac{\partial^2 T}{\partial \psi^2} + \frac{p_o}{p_q} \frac{Q}{c_p} \quad , \tag{F.2}$$

The wall heat flux is given by

$$q_w = -k_o \frac{\rho_w}{\rho_o} \frac{\partial T}{\partial \psi}\bigg|_w = -k_o \frac{T_o}{T} \frac{p}{p_o} \frac{\partial T}{\partial \psi}\bigg|_w \quad . \tag{F.3}$$

It was assumed that the flame propagates up to the wall at a constant velocity, and that the heat generation is uniform throughout the flame. Thus the source term in the energy equation was taken to be a moving, constant strength source of finite extent, and he strength of the source is

$$Q = \frac{c_p \Delta T_f S_u}{L_f} \quad .$$

The maximum heat flux will occur during the time when the flame is at the wall, which is denoted as the "second period". At the start of the second period, the front of the source term has just made contact with the wall, and the back of the source term is located a distance Δx_f (the flame thickness) from the wall. The back of the source term continues to propagate at a velocity S_u (the flame speed) towards the wall. The duration of the flame wall interaction is thus

$$t_f = \frac{\Delta x_f}{S_u} \quad ,$$

giving a source strength of

$$Q = \frac{c_p \Delta T_f}{t_f} \quad . \tag{F.4}$$

The problem as formulated is linear, and may be considered to be the superposition of the following three problems:

1) A uniform source term from $z = 0$ to $z = \infty$, for $0 < t < t_f$.

2) A uniform sink term whose front is located at $z = L_f$ at the start of the second period, and which propagates towards the wall with a speed of U_f.

3) The temperature distribution at the start of the second period.

The effect of 1) on the wall heat flux is much greater than the effect of 2) or 3). Thus the important contribution to the heat flux is obtained by considering a gas of semiinfinite extent, at the wall temperature, which has uniform heat generation throughout for a finite period of time, t_f. Combining F.2 and F.4, the problem then reduces to

$$\frac{\partial T}{\partial t} = \alpha_o \frac{\partial^2 T}{\partial \psi^2} + \frac{p_o}{p_q}\frac{\Delta T_f}{t_f} \quad ; \quad 0<t<t_f \tag{F.5}$$

with

$$T(\psi,0) = T_o \quad .$$

The solution of the above equations gives the heat flux at the wall to be

$$q_w = \frac{2k_o \Delta T_f}{\sqrt{\pi \alpha_o t_f}}\left[\frac{p_q}{p_o}\right]^{1/2}\left[\frac{t}{t_f}\right]^{1/2} \quad ; \quad 0<t<t_f$$

The maximum wall heat flux will occur at the moment when the source stops (t = t_f), and is given by

$$q_{w_{max}} = \frac{2k_o \Delta T_f}{\sqrt{\pi \alpha_o t_f}}\left[\frac{p_q}{p_o}\right]^{1/2} \tag{F.6}$$

The value of t_f was taken from wall temperature measurements to be the total time for quenching.

For comparison with the results of Chapter 4, it will be convenient to introduce the characteristic heat flux and time. From Appendix E, the characteristic heat flux is given by

$$q_c = (\rho S_u c_p \Delta T_f)_{P_q, T_u} \tag{E.19}$$

where the subscript u refers to the state of the unburnt gas prior to quenching. Using the assumed property variations, we get

$$q_c = \rho_o S_u c_p \Delta T_f \left[\frac{p_q}{p_o}\right]\left[\frac{T_o}{T_u}\right]$$

The characteristic time,

$$t_c = \left[\frac{\alpha}{S_u^2}\right]_{P_q, T_u} \tag{E.18}$$

becomes

$$t_c = \frac{\alpha_o}{S_u^2}\left[\frac{p_o}{p_q}\right]\left[\frac{T_u}{T_o}\right]^2$$

Dividing Equation F.6 by $q_c\sqrt{t_c}$ gives

$$\frac{q_{w_{max}}}{q_c}\left[\frac{t_f}{t_c}\right]^{1/2} = \frac{2}{\sqrt{\pi}} \quad . \tag{F.7}$$

REFERENCES

Afgan, N.H. and Beer, J.M. (eds.), Heat Transfer in Flames, Scripta Book Company, New York, (1974).

Alkidas, A.C. and Myers, J.P., "Transient Heat-Flux Measurements in the Combustion Chamber of a Spark-Ignition Engine", ASME Report No. 81-WA/HT-1 (1981).

Aly, S.L. and Hermance, C.E., "A Two-Dimensional Theory of Laminar Flame Quenching", Combustion and Flame, **40**, 173-185 (1981).

Andrews, G.E. and Bradley, D., "The Burning Velocity of Methane-Air Mixtures", Combustion and Flame, **19**, 275-288 (1972).

Annand, W.J.D., "Heat Transfer in the Cylinders of Reciprocating Internal Combustion Engines", Proceedings of the Institution of Mechanical Engineers, **177**, 973-990 (1963).

Ballal, D.R. and Lefebvre, A.H., "Ignition and Flame Quenching in Flowing Gas Mixtures", Proceedings of the Royal Society of London, A. 357, 163-181 (1977).

Bechtel, J.H. and Blint, R.J., "Structure of a Laminar Flame-Wall Interface by Laser Raman Spectroscopy", General Motors Research Publication GMR-3162 (1979).

Borgnakke, C., Arpaci, V.S. and Tabaczynski, R.J., "A Model for the Instantaneous Heat Transfer and Turbulence in a Spark Ignition Engine", **SAE Technical Paper Series**, no. 800287 (1980).

Bradley, D. and Mitcheson, A., "Mathematical Solutions for Explosions in Spherical Vessels", Combustion and Flame, **26**, 201-217 (1976).

Buckmaster, J., "The Quenching of Two-Dimensional Premixed Flames", Acta Astronautica, **6**, 741-769 (1979).

Carlslaw, H.S. and Jaeger J.C., Conduction of Heat in Solids, Oxford University Press, London (1948).

Carrier, G.F., Fendell, F.E. and Feldman, P.S., "Interaction of a Planar Laminar Premixed Flame with a Perpendicular Wall", SAE Technical Paper Series, no. 800285 (1980).

Clendening Jr., C.W., Shackelford, W. and Hilyard, R., "Raman Scattering Measurements in a Side-Wall Quench Layer", Eighteenth Symposium (International) on Combustion, 35-42 (1981).

Cloutman, L.D., Dukowicz, J.K., Ramshaw, J.D. and Amsden, A.A., CONCHAS-SPRAY: A Computer Code for Reactive Flows with Fuel Sprays, Los Alamos National Laboratory report LA-9294-MS (1982).

Daniel, W.A., "Flame Quenching at the Walls of an Internal Combustion Engine", Sixth Symposium (International) on Combustion, 886-894, (1956).

Eichelberg, G., "Some New Investigations on Old Combustion-Engine Problems", Engineering, p. 463, October 27, 1939.

Greif, R., Namba, T. and Nikanjam, N., "Heat Transfer During Piston Compression Including Side Wall and Convection Effects", Internation Journal of Heat and Mass Transfer, **22**, 901-907 (1979).

Groff, E.G., "The Cellular Nature of Confined Spherical Propane-Air Flames", General Motors Research Publication GMR-3522 (1981).

Heperkan, H.A., "An Experimental and Theoretical Study of Heat Transfer with Combustion", Ph.D. Thesis, U. C. Berkeley (1980).

Hocks, W., Peters, N. and Adomeit, G., "Flame Quenching in Front of a Cold Wall under Two-Step Kinetics", Combustion and Flame, **41**, 157-170 (1981).

Ishikawa, N., "Studies of Wall Flame Quenching and Hydrocarbon Emissions in a Model Spark Ignition Engine", Ph.D. Thesis, U. C. Berkeley (1978).

Isshiki, N. and Nishiwaki, N., "Basic Study on Inside Convective Heat Transfer of Internal Combustion Engines", Proceedings of the Fifth International Heat Transfer Conference, **II**, 344-348 (1974).

Kays, W.M. and Crawford, M.E., Convective Heat and Mass Transfer, Second Edition, McGraw-Hill, New York (1980).

Keck, J.C., "Thermal Boundary Layer in a Gas Subject to a Time Dependent Pressure", Letters in Heat and Mass Transfer, **8**, 313-319 (1981).

Keck, J.C. and Ferguson, C.R., "On Laminar Flame Quenching and Its Application to Spark Ignition Engines", Combustion and Flame, **28**, 197-205 (1977).

Keiper, R. and Spurk, J.H., "Methane Oxidation Near a Cold Wall", Journal of Fluid Mechanics, **113**, 333-346 (1981).

Kilham, J.K. and Purvis, M.R.I, "Heat Transfer From Normally Impinging Flames", Combusition Science and Technology, **18**, 81-90 (1978).

Krieger, R.B. and Borman, G.L., "The Computation of Apparent Heat Release for Internal Combustion Engines", ASME Paper 66-WA/DGP-4, (1966).

Kurkov, A.P., "A Theoretical Study of Flame Extinction by a Cold Wall and Flame Ignition by a Hot Surface", Ph.D. Thesis, University of Michigan (1967).

Leipmann, H.W. and Roshko, A., Elements of Gasdynamics, John Wiley and sons, New York (1957).

Lund, C.M., HCT - A General Computer Program for Calculating Time-Dependent Phenomena Involving One-Dimensional Hydrodynamics, Transport, and Detailed Chemical Kinetics, Lawrence Livermore National Laboratory report UCRL-52504 (1978).

Markstein, G.H., Nonsteady Flame Propagation, Pergamon Press, New York (1964).

Mondt, J.R., "Heat-Transfer Research on Internal-Combustion-Engine Systems", General Motors Ressearch Publication GMR-4147 (1982).

Nikanjam, M. and Greif, R., "Heat Transfer During Piston Compression", Journal of Heat Transfer, **100**, No. 3, 527-530 (1978).

Ohtake, K., "Heat Transfer with Surface Reaction", from Mori, Y., Ohtake, K. and Ishizuka, "Effect of Surface Reaction on Heat Transfer", The Transactions of The Japan Society of Mechanical Engineers, **38**, 313 (1972), 2333.

Paillard, C., Dupre, G., Combourieu, J., Fokeev, V.P., Gvozdeva, L.G. and Bazhenova, T.V., "Pressure and Wall Heat Transfer behind a Hydrogen/Azide Detonation Wave in Narrow Tubes", in Gasdynamics of Detonations and Explosions, Vol. 75 of Progress in Astronautics and Aeronautics, AIAA, N.Y., N.Y., pgs. 134-149 (1981).

Rosner, D.E., "Correlation and Prediction of Boundary Layer Energy Transfer Rates in the Presence of Chemical Reactions and Mass Injection", Combustion Science and Technology, **10**, 97-108 (1975).

Schefer, R.W. and Robben, F., "Catalyzed Combustion of Lean Fuel/Air Mixtures", Laurence Berkeley Laboratory, Report 10842 (1980).

Schulte, E.H., "Impingement Heat-Transfer Rates from Torch Flames", Journal of Heat Transfer, Series C, **94**, No. 2, 231-233 (1972).

Spalding, D.B., "A Theory of Inflammibility Limits and Flame-Quenching", Proceedings of the Royal Society, **240**, No. 1220, 83-100, (1957).

Sivashinsky, G.I., "Hydrodynamic Theory of Flame Propagation in an Enclosed Volume", Acta Astronautica, **6**, 613-645 (1979).

Tewari, G.P. and Weinberg, F.J., "Structure of Flame Quenched by Cold Surfaces", Proceedings of the Royal Society of London, **A296**, 546-565 (1966).

von Karman, T. and Millan, G., "Thermal Theory of a Laminar Flame Front Near a Cold Wall", Fourth Symposium (International) on Combustion, 173-177 (1952).

Westbrook, C.K., Adamczyk, A.A. and Lavoie, G.A., "A Numerical Study of Laminar Flame Wall Quenching", Combustion and Flame, **40**, 81-99 (1981).

Westbrook, C.K. and Dryer, F.L., "Simplified Reaction Mechanisms for the Oxidation of Hydrocarbon Fuels in Flames", Combustion Science and Technology, **27**, 31-43 (1981).

Williams, F.A., Combustion Theory - The Fundamental Theory of Chemically Reacting Flows, Addison-Wesley, Palo Alto (1965).

Woodard, J.B., "An Experimental and Theoretical Study of Heat Transfer in Constant Volume and Compression-Expansion Systems Including the Effects of Flame Propagation", Ph.D. Thesis, U.C. Berkeley, March 1982.

Woschni, G., "A Universally Applicable Equation for the Instantaneous Heat Transfer Coefficient in the Internal Combustion Engine", SAE Technical Paper Series, no. 670931 (1967).

Yamazaki, S. and Ikai, S., "Study on Laminar One-Dimensional Premixed Flame with Heat Loss", translated by Kazutomo Ohtake, Transactions of The Japan Society of Mechanical Engineers, **37**, p.121 (1971).

This report was done with support from the Department of Energy. Any conclusions or opinions expressed in this report represent solely those of the author(s) and not necessarily those of The Regents of the University of California, the Lawrence Berkeley Laboratory or the Department of Energy.

Reference to a company or product name does not imply approval or recommendation of the product by the University of California or the U.S. Department of Energy to the exclusion of others that may be suitable.

LAWRENCE BERKELEY LABORATORY
TECHNICAL INFORMATION DEPARTMENT
UNIVERSITY OF CALIFORNIA
BERKELEY, CALIFORNIA 94720